REPUBLIC OF TÜRKİYE

ALTINBAŞ UNIVERSITY

Institute of Graduate Studies

Biomedical Sciences

DETERMINATION OF THE ROLE OF PYRIDOSTIGMINE TREATMENT IN MYASTHENIA GRAVIS DISEASE AT MOLECULAR LEVEL BY INFRARED SPECTROSCOPY

Ceren ÇELİK

Master's Thesis

Supervisor

Prof. Dr. Feride SEVERCAN

Istanbul, 2023

DETERMINATION OF THE ROLE OF PYRIDOSTIGMINE TREATMENT IN MYASTHENIA GRAVIS DISEASE AT MOLECULAR LEVEL BY INFRARED SPECTROSCOPY

Ceren ÇELİK

Biomedical Sciences

Master's Thesis

ALTINBAŞ UNIVERSITY

2023

The thesis titled DETERMINATION OF THE ROLE OF PYRIDOSTIGMINE TREATMENT IN MYASTHENIA GRAVIS DISEASE AT MOLECULAR LEVEL BY INFRARED SPECTROSCOPY prepared by CEREN ÇELİK and submitted on 27/04/2023 has been **accepted unanimously** for the degree of Master of Science in Biomedical Sciences.

Asst. Prof. Dr. Ayça DOĞAN	Prof. Dr. Feride SEVERCAN
Co-Supervisor	Supervisor

Thesis Defense Committee Members:

Prof. Dr. Feride SEVERCAN	Department of Biophysics, Altınbaş University	_____
Asst. Prof Dr. Şebnem GARİP USTAOĞLU	Department of Medical Biochemistry, Altınbaş University	_____
Assoc. Prof. Dr. Rafig GURBANOV	Department of Bioengineering, Bilecik Şeyh Edebali University	_____

I hereby declare that this thesis meets all format and submission requirements for a Master's Thesis.

Submission date of the thesis to Institute of Graduate Studies:____/___/____

I hereby declare that all information/data presented in this graduation project has been obtained in full accordance with academic rules and ethical conduct. I also declare all unoriginal materials and conclusions have been cited in the text and all references mentioned in the Reference List have been cited in the text, and vice versa as required by the abovementioned rules and conduct.

Ceren ÇELİK

Signature

DEDICATION

I wish to express my sincere thanks to my esteemed advisor Prof. Dr. Feride SEVERCAN for her valuable guidance, support, and understanding throughout the research.

I am thankful my co-advisor Asst. Prof. Dr. Ayça DOGAN who was with me during my graduation thesis and spared her precious time.

I would like to thank Asst. Prof. Dr. Nazlı EZER OZER, Asst. Prof. Dr. Fulya KUCUKCANKURT, and Dr. Zeynep GUNGORDU DALAR for sharing their knowledge and experiences.

I am thankful to Melike Nur YANGIN for her support and friendship during my master's and thesis phase.

I would like to thank Ipek OZYURT and Ayşe Suna CETIN for their help and support during my thesis work.

I would like to thank Assoc. Prof. Dr. Rafig GURBANOV for supporting me throughout my academic life.

I would like to thank also my friend Alper TEKIN who supported me and did not spare any kind of help.

I am grateful to my family who supported me in all the decisions I made and were always there for me.

PREFACE

This thesis was supported by The Scientific and Technological Research Council of Türkiye (TUBITAK) with the Project number: TUBITAK-SBAG-1003-218S986 and 218S988.

ABSTRACT

DETERMINATION OF THE ROLE OF PYRIDOSTIGMINE TREATMENT IN MYASTHENIA GRAVIS DISEASE AT MOLECULAR LEVEL BY INFRARED SPECTROSCOPY

ÇELİK, Ceren

M.Sc., Biomedical Sciences, Altınbaş University,

Supervisor: Prof. Dr. Feride SEVERCAN

Co-Supervisor: Asst. Prof. Dr. Ayça DOĞAN

Date: April / 2023

Pages: 89

Myasthenia gravis, one of the neuromuscular junction diseases, is a rare autoimmune disease with extensiveness of 15-20 per 100,000 people. Ptosis and skeletal muscle weakness are the most characteristic features of this antibody-mediated disease. Although skeletal and extraocular muscles are mostly affected in patients, violent involvement of respiratory muscles is observed in some of the patients. Due to the violent involvement of the muscles used in breathing, complications called myasthenic crisis, which can be fatal, develop. The illness may progress from ocular MG to generalized MG after at least two years. People with ocular symptoms may receive therapy with acetylcholinesterase inhibitors, called symptomatic therapy since ocular symptoms are characteristic signs of the disease. Pyridostigmine is the most commonly used medicine for this treatment. The quantity of acetylcholine is increased at the neuromuscular junction by inhibition of the enzyme acetylcholinesterase, which hydrolyzes acetylcholine. Thus, neuromuscular transmission is supported.

In this thesis study, the role of pyridostigmine treatment in the pathogenesis of MG was investigated at the molecular level by infrared spectroscopy by comparing the serum of

patients using and not using pyridostigmine and control. Our results revealed that the use of pyridostigmine reduced the elevated effect of MG on saturated lipid, DNA concentration, and protein phosphorylation and approaches the control values. These results clearly indicate that Pyridostigmine has a recovery impact against MG-induced alterations in serum biomolecules.

Keywords: Myasthenia Gravis, Rare Disease, Infrared Spectroscopy, Spectral Characterization, Pyridostigmine.

TABLE OF CONTENTS

Pages

LIST OF TABLES

Pages

LIST OF FIGURES

Pages

ABBREVIATIONS

MG	:	Myasthenia Gravis
C	:	Control
MG+M	:	A Patient Group Using Pyridostigmine
ACh	:	Acetylcholine
AChR	:	Acetylcholine Receptor
AChE	:	Acetylcholinesterase
LRP4	:	Low-Density Lipoprotein Receptor Related Protein 4
MuSK	:	Muscle Spesific Kinase
IR	:	Infrared
FTIR	:	Fourier Transform Infrared Spectroscopy
ATR	:	Attenuated Total Reflectance
EM	:	Electromagnetic
E	:	Energy
THz	:	Tera Hertz
NMR	:	Nuclear Magnetic Resonance
CD	:	Circular Dichroism
ESR	:	Electron Spin Resonance
UV	:	Ultraviolet
VIS	:	Visible
Abs	:	Antibody

RNA	:	Ribonucleic Acid
DNA	:	Deoxyribonucleic Acid
CD	:	Cluster Of Differentiation
NMJ	:	Neuromuscular Junction
HLA	:	Human Leukocyte Antigen
EO-MG	:	Early-onset MG
LO-MG	:	Late-onset MG
EPSP	:	Excitatory Postsynaptic Potential
RNS	:	Repetitive Nerve Stimulation
SFEMG	:	Single Fiber Electromyography
RIP	:	Radioimunoprecipitation
VGKCs	:	Voltage-gated Potassium Channels
LEMS	:	Lambert-Eaton Myasthenic Syndrome
ROS	:	Reactive Oxygen Species
ELISA	:	Enzyme-Linked Immunosorbent Assays
RIPA	:	Radioimmunoprecipitation Assay
CBA	:	Cell-based Assay
IVIG	:	Intravenous Immunoglobulin
NIR(S)	:	Near-Infrared Spectroscopy
MR	:	Manetic Resonance
MW	:	Microwave

Ab/ Abs	:	Antibody/ Antibodies
Th	:	T Helper
ColQ	:	Collagen Q
IFN	:	Interferon
IL	:	Interleukin
Ig/Igs	:	Immunoglobulin/ Immunoglobulins
ATP	:	Adenosine Triphosphate
BAFF	:	B Cell Activating Factor
MHC	:	Major Histocompatibility Complex
MAC	:	Membranous Attack Complexes
CMAP	:	Compound Muscular Action Potential
TCR	:	T Cell Receptor
PTPN22	:	Protein Tyrosine Phosphatase Non-Receptor Type 22
CTLA4	:	Cytotoxic T-Lymphocyte Associated Protein 4
TNF	:	Tumor Necrosis Factor
miRNA	:	MicroRNA
MGFA	:	Myasthenia Gravis Foundation of America
WHO	:	World Health Organization
CT	:	Computed Tomography
MIR	:	Magnetic Resonance Imaging
EDTA	:	Ethylenediamine Tetraacetic Acid

HDL	:	Serum Cholesterol
LDL	:	Serum Cholesterol
CRP	:	C-reactive Protein
ZnSe	:	Zinc Selenide
Ge	:	Germanium
Si	:	Silicon
Ca	:	Calcium
Na	:	Sodium
SEM	:	Standard Error of Mean
Hz	:	Hertz
s	:	Second
J	:	Joule
cm	:	Centimeter
nm	:	Nanometer
m	:	Meter
µm	:	Micrometer
ml	:	Milliliter
µL	:	Microliter
kD	:	Kilodalton
kg	:	Kilogram
g	:	Gram

1. INTRODUCTION AND PURPOSE

Myasthenia gravis is among the neuromuscular junction disorders as a rare autoimmune disease, seen in 15-20 per 100,000 patients (Beloor Suresh & Asuncion, 2022:1). Ptosis and skeletal muscle weakness are the most characteristic features of this antibody-mediated disease. Although skeletal and extraocular muscles are mostly affected in patients, severe involvement of respiratory muscles is observed in some of the patients. Due to the violent involvement of the muscles used in breathing, life-minacious complications called myasthenic crisis develop (Sieb, 2014: 409). After at least two years, the condition may progress from ocular symptoms to generalized Myasthenia Gravis. Acetylcholinesterase inhibitors, often known as symptomatic treatment, can be used to treat individuals with ocular Myasthenia Gravis since ocular symptoms are typical illness presentations (Hehir & Silvestri, 2018: 255). Pyridostigmine is the most commonly used medicine for this therapy. The quantity of acetylcholine is increased at the neuromuscular junction by inhibition of the enzyme acetylcholinesterase, which hydrolyzes acetylcholine. Thus, neuromuscular transmission is supported (Ozdemir & Alagöz, 2018: 3). Pathological conditions such as disease, vaccine-drug use, exposure to chemical substances, genetic infrastructure and modifications cause changes in the amounts, ratios, structures and functions of biomolecules belonging to biological systems. To obtain the infrared (IR) spectra unique to the system under study, these changes are mirrored in the vibration spectra of the samples employed (Dogan, Gurbanov, Severcan, & Severcan, 2021: 550). IR spectroscopy is an essential method that enables the characterization of these molecules and their interactions with each other by showing different vibrational groups of lipid, carbohydrate, protein, nucleic acids (RNA, DNA) molecules in a biological system in a single spectrum (Gok, Aydın, Sural, Zorlu, Bayol, & Severcan, 2016: 968).

This molecular-level study is aimed to determine the role of pyridostigmine treatment in Myasthenia Gravis pathogenesis via infrared spectroscopy by comparing the sera of pyridostigmine user and non-user patients and control.

2. GENERAL INFORMATION

2.1 NEUROMUSCULAR JUNCTION

The synaptic connection between the terminal end of a motor nerve and a muscle forms the neuromuscular junction (NMJ) (Omar, Marwaha, & Bollu, 2022). The terminal branch of the presynaptic motor axon, the postsynaptic muscle membrane, and the synaptic space between the two form the neuromuscular junction structure (Sirin-Inan, 2018: 3).

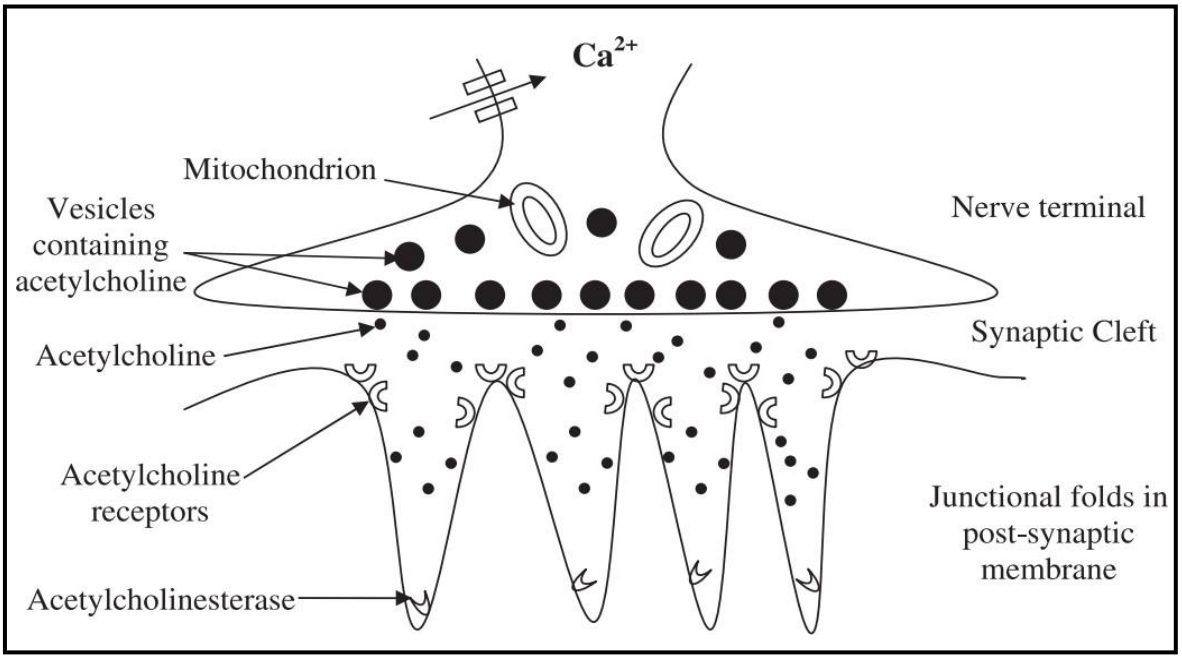

Figure 2.1: General Structure of the Neuromuscular Junction [Turner, 2007: 16].

There are neurotransmitters, which are chemical substances that enable communication between neurons or between a neuron and another type of cell. Acetylcholine (ACh) is synthesized in the terminal region of motor axons and is packaged in vesicles. This packaged ACh is called quanta (Yavuz, 2019: 10). Choline and acetyl-CoA and choline acetyltransferase enzyme are used in the synthesis of ACh (Omar et al., 2022). The synaptobrevin protein controls the storage of ACh vesicles, their mobilization by Rab3A, and their fusion with the presynaptic membrane (Sirin-Inan, 2018:3). In response to an electrical impulse reaching the motor axon, voltage-gated calcium channels in the terminal region open, allowing calcium ions to enter the cell. The action potential induces the discharge of ACh in the acetylcholine vesicles into the synaptic cleft via voltage (Oger & Frykman, 2015: 127). Binding to synaptobrevin, and syntaxin proteins ensure exocytosis of

ACh. Synaptotagmin controls this process by being sensitive to Ca2+ ions. ACh crossing the synaptic gap reaches the postsynaptic muscle membrane. The postsynaptic muscle membrane (End plate membrane) enlarges the surface area by forming a recessed and protruding structure (Omar et al., 2022). This region is rich in ion channels and is located above the membrane folds of the nicotinic acetylcholine receptor (AChR) to which acetylcholine will bind. The acetylcholine receptor is a ligand-gated ion channel and consists of two alpha, a beta, a gamma, and an epsilon subunit. AChR is kept enveloped by the proteins MuSK, ryanodine, agrin, titin, and rapsyn (Oger & Frykman, 2015: 127).

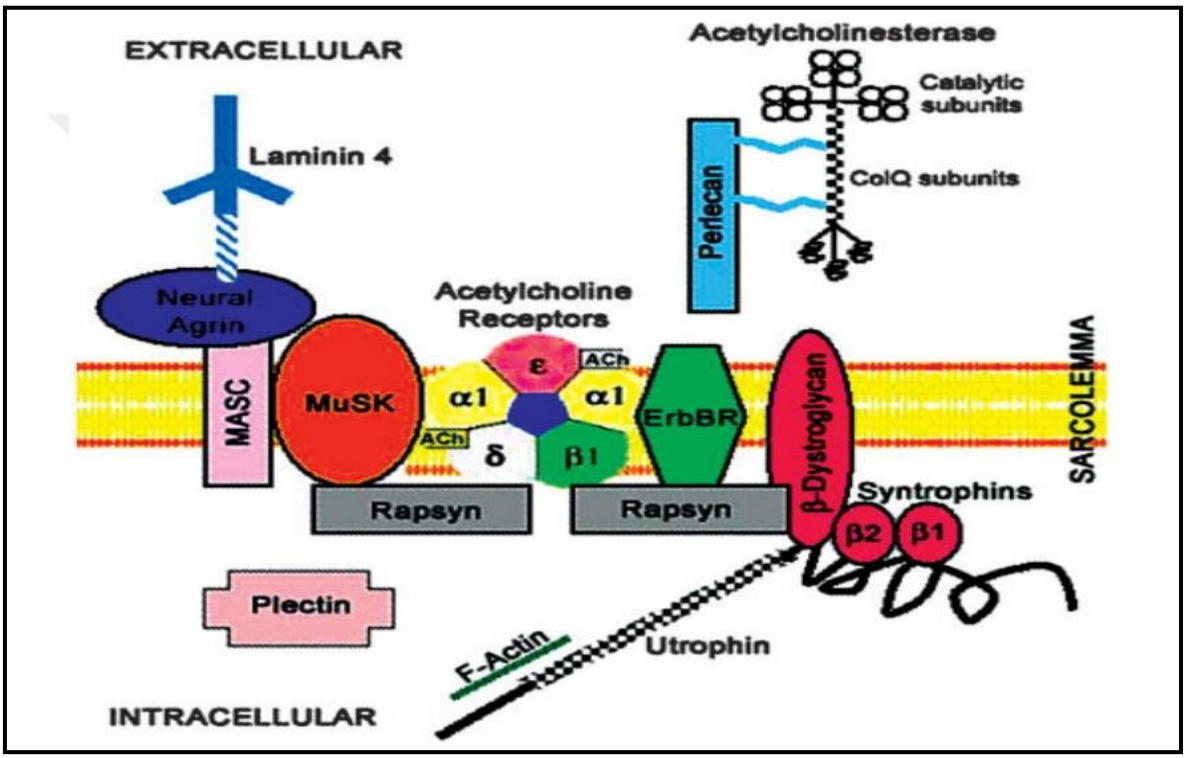

Figure 2.2: Protein Composition of a Mammalian Neuromuscular Junction [Hughes, Kusner, & Kaminski, 2006: 450].

By binding acetylcholine to ACh receptors (AChRs), their associated ion channels are opened (Vincent, 2002: 797). Sodium ions enter the cell and depolarization occurs. Thus, when the depolarization reaches the threshold, the action potential causes muscle contraction (Ha & Richman, 2015: 2). Afterwards, acetylcholinesterase, which is found in synaptic folds bound to the basal membrane, breaks down the acetylcholine that has been separated from its receptor and splits it into acetyl and choline (Turner, 2007: 17). The motor axon terminal absorbs choline and uses it to create ACh (Sirin-Inan, 2018: 4). VGKCs open, causing the

motor nerve terminal to repolarize. Targets for antibody-mediated neurological diseases include VGKCs and AChRs (Vincent, 2002: 799). Muscle contraction occurs as a result of the electrochemical synapse (Oger & Frykman, 2015: 127).

2.1.1 Neuromuscular Junction Disorders

Neuromuscular transmission disorders may occur at the neuromuscular junction due to genetic, toxicological, or immunological causes (Querol, & Illa 2013: 459). Autoimmune neuromuscular junction diseases are rare diseases (Punga, Maddison, Heckmann, Guptill, & Evoli, 2022: 176) Myasthenia gravis is the leading neuromuscular disease in the group of rare diseases. Antibodies against neuromuscular conduction nicotinic Ach receptors are the root cause of the autoimmune illness myasthenia gravis. It is signalize by symptoms such as muscle weakness and fatigue and will be thoroughly explained in the section that follows (MCGrogan, Sneddon, & de Vries, 2010: 171). Antibody-mediated neuromuscular junction transmission disorders include myasthenia gravis, Lambert Eaton myasthenic syndrome (LEMS), and acquired neuromyotonia (Isaac syndrome) (Hill, 2003: 32). Isaacs syndrome is an antibody-mediated disease of the potassium channel. It is clinically characterized by slow muscle relaxation and muscle cramps. Isaac syndrome creates peripheral nerve hyperexcitability disorders acquired with Morvan syndrome, which has common clinical features (Watanabe, 2013: 1067). LEMS is an autoimmune disease that produces antibodies against motor nerve presynaptic voltage-gated calcium channels and affects acetylcholine release (Ha & Richman, 2015: 3; Hughes et al., 2006: 457). Congenital myasthenic syndromes occur due to mutations in neuromuscular junction proteins (Hill, 2003: 32). The number of mitochondria is quite high in the presynaptic motor nerve terminal and postsynaptic junction folds. For this reason, it appears to be common in neuromuscular junction conduction problems (Braz, Shiau, Gorman, Schaefer, McFarland, Taylor, Turnbull, & Whittaker, 2021: 102). Mitochondrial diseases that cause defects in ATP synthesis and oxidative phosphorylation are common metabolic diseases (Gervasoni, Primiano, Marini, Sabino, Biancolilo, Calvani, Picca, Marzetti, Persichilli, Urbani, Servidei, & Primiano, 2020: 1). A mitochondrial condition called primary mitochondrial myopathies is characterized by assaults that resemble strokes (Montano, Gruosso, Carelli, Comi, Filosto, Lamperti, Mongini, Musumeci, Servidei, Tonin, Toscano, Modenese, Primiano, Valentino, Bortolani, Marchet, Meneri, Tavilla, Siciliano, & Mancuso, 2020: 2). Some symptoms of

ptosis and muscle weakness are seen in both mitochondrial myopathy and patients with myasthenia gravis. Studies have indicated that it is difficult to distinguish between the two diseases clinically (Braz et al., 2021: 97). Gervasoni et al. determined the biochemical profile of muscle samples, facilitating the detection of primary mitochondrial myopathies using the FTIR technique (Gervasoni et al., 2020). As demonstrated in another study, the NIRS (Near-Infrared Spectroscopy) technique can measure intramuscularly, providing local tissue oxygenation information regarding mitochondrial myopathy. Thus, patients with mitochondrial myopathy of varying severity can be identified (van Beekvelt, van Engelen, Wevers, & Colier, 1999: 667). Apart from these, neurotoxins also cause neuromuscular transmission disorders. Botulinum toxin is a neurotoxin that causes botulism in smooth and striated muscles. *Clostridium botulinum* bacteria causes this toxin. There are eight varieties of botulinum toxin. Botulinum neurotoxin is -150 kD single-chain polypeptides. It is transported to the neuronal cell cytosol by binding to specific receptors on the presynaptic membranes. It blocks the release of ACh by disrupting the release of neurotransmitters (Ha & Richman, 2015: 4; Nalbantoglu & Adatepe, 2015: 241, Singh, Wasacz, Strand, Jakobsen, & DasGupta, 1990: 705, 706). It causes botulism, ptosis, diplopia, respiratory muscle weakness, and paralysis (Turner, 2007: 19). Botulinum neurotoxins can be analyzed by IR spectra (FTIR spectroscopy technique) and it is possible to learn things like if their polypeptides contain sizable amounts of both a-helix and b-pleated sheets layers (Singh et al., 1990: 711). Venoms of creatures such as snakes, scorpions, and spiders act as a neurotoxin and impair neuromuscular transmission (Nalbantoglu & Adatepe, 2015: 242, Vincent et al., 2001: 2125). Snake venom by blocking Ach or reducing Ach release, Black widow spider and scorpion venom can impair neuromuscular transmission by increasing neurotransmitter release and depleting Ach stores. Organophosphate compounds irreversibly phosphorylate a serine residue in the hydroxyl group in the active site of the acetylcholinesterase (AChE) enzyme, resulting in irreversible AChE inhibition (Nalbantoglu & Adatepe, 2015: 242, Ha & Richman, 2015: 4,5).

2.2 MYASTHENIA GRAVIS

Muscle prostration and exhaustion are the main symptoms of the autoimmune antibody-mediated neuromuscular illness myasthenia gravis (MG) (Romi, Hong & Gilhus, 2017: 9). Neuromuscular diseases are in the group of rare diseases and the most common one is

myasthenia gravis with an incidence of 15-25/100.000 (Wang, & Yan, 2017: 2). When etymologically analyzed, the term myasthenia gravis refers to extreme muscle weakness. Here, it derives from the Latin/Greek word gravis, which means harsh. Myasthenia is the Greek/Latin word for muscle weakness (Al-Zwaini, & Al-Mayahi, 2019: 1). The development of autoantibodies versus the nicotinic-type acetylcholine receptor (AChR) is the primary pathophysiologic process in myasthenia gravis (Owe, Daltveit & Gilhus, 2006: 33). Antibodies against acetylcholine receptors (AChRs), muscle-specific kinase (MuSK), and low-density lipoprotein receptor-associated protein 4 (LRP4) are most common in the pathophysiology of myasthenia gravis. Cortactin, titin, KV1.4, ryanodine receptors, agrin, and Collagen Q (ColQ) antibodies have also been linked to MG in addition to these ones (Gilhus, Skeie, Romi, Lazaridis, Zisimopoulou, & Tzartos, 2016: 260). Muscle fatigue, which is characterized by the disease, affects the bulbar and skeletal muscles, while the heart and smooth muscles are not affected (Owe et al., 2006: 33). As a clinical feature, it is characterized by voluntary muscles. Eye muscle weakness and subsequent diplopia and ptosis are symptoms of decreased electrical impulse conduction at the neuromuscular junction in the early stage of the disorder. The onset of respiratory muscle weakening is a rare occurrence. In addition, difficulties in articulation, chewing, and swallowing may develop due to oropharyngeal weakness. The deterioration of the respiratory muscles and difficulties swallowing can lead to a catastrophic myasthenic crisis. Situations in which a myasthenic crisis occurs are a life-threatening indicator of MG (Sieb, 2014: 409; Gilhus et al., 2016: 259). Neuromuscular blocking agents, heat, infections, emotional stress, pregnancy, previous surgeries, medications, immunization, and worsening of chronic medical diseases may stimulate the onset of the disease (Beloor Suresh & Asuncion, 2022: 2).

2.2.1 Pathophysiology

Myasthenia gravis is caused by antibodies against certain extracellular or transmembrane muscle proteins. Acetylcholine's ability to operate at the neuromuscular junction can be affected by antibodies against AChR, MuSK, or LRP4, either directly or indirectly. It remains unclear whether antibodies to Agrin play a pathogenic role. Sick people with myasthenia gravis have been found to have antibodies against transmembrane proteins such ColQ and Kv1.4, however it is unknown how these proteins contribute to the onset of the

illness. Although they are not harmful in myasthenia gravis, intracellular proteins like titin, ryanodine receptor, and cortactin may operate as distinctive indicators of thymoma existence and disease severity. When the function of acetylcholine is impaired, ion release from the presynaptic membrane decreases. As a result, muscle contraction decreases (Gilhus, Tzartos, Evoli, Palace, Burns, & Verschuuren, 2019: 1,5,6). The presynaptic motor nerve terminal produces acetylcholine (ACh), which is then transported across the synaptic gap to the postsynaptic muscle membrane. By forming multiple branches, the motor neuron axon connects to the muscle fibers. Presynaptic axon terminals reaching the target are devoid of the myelin sheath and contain vesicles containing Ach. Ca^{2+} enters the cell when presynaptic voltage-gated Ca^{2+} channels open as the nerve action potential achieve the synaptic end. However, ACh-containing synaptic vesicles are released into the synaptic vacancy after fusion with the presynaptic membrane. Released ACh molecules bind to AChRs situated in the postsynaptic membrane and open the channel structure. Na^{+} flows into the muscle fiber through the opened channels. As a result, depolarization and muscle contraction occur. Muscle relaxation requires Ca^{2+} ions.

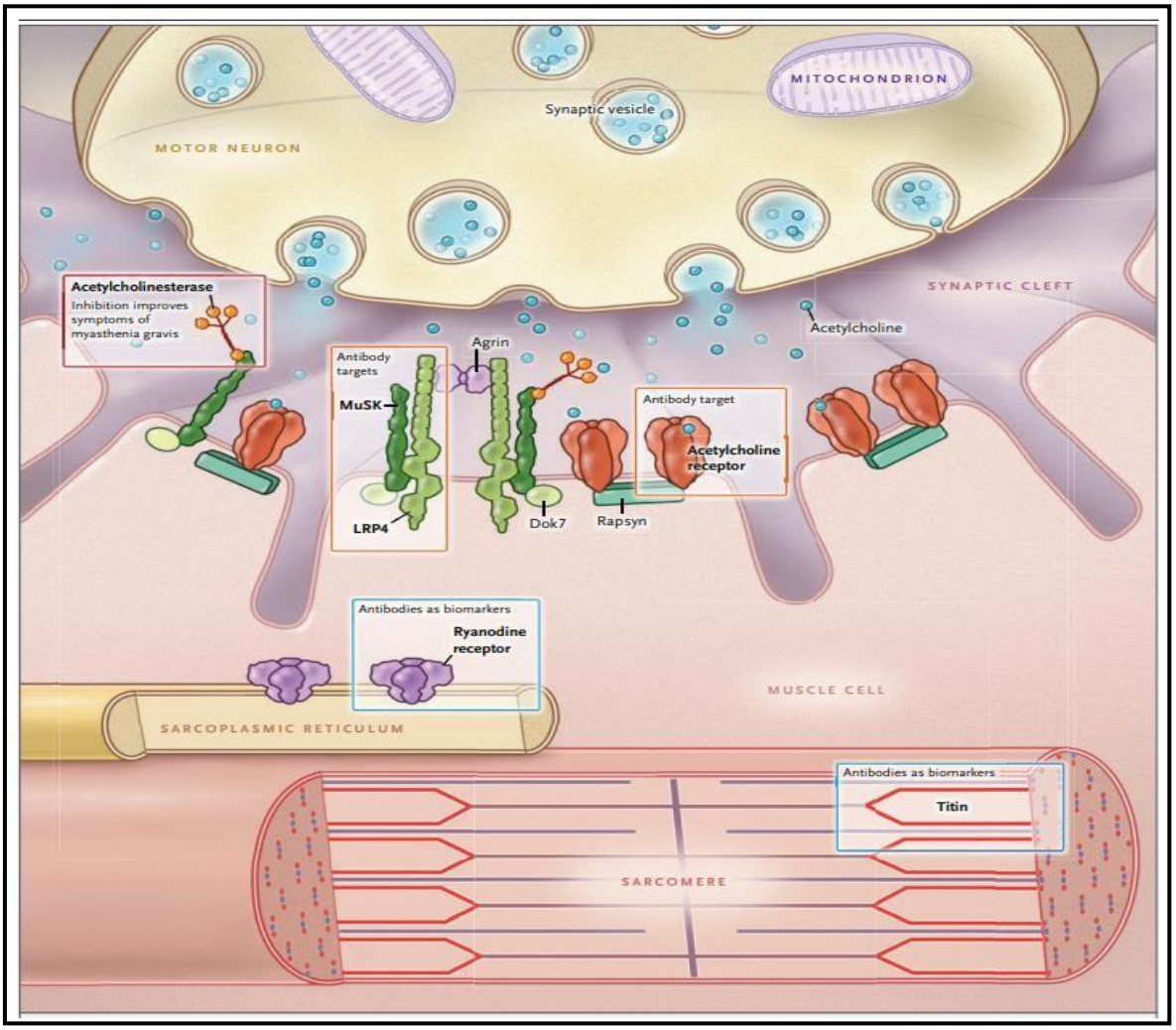

Figure 2.3: Pathogenesis of Myasthenia Gravis and Neuromuscular Junction [Gilhus et al., 2016: 2571].

Although Ach release occurs in myasthenia gravis disease, it has less of an impact on the postsynaptic membrane. There are less Ach receptors in the muscle endplate membrane as a result of the formation of autoantibodies against AChRs. Accordingly, insufficiency of muscle action potential causes muscle weakness (Al-Zwaini, & Al-Mayahi, 2019: 2).

There are 3 different contraption by which anti-AChR Antibodies affect neuromuscular transmission:

a. Binds to the NMJ and activates the complement system.
b. It increases the uptake into the cell and the breakdown of AChR molecules by cross-linking to AChR.

c. It blocks the function of AChR by binding to the region on the receptor where Ach will bind.

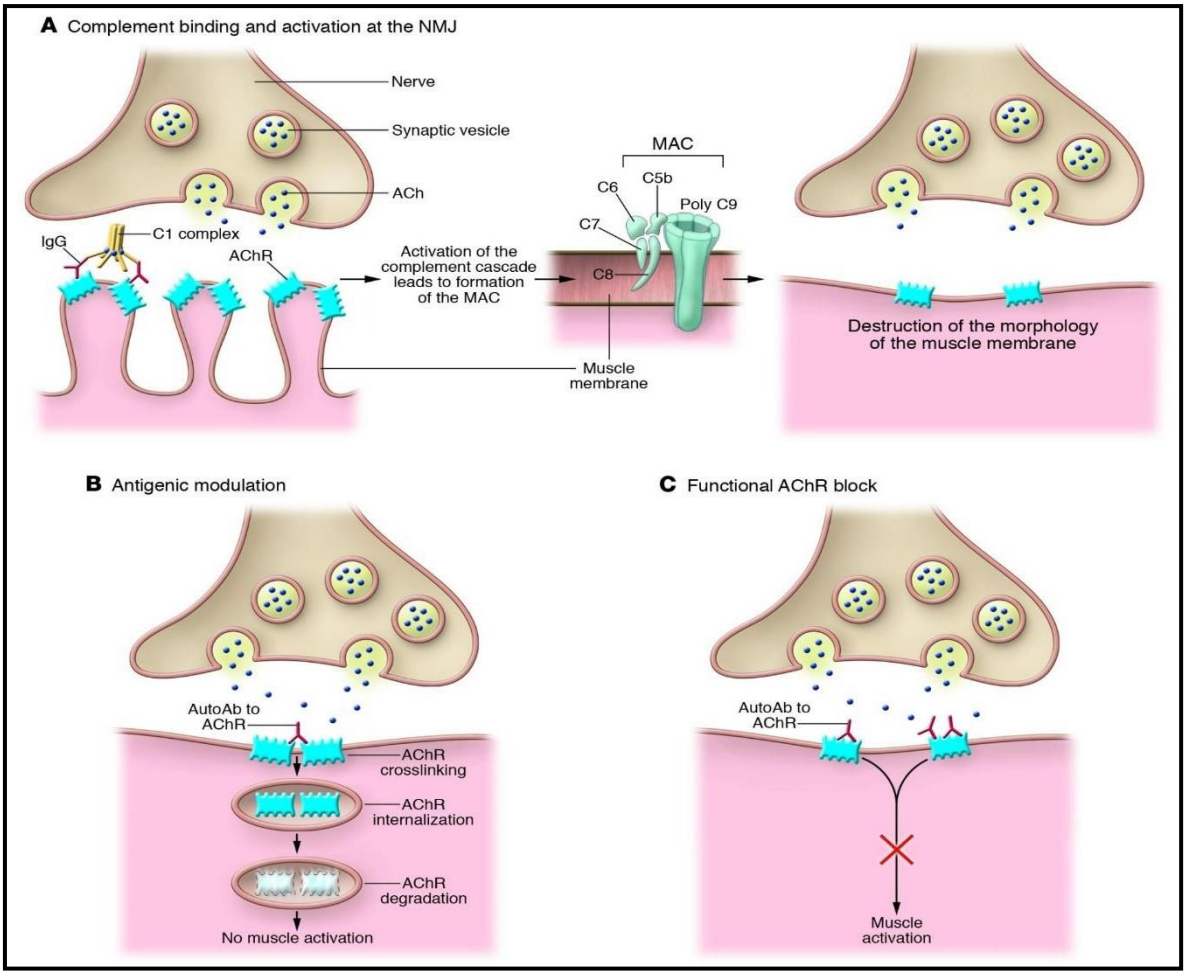

Figure 2.4: Mechanisms of Action of anti-AChR Abs on the Neuromuscular Junction [Conti-Fine, Milani, & Kaminski, 2006: 2846].

2.2.2 Immunity and Thymus in Myasthenia Gravis

When it comes to the beginning and development of myasthenia gravis, type-II hypersensitivity reaction is crucial. It is clear from the development of autoantibodies that the illness is an autoimmune condition mediated by B-cells. T cells help this develop. Additionally, $CD4^+$ T cells are what fuels the immunopathogenesis of MG illness. When macrophage and dendritic cells are activated, they become antigen-presenting cells and phagocytose the antigen. These antigens are degraded into peptide subdivisions. Antigens are transported to the surface of the cell via the MHC-II complex. With the help of CD3+ complex and CD4+ receptors, specific T helper (Th) cells recognize the antigen. When T

cells are activated, they stimulate B lymphocytes by releasing interferon (IFN)-γ and interleukin (IL)-17. Activated B cells that proliferate clonally transform into antibody-producing plasma cells. These autoantibody-producing cells create an autoimmune reaction by binding to target antigens on the cell surface (Conti-Fine, Milani, & Wang, 2008: 193).

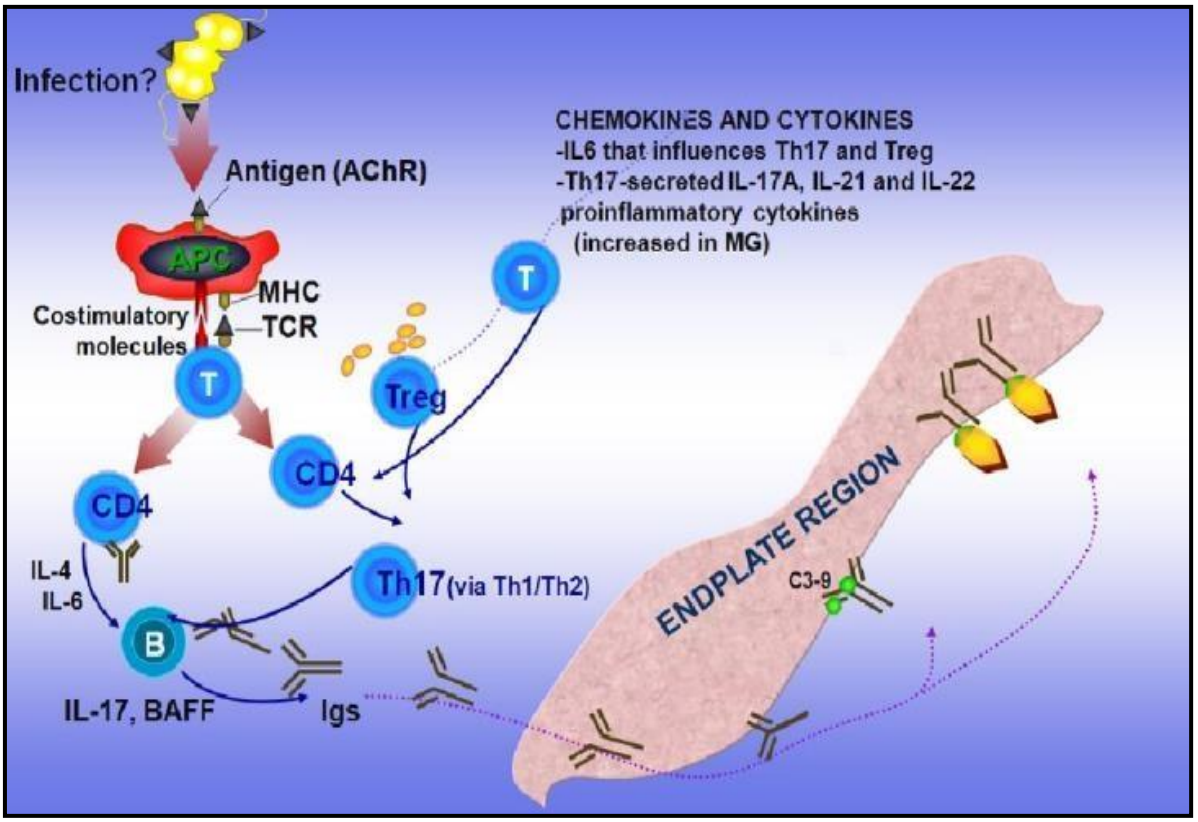

Figure 2.5: Immune Cell Interactions Resulting in the Formation of Autoantibodies are Seen in MG [Dalakas, 2015: 319].

In autoimmune disorders, the percentage of $CD3^+$, $CD4^+$ cells is used to characterize the disease. T cells that act as helper/inducers are $CD3^+$ and $CD4^+$. Suppressor/cytotoxic T cells are $CD3^+$ and $CD8^+$ (McBride & Striker, 2017: 1).

Relationships among B and T cells are crucial for the immunopathogenesis of MG. Transmembrane calcium channel $CD20^+$ act a crucial part in the activation, proliferation, and differentiation of B cells (Du, Mills, & Mao-Draayer, 2017: 1). $CD71^+$ is the transferrin receptor in mononuclear cells. Expression of $CD71^+$ parallels the realization of cell activation, growth control, and cell proliferation. Iron in plasma binds to transferrin, producing apo transferrin. Apotransferrin attach to $CD71^+$ on the cell surface (Kinik, Tuncer,

& Altay, 1999: 494). Iron stimulate the formation of Reactive Oxygen Species and acts as a catalyst in lipid peroxidation (Hübscher, 2003: 524). Although it showed an increase in $CD71^+$ expression in anti-AChR positive MG patients, there is no study on the evaluation of the relationship between this increase and the pathogenesis of MG (Ragheb, Bealmear & Lisak, 1999:63).

For T-cell differentiation and central tolerance, the thymus is crucial. Most thymic cells under physiologically normal circumstances are made up of thymocytes and stromal cells; B cells are few in number. Thymus gland abnormalities usually occur in MG. In individuals with MG, follicular hyperplasia, in which foci with a high number of B cells are formed (germinal centers), may be in question. This is seen in AChR Ab-positive patients. From the point of gender, men are affected more often than women. From the point of age, the aged are affected more often than younger individuals (Oger, & Frykman, 2015: 128).

2.2.3. Genetic Basis in Myasthenia Gravis

Despite the fact that myasthenia gravis is an autoimmune disease, hereditary influences should not be disregarded. Human leukocyte antigen (HLA) loci and some variants of non-HLA genes are associated with disease MG susceptibility (Sathasivam, 2014: 8). It is known that the genes for the human leukocyte antigen class I and class II are connected to MG. Numerous studies have supported the link between early-onset MG linked to thymic follicular hyperplasia and HLA B8 (MHC class I) and -DR3 (MHC class II). Late-onset MG is related to HLA-DR2-B7. In MuSK-MG cases, a link with HLA-DR14-DQ5 has been noted. The genes linked to MG in addition to HLA involve PTPN22, IFN-g, IL-1b, IL-10, TNF-a, and CTLA-4. The PTPN22 gene, which transcribes a member of the tyrosine phosphatase subfamily, prevents T cell activation by interfering with T cell signaling. The highly polymorphic CY-TLA-4 molecule controls immunity by preventing T cells from becoming overly activated. A particular TNF-a allele that causes TNF-a production is present in women with early-onset MG. Additively, the AChR promoter is genetically linked to autoimmune MG (Berrih-Aknin, Frenkian-Cuvelier, & Eymard, 2014: 146).

There have been reports of abnormal miR(320a,155, and 146a) and let-7c expression in immune cells as well as miR-150 and 21 expression in blood serum in MG. In the transcriptome and methylome profile analysis by Mamrut et al., it was suggested that genetic

predisposition is important in the pathogenesis of MG (Wang & Yan, 2017: 3; Mamrut, Avidan, Truffault, Staun-Ram, Sharshar, Eymard, Frenkian, Pitha, de Baets, Servais, Berrih-Aknin & Miller, 2017: 62).

2.2.4 Epidemiology

In 1672, myasthenia gravis was first characterized. But Indian Chief Opechancanough's case may be the first known instance of MG. It has been reported by historians that the chief's muscles lost their elasticity and opened his eyelids with help (Trouth, Dabi, Solieman, Kurukumbi, & Kalyanam, 2012: 1). Between 3 to 30 cases of MG occur annually for every million people. Both sexes experience an increase in MG incidence with age (Sathasivam, 2014: 6). The rise in immune-related issues with aging may have contributed to the increase in incidence. It is rare (up to 3/1,000,000/year) and typically does not correlate with age in boys aged 0 to 19. The incidence is high in girls (up to 11/1,000,000 per year), and it rises with age (MCGrogan et al., 2010: 173). Pediatric MG is rare. Transient neonatal MG with placental antibody transfer in maternal autoimmune MG occurs as a self-limiting disease (Juel & Massey, 2007: 2). There is little geographical variation in the incidence and prevalence of myasthenia gravis. Of course, this does not apply to every subgroup of the disease. For example; Juvenile (MG occurring in children) is higher in Asian ethnicities. There are epidemiological data showing that the prevalence of LRP4-associated myasthenia gravis is half that of the MuSK type. MuSK and LRP4 antibodies are present in 25% and 19%, respectively, of individuals with MG without AChR antibodies. The incidence and prevalence of the disease associated with MuSK is 2.9 per million. It is more widespread in the south than in northern Europe (Gilhus & Verschuuren, 2015: 1025). Between 1970 and 2000, incidence rates in Europe varied between 4.1 and 30/1,000,000/year (Berrih-Aknin et al., 2014: 145).

2.2.5 Classification

Myasthenia gravis can be categorized according to more than one condition. It is categorized by antibody type, clinical status (ocular or generalized), age of onset, and thymic pathology.

2.2.5.1. Classification age of onset

In accordance with, the age of onset, myasthenia gravis is split into two categories. Early-onset myasthenia gravis is categorized as beginning before the age of 50, whereas late-onset myasthenia gravis is categorized as beginning beyond the age of 50.

In the early onset type of the disease (EOMG), the earliest symptoms appear before the age of 50. Thymoma patients are not included in this group. Women are more likely than men to have thymic follicular hyperplasia, yet this group responds to thymectomy. There are more female patients than male, with a 3:1 gender split. This dominance may be impacted by sex hormones. In addition, early-onset myasthenia gravis is linked to HLA-DR3, HLA B8, and other autoimmune risk genes. After age 50, the early signs of late-onset myasthenia gravis (LOMG) appear. Men have a somewhat higher prevalence of late-onset MG. When a tumor develops in the thymic epithelial cells, it is called a thymoma, seen during imaging or surgery. In addition, thymic hyperplasia is rarely seen. Patients in this group generally do not respond to thymectomy. Bulbar involvement is a serious symptom that occurs. In contrast to patients with other types of the disease, thymoma patients were shown to have autoantibodies against anti-ryanodine, anti-titin, or anti-striated muscle (Gilhus & Verschuuren, 2015: 1026; Berrih-Aknin et al., 2014: 145).

2.2.5.2. Classification by antibody

In MG, prognosis and treatment are affected by the antibody profile. Therefore, autoantibodies control the primary immunological profile. In MG, antibodies against the muscular membrane's acetylcholine receptor are more prevalent. About half of the patients who are ocular have AChR autoantibodies. 90% of severe MG and 80-85% of widespread MG exhibit AChR positive. Some patients whose AChR antibodies were undetectable turned out to have positive Muscle-Specific Kinase antibodies. Of all MG patients, 1–10% have MuSK antibodies. It is seen in 5-7% of generalized MG types. It is less common in ocular MG (Yavuz, 2019: 23). If patients who do not have AChR autoantibodies do not additionally have MuSK autoantibodies, these patients are called double seronegative. A proportion of double seronegative patients have antibodies to LRP4. If this antibody is also absent, it is called triple seronegative (Zhang, Shen, Bealmear, Ragheb, Xiong, Lewis, Lisak, & Mei, 2014: 1).

2.2.5.3. Classification according to clinical condition (ocular or generalized)

Muscle weakening that just affects the eye muscles in 20% of MG patients causes ptosis or diplopia (Hehir & Silvestri, 2018: 255). Ocular myasthenia gravis is the defining feature of these patients. Generalized myasthenia gravis is more likely to occur in patients with an ocular manifestation. Therefore, patients can be categorized as ocular if they do not experience the onset of generalized myasthenia gravis for at least 2 years and after. Antibodies to AChR are typically identified in ill with ocular myasthenia gravis, although antibodies to MuSK are uncommon (Gilhus & Verschuuren, 2015: 1027). 85% of MG patients are generalized myasthenia gravis. These patients often have thymic abnormalities (Berih-Aknin, 2014: 145). The clinical features of generalized MG are characterized by facial, bulbar, neck, or sometimes marked muscle atrophy and respiratory muscle weakness. When muscle groups such as the paraspinal and upper esophageal muscles are involved, respiratory crisis often occurs (Trouth et al., 2012: 2). Immunosuppressants are used to treat patients with generalized MG. Acetylcholinesterase inhibitors are the only drugs that can be used to treat people with ocular MG. Due to the severe nature of ocular muscle weakness and the potential necessity for immunosuppressive medication in those ill with ocular MG, acetylcholinesterase alone may fail (Hehir & Silvestri, 2018: 255).

2.2.5.4. Classification thymoma

Thymomas are a result of epithelial cells developing abnormally and are linked to autoimmune disease. AChR-like, titin-like, and ryanodine-receptor-like epitopes are just a few examples of the many self-similar antigens that neoplastic epithelial cells in thymomas express. Thymomas are present in 10-15% of myasthenia gravis ills. Ill with widespread MG frequently experience it, and AChR antibody is found. MG patients usually have B1 or B2 type of thymoma. Thymectomy is indicated in patients (Hehir & Silvestri, 2018: 255; Trouth et al., 2012: 2).

Table 2.1: Histopathological Classification of Thymoma according to WHO [Yavuz, 2019: 29].

TYPE	Histopathological Description
A	Medullary
AB	Mixed
B1	Predominant Cortical
B2	Tortical
B3	Well Differentiated Thymic Carcinoma
C	Thymic Carcinoma

Table 2.2: Clinical Classification of Myasthenia Gravis by MGFA [Trouth et al., 2012: 2].

CLASS	Clinical Description
I	(i) any ocular muscle weakness (ii) can have weakness of eye closure (iii) all different muscle strengths are normal
II	(i) mild weakness influencer muscles other than ocular muscles (ii) can also have ocular muscle weakness of any severity
IIa	(i) mainly affecting limb, axial muscles, or both (ii) can also have lesser involvement of oropharyngeal muscles.

Table 2.2: Clinical Classification of Myasthenia Gravis by MGFA [Trouth et al., 2012: 2] ‘‘Table Continued’’.

IIb	(i) mainly affecting oropharyngeal, respiratory muscles, or both, (ii) can also have lesser or equal involvement of limb, axial muscles, or both.
III	(i) mid weakness affecting muscles other than ocular muscles, (ii) can also have ocular muscle weakness of any severity.
IIIa	(i) mainly affecting limb, axial muscles, or both, (ii) can also have lesser involvement of oropharyngeal muscles.
IIIb	(i) mainly affecting oropharyngeal, respiratory muscles, or both, (ii) can also have lesser or equal involvement of limb, axial muscles, or both.
IV	(i) violent weakness affecting muscles other than ocular muscles, (ii) can also have ocular muscle weakness of any severity.
IVa	(i) mainly affecting limb, axial muscles, or both, (ii) can also have lesser involvement of oropharyngeal muscles.
IVb	(i) mainly affecting oropharyngeal, respiratory muscles, or both, (ii) can also have lesser or equal involvement of limb, axial muscles, or both.
V	(i) intubation with or without mechanical ventilation, except when employed during routine postoperative management, (ii) the use of a feeding tube without intubation places the patient in class IVb.

2.2.6. Symptoms

The most familiar symptom of Myasthenia Gravis is fatigued weakness. In this case, weakness may develop or may manifest itself with effort. Ptosis, diplopia, and blurred vision

can by virtue of the involvement of extraocular muscles or the involvement of levator palpebrae muscles. Weakness of the bulbar and facial muscles causes expressionless face formation. In addition, it causes difficulties in speaking, chewing, and swallowing (Trouth et al., 2012: 4). Neck flexors and neck extensor muscles are weak. Although the neck extensor muscles are typically weaker than the neck flexor muscles, the dropped head syndrome can still happen if these muscles aren't strong enough. Ill with neck extensor weakness can develop posterior neck myalgias despite the fact that MG causes painless weakness (Juel & Massey, 2007: 3). Localized muscle weakness in the ocular muscles is called ocular myasthenia gravis. It is called generalized myasthenia gravis when it is not limited to the ocular muscles, but spreads to other skeletal muscles and affects them. Respiratory or bulbar paralysis attacks that threaten the patient's life may occur, these are myasthenic crises. A cholinergic crisis, including hypersalivation, lacrimation, sweating, vomiting, and cholinergic symptoms associated with miosis, may occur when patients use excessive anticholinesterase medication (Vincent, Palace, & Hilton-Jones, 2001: 2123).

2.2.7 Diagnostic Methods in Myasthenia Gravis Disease

To understand whether a patient has MG, it is diagnosed through examination findings, diagnostic tests, and clinical symptoms. The combination of present symptoms and examination findings is confirmed by positive anti-AChR antibodies in a major proportion of ill. Additionally, the diagnosis of the disease is vulnerable to the existence of antibodies to MuSK and LRP4. If antibodies are negative, neurophysiological tests are used. If the ptosis is reversed by placing ice in the eye with ptosis, the ice test responds to treatment and provides a diagnosis. Thymic status can be determined using mediastinal imaging. The presence of thymoma can be detected on imaging, but this is not specific to the definition of thymic hyperplasia. Diagnosis of MG can be difficult because it is a rare disease and can be confused with other defects in neuromuscular transmission (Gilhus et al., 2016: 2570; Vincent et al., 2001: 2125).

2.2.7.1 Antibody tests

85–90% of people with a broad form of MG illness have AChR antibodies. AChR antibodies serve as a marker for myasthenia gravis (Vincent et al., 2001: 2125) 10-20% of individuals with generalized MG lack AChR antibodies, these patients qualify as seronegative MG

patients. Approximately 40 to 70% of seronegative ill have anti-MuSK autoantibodies. Patients are tested for the less common LRP4 antibodies if they do not have both MuSK and AChR antibodies (double seronegative). Between 2 and 50% of double seronegative ill have anti-LRP4 antibodies. When AChR, MuSK, and LRP4 antibodies cannot be found in the blood sera of triple seronegative MG ills, Agrin or COLQ antibodies can be thought of as viable targets. Antibodies are discovered using antigen-specific antibody assay techniques such cell-based assays (CBAs), radio-immunoprecipitation assays (RIPAs), and enzyme-linked immunosorbent assays (ELISAs) (Trakas & Tzartos, 2018: 111; Zhang et al., 2014: 1; Oger & Frykman, 2015: 129).

2.2.7.2 Electrophysiologic tests

Electrophysiological tests can be applied to patients who are seronegative in the antibody test. These tests include single fiber electromyography (SFEMG) and repeated nerve stimulation (RNS) testing. They provide information about delays at the neuromuscular junction. Before these tests are applied, the functioning of nerves and muscles is determined. RNS at 2-5 Hz depletes acetylcholine stores at the neuromuscular junction. In neuromuscular junction disorders, the factor of safety decreases. Some endplate potentials may not reach the depolarization threshold, as RNS will further increase this reduction. Action potentials in the muscle fibers do not result as a result. The compound muscular action potential (CMAP), which has a lower amplitude and area with fewer individual muscle fiber action potentials, has a lower response. A diagnostic indicator for MG is an excitatory postsynaptic potential (EPSP) drop of 10% or more between the first and fifth stimulation. Compared to ocular MG, the RNS test is more sensitive in generalized MG. The RNS test's sensitivity is typically 75%, however the specificity changes depending on which nerve is being examined. The most accurate diagnostic procedure for identifying abnormalities of neuromuscular conduction is SFEMG. The SFEMG test can be used to determine the diagnosis of MG in patients with normal RNS testing. With the aid of a special concentric needle, individual muscle fiber action potentials produced by a single motor neuron are recorded. Neuromuscular jitter is the lag between firing one muscle fiber potential into another. Because of the decreased neuromuscular transmission in MG, the jitter will rise. SFEMG has a sensitivity of up to 99% in generalized MG, but only about 80% in ocular MG (Beloor Suresh & Asuncion, 2022; Juel & Massey, 2007: 4; Sathasivam, 2014: 9).

2.2.7.3 Edrophonium (tensilon) test

Edrophonium chloride helps acetylcholine maintain the length of its action at the neuromuscular junction by acting as an acetylcholinesterase inhibitor. The intravenous administration of edrophonium. The patient experiences less ptosis or diplopia symptoms. The susceptibility of the test for identification MG is between 71.5% and 95%. Some young children and babies may be tested with neostigmine. Because neostigmine is longer-effective. Physostigmine and neostigmine (pyridostigmine) were used before the edrophonium test was used for the diagnosis of MG. Edrophonium is also known as the Tensilon test as it is supplied by a manufacturer called Tensilon (Pasnoor, Dimachkie, Farmakidis, & Barohn, 2018: 262-263).

2.2.7.4 Ice pack test

For patients with droopy eyelids, ice is applied with an ice pack for nearly 5 minutes. The acetylcholinesterase enzyme is suppressed by the cold effect. Since the degradation of acetylcholine will be slowed down, neuromuscular transmission is temporarily improved. If there is a recovery of more than 2 mm in the eyelid, the test is positive. It is exclusive to 80-90% MG (Yangın, Zorlu, & Severcan, 2022: 108).

2.2.7.5 Imaging

There are two ways to check if a patient has a thymoma or thymic hyperplasia. These are magnetic resonance imaging (MRI) and computed tomography (CT) (Sathasivam, 2014: 10).

2.2.8 Treatment

There are four basic treatment methods for the treatment of MG (Trouth et al., 2012: 6).

These;

a. Use of acetylcholinesterase inhibitors qualified as symptomatic therapy,
b. Chronic long-term immunomodulatory therapy with immunosuppressive drugs,
c. Immunomodulatory therapy with plasmapheresis or intravenous immunoglobulin,
d. Surgical intervention (Thymectomy).

2.2.8.1 Symptomatic treatment (acetylcholinesterase inhibitors)

The use of pyridostigmine, which is an acetylcholinesterase inhibitor, is one of the leading symptomatic treatments. Inhibition of acetylcholine esterase at the neuromuscular junction has a symptomatic effect, especially in autoimmune MG. Agents that inhibit acetylcholinesterase increase the bioavailability of ACh in the synaptic cleft. Individuals with anti-MuSK antibodies do not respond to acetylcholinesterase inhibition, while individuals belonging to other subgroups of Myasthenia gravis disease respond to acetylcholinesterase inhibition. It provides excellent responsiveness, especially in juvenile MG. Pyridostigmine is the most widely used acetylcholinesterase inhibitor. Neostigmine or ambenonium chloride can also be used as acetylcholinesterase inhibitors, but pyridostigmine is more effective in most patients (Gilhus et al., 2019: 10; Gilhus, 2016: 2575).

2.2.8.1.1 Pyridostigmine

Pyridostigmine is the extensively used acetylcholinesterase inhibitor in the treatment of symptomatic MG. Anticholinesterases, also known as acetylcholinesterase inhibitors, are a tool used to treat the symptoms of MG. Since the 1950s, pyridostigmine has been utilized. The serine hydrolase enzyme class includes the hydrolytic enzyme acetylcholinesterase. The central nervous system and autonomic nervous system's cholinergic synapses depend on this enzyme to hydrolyze acetylcholine. This enzyme is found at nerve endings and cholinergic synapses or junctions at the postjunctional or postsynaptic membrane. Drugs that inhibit AChE are acetylcholinesterase inhibitory agents. Inhibition of acetylcholinesterases leads to increased ACh at nerve synapses and neuromuscular junctions. Thus, neuromuscular transmission is increased. Pyridostigmine bromide is a reversible AChE inhibitor derived from carbamate. They provide short-term improvement, that is, they do not change the pathophysiological process that causes and maintains MG. Patients with anti-MuSK antibodies respond less favorably to acetylcholinesterase inhibitors such as pyridostigmine than other subgroups of MG. There is individual variation in how well other subcategories of MG respond to acetylcholinesterases in terms of the amount of weakness alleviation, ideal dosage, and tolerability. Some people regain their muscle power, while others continue to have variations. In this case, patients are accompanied by other treatment methods. Administration of acetylcholinesterase inhibitors in very high doses involves the risk of poisoning called a 'cholinergic crisis'. Dosage optimization is important. In addition, the use

of pyridostigmine in elderly patients may cause bradycardia. Characteristic side effects of pyridostigmine; diarrhea, abdominal cramps, nausea, and increased salivation, as well as urinary urgency and increased sweating (Ozdemir & Alagöz, 2018: 3-5; Maggi & Mantegazza, 2011: 694; Gilhus, 2016: 2575; Sieb, 2014: 412; Gilhus et al., 2019: 10).

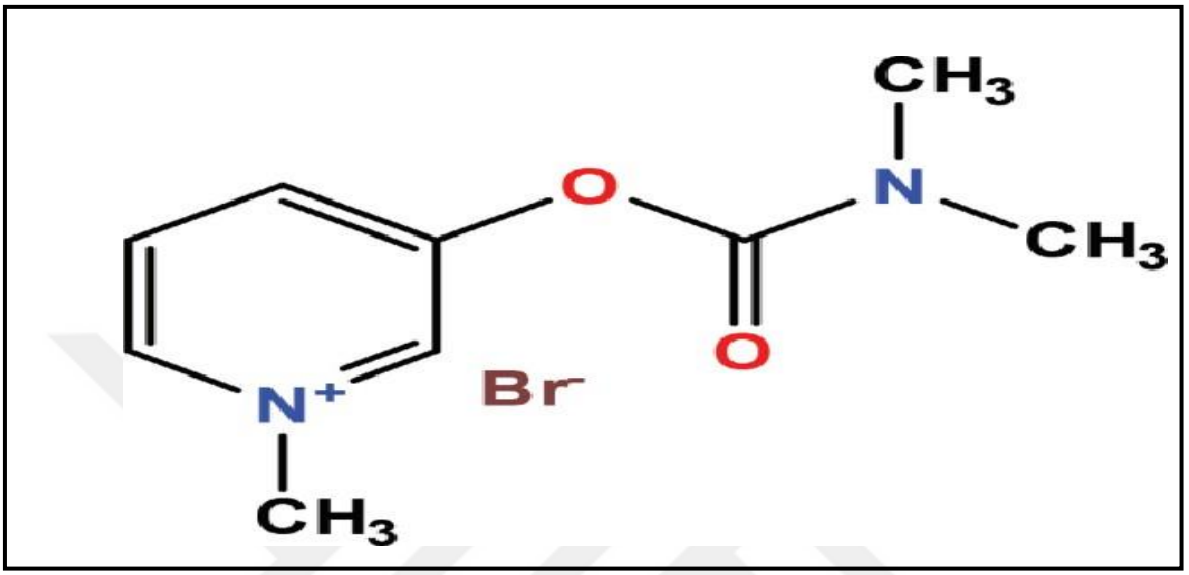

Figure 2.6: Chemical Structure of Pyridostigmine [Ozdemir & Alagöz, 2018: 5].

2.2.8.2 Immunosuppressive treatment

In the treatment of MG, immunosuppressants are used as long-term corticosteroid-sparing agents (Sathasivam, 2014: 12). Immunotherapies based on steroids and other immunosuppressants should be administered in patients for whom acetylcholinesterase inhibitor therapy is not sufficient. Azathioprine, mycophenolate mofetil, methotrexate, or cyclophosphamide can be used as antimetabolites in immunosuppression, and tacrolimus and cyclosporine can be used as calcineurin inhibitors (Gilhus et al., 2019: 10). In addition, according to recent studies, two monoclonal antibodies, rituximab, and eculizumab, have promising potential for treatment. Looking at the mechanisms of the effect of immunosuppressive drugs, they result in a variety of alterations, such as the inhibition of T cell activation and the interfering with T and B cell proliferation by stopping the cell cycle, as well as the decline of circulating T cells and activation or suppression of target genes (Menon, Barnett, & Bril, 2020: 2).

2.2.8.3 Immunomodulatory treatment

In the lead up to surgery, intravenous immunoglobulin (IVIG) or plasma exchange (plasmapheresis) are advised to stabilize the patient. It is also employed when immunosuppressive medication is ineffective (Beloor Suresh & Asuncion, 2022).

Plasma exchange is performed in myasthenic crises and before surgery (including thymectomy) to stabilize muscle function. One or two volumes of plasma can be exchanged three times a week, with a maximum of six. Plasmapheresis treatment performs better for MuSK MG patients than IVIG. Plasma exchange provides a solution by eliminating circulating pathogenic antibodies and other factors. When antibodies that block AChR function are removed, recovery can be observed shortly after plasma exchange (Kaminski, 2018: 178).

Patients with MG receive 0.4 g of immunoglobulin per kilogram of body weight per day, which is isolated from the plasma of hundreds of donors receiving ethanol cryoprecipitate. Healing begins to show its effect within a week and continues for a month (Yangın et al., 2022: 110).

IVIG therapy for MG immunopathogenesis includes inhibiting pathogenic cytokines from activating B and T cells, decreasing antibody production, neutralizing autoantibodies using anti-idiotypic antibodies, preventing the formation of membranous attack complexes (MAC), and inhibiting complement (Dalakas, 2018: 118).

2.2.8.4 Surgical intervention (thymectomy)

Ill with MG produce anti-AChR antibodies when their thymus is active. While thymic hyperplasia is observed in 60-70% of patients, 10-15% of them have thymoma (Yangn et al., 110). Men over the age of 40 are more likely than women to experience it. Children are rarely affected by it. The tumor tissue is removed with a thymectomy. Ill with early-onset and anti-AChR conditions may benefit from thymectomy as a treatment. Ill with anti-MuSK or anti-LPR4 antibodies is not recommended for thymectomy. The patient may continue to need immunosuppressants even after a thymectomy (Dalakas, 2018: 118; Kaminski 2018: 180; Gilhus et al., 2016: 2578).

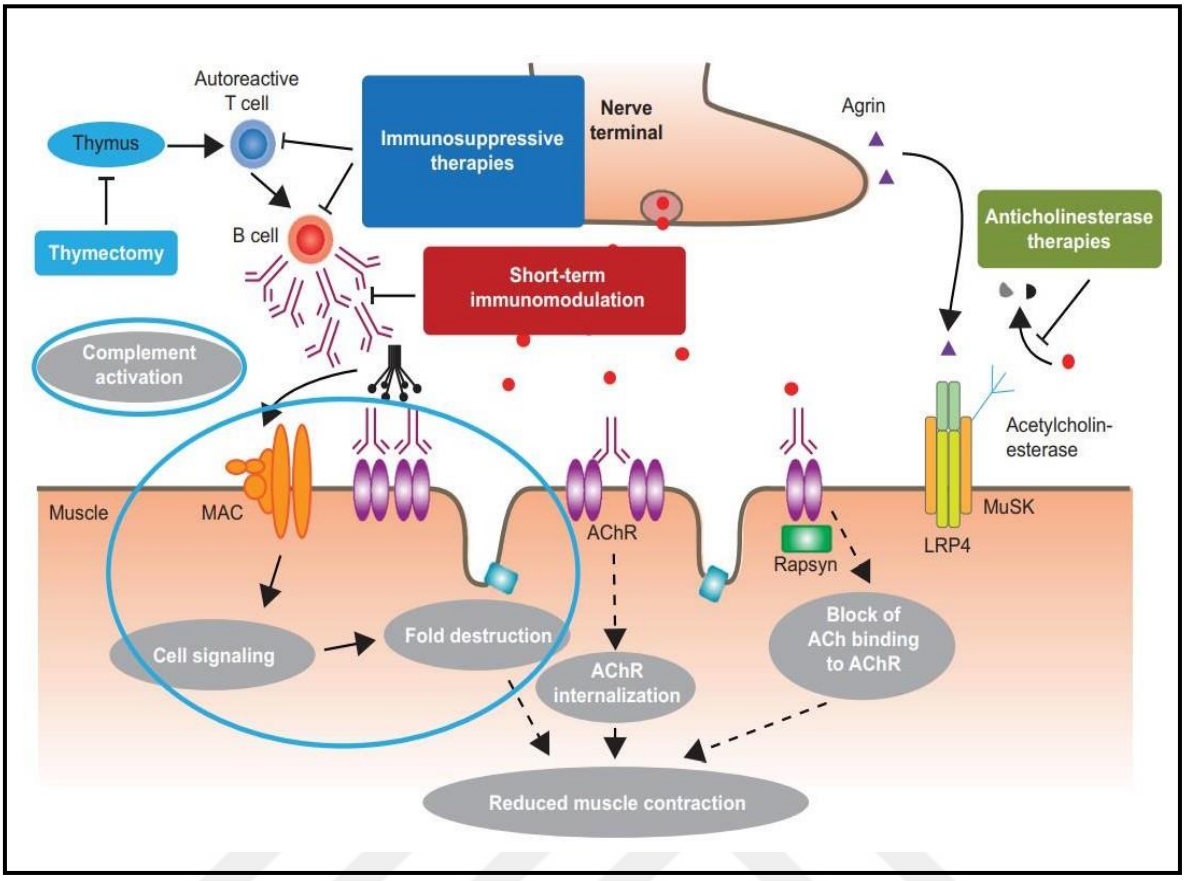

Figure 2.7: Current Treatments for People with Myasthenia Gravis [Howard, 2017: 124].

2.3 SPECTROSCOPY

2.3.1 Fundamentals of Spectroscopy

The investigation of how electromagnetic radiation (light) interacts with substances is referred to as spectroscopy. In accordance with Maxwell's classical theory, electromagnetic radiation is defined as two perpendicular electric and magnetic fields oscillating in a single plane at right angles to one another (Stuart, 2004: 3; Andrews, 2017: 430, Emery & Camps, 2017: 43). Light is dual nature, both wave and a corpuscle (Spahıu, 2015: 16). Figure 2.3.1 depicts an electromagnetic wave containing both magnetic and electric fields, as well as the definitions of frequency and wavelength.

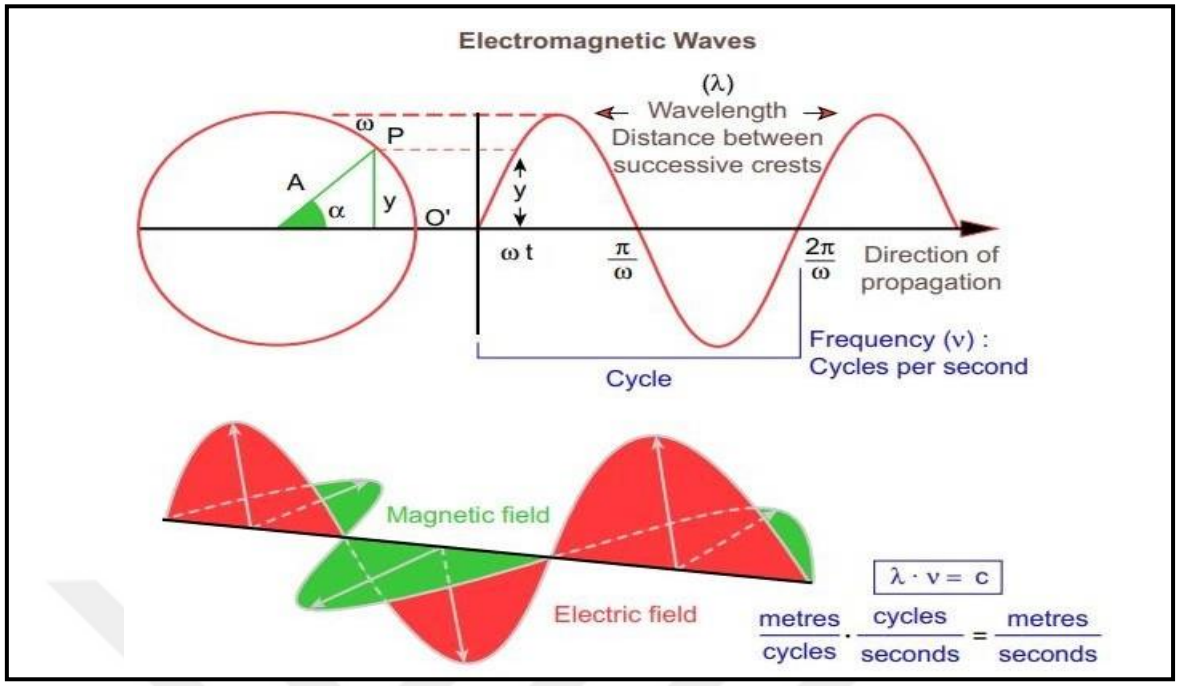

Figure 2.8: Electromagnetic Wave [Emery & Camps, 2017: 45].

The frequency (ν) is the total number of waves produced each second, while the wavelength (λ) is the distance between the crests of the two waves, and the period (T) is the amount of time it takes to cross the wavelength.

$$\lambda = cT \tag{2.1}$$

$$T = 1/\nu \tag{2.2}$$

$$c = \lambda \, . \, \nu \tag{2.3}$$

The speed of light ($c = 3\text{x}108$ ms^{-1})—the result of frequency and wavelength—is the constant velocity of EM waves in a vacuum.

By means of the Bohr equation, the energy (E) of the electromagnetic wave can be calculated.

$$\Delta E = h\,\nu \tag{2.4}$$

In this equation, h gives the Planck constant ($6{,}6\text{x}10^{-34}$ Js^{-1}).

The wavenumber (cm^{-1}) is the adverse of the wavelength, in infrared (IR) spectroscopy. It is expressed as:

$$\bar{\nu} = 1/\lambda \qquad (2.5)$$

When this equation is combined with the Bohr equation, the equation $E = h\nu = hc\,\bar{\nu}$ is obtained.

It is seen that the frequency and number of waves are straight commensurate to the energy (Stuart, 2004: 4).

As a result of the interaction of a substance and electromagnetic radiation, data known as spectrum is produced. The spectrum includes a band with properties of band position, bandwidth, and band density/area. These bands, with their uniqueness, provide an understanding of the molecular structure (Mollaoglu Dogan, Ozyurt, & Severcan, 2018: 1). The properties of the various spectral regions are shown in figure 9 (Andrews, 2017: 429).

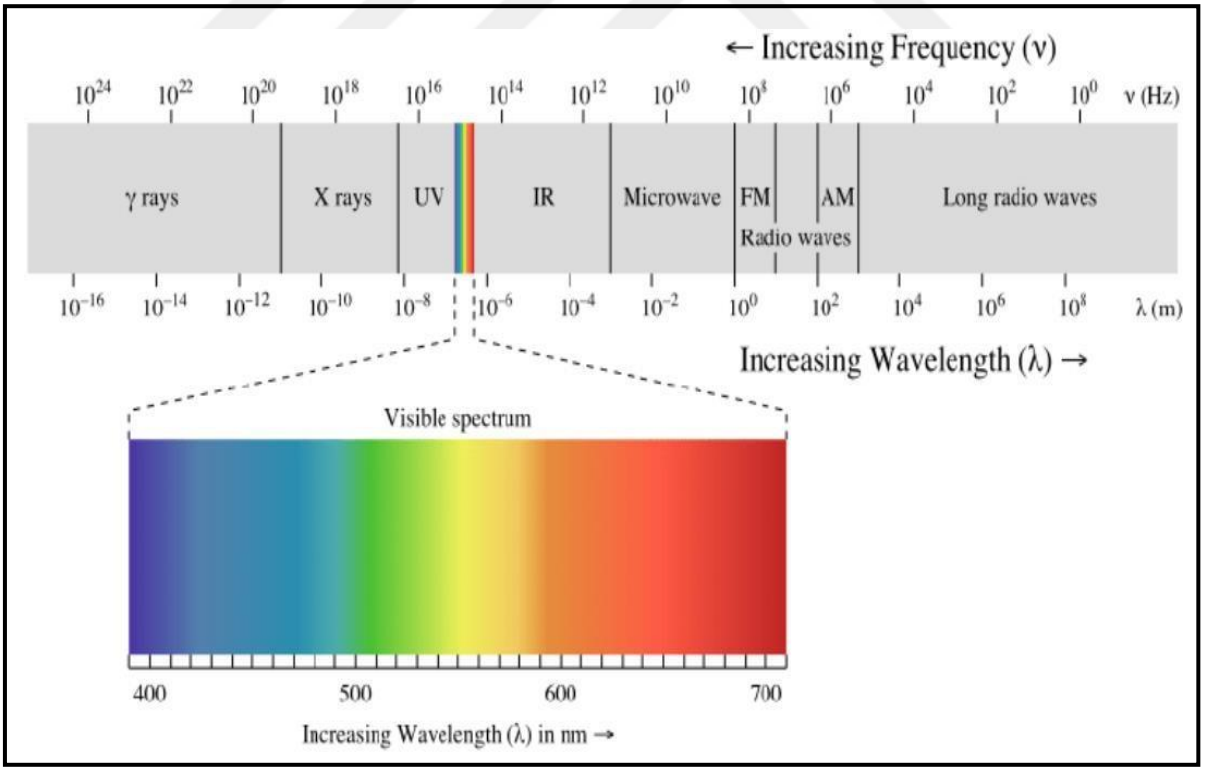

Figure 2.9: Regions of the Electromagnetic Spectrum [Stief, 2014: 326].

The spectrum is the graph of the energy density. Between the energy levels of atoms or molecules, radiation is diverted. In other words, a molecule is energized to a higher level (Freifelder, 1982: 14; Garip, 2012: 29). An energy level diagram in Figure 2.3.3 shows the earliest excited states of the ground and energy levels. The lowest of the energy states is the ground state. As higher energy states are ascended, this is called the excited state. The term spectrum refers to the dispersion of all photon energy over the observable frequency gap. The spectrum is obtained by plotting this distribution as a function of either wavelength or frequency (Emery & Camps, 2017: 46).

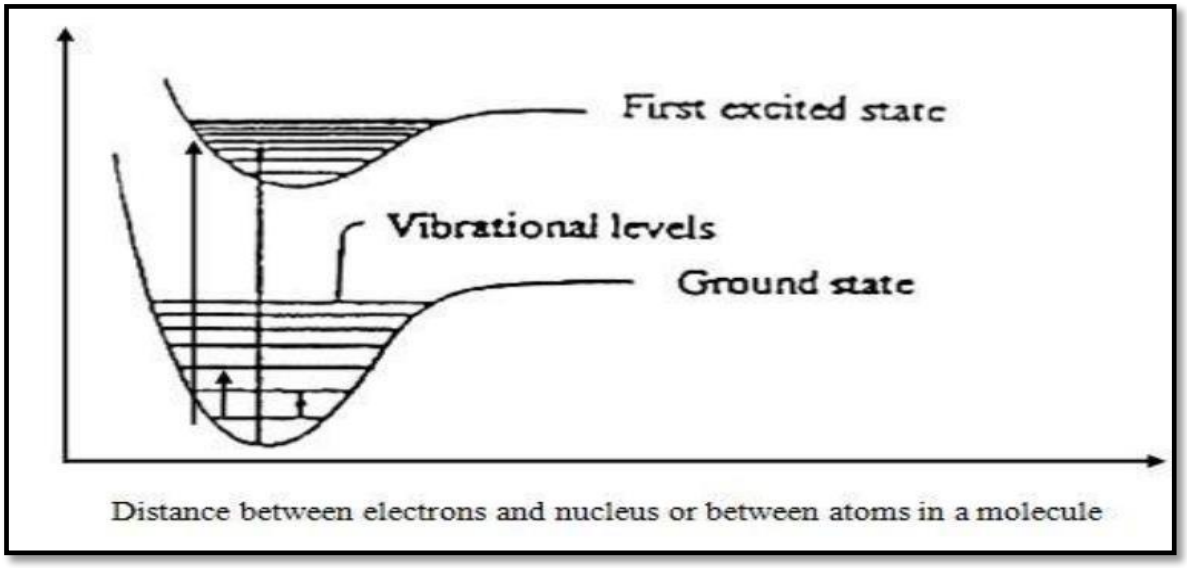

Figure 2.10: An Energy Diagram [Gurbanov, 2010: 33].

When a molecule interacts with electromagnetic radiation (light), the result emerges in three different ways; scattering, absorption, and emission are shown in Figure 2.3.4 (Campbell, & Dwek, 1984: 18).

If the propagation direction shifts, scattering will happen.

Energy is transferred to the molecule during absorption.

Emission happens if the molecule emits energy (Aydogan, 2019: 23).

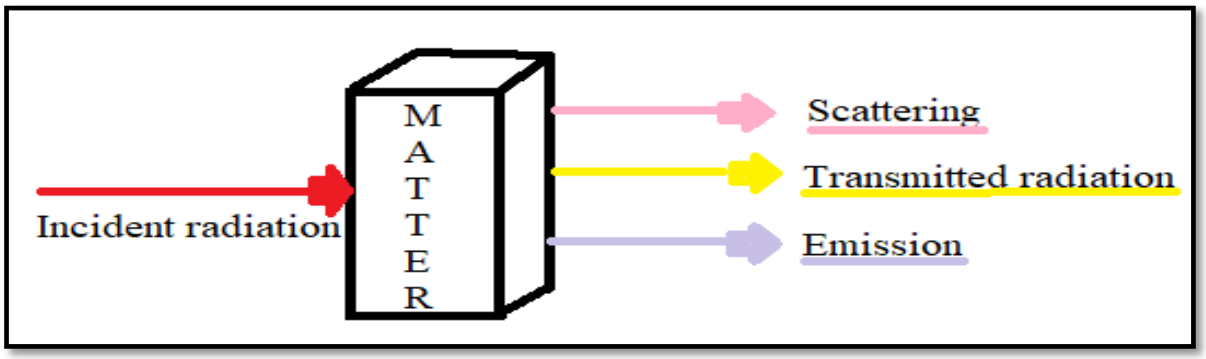

Figure 2.11: When a Sample Interacts with Electromagnetic Radiation, It Results in Absorption, Scattering, or Emission [Campbell, & Dwek, 1984: 18].

In quantum mechanics, an excited molecule is excited by absorbing a discrete amount of energy. This amount of energy (quanta) that the molecule will absorb; is equivalent to the energy distinction among the ground state and the excited state (Mousa Abbas, 2016: 7).

The fundamental molecular energy levels are electronic transition, vibrational, Rotational, and transitional (Campbell, & Dwek, 1984: 16).

The equation: describes the total energy. Total = Rotation + Vibration + Electronic + Transition + Nuclear spin orientation+ Electron spin orientation (Campbell, & Dwek, 1984: 15). (2.6)

2.3.2 Vibrational Spectroscopy

The infrared zone of the electromagnetic spectrum provides knowledge of molecular vibrations (wavelength 100µm - 1µm). The spectroscopic technique attributed to this region is vibrational spectroscopy (Hashimoto, 2018: 1). Vibrational spectroscopy contains Infrared (IR), Raman, and Tera Hertz (THz) spectroscopy as seen in figure 2.3.5 (Mollaoglu Dogan et al., 2018: 2).

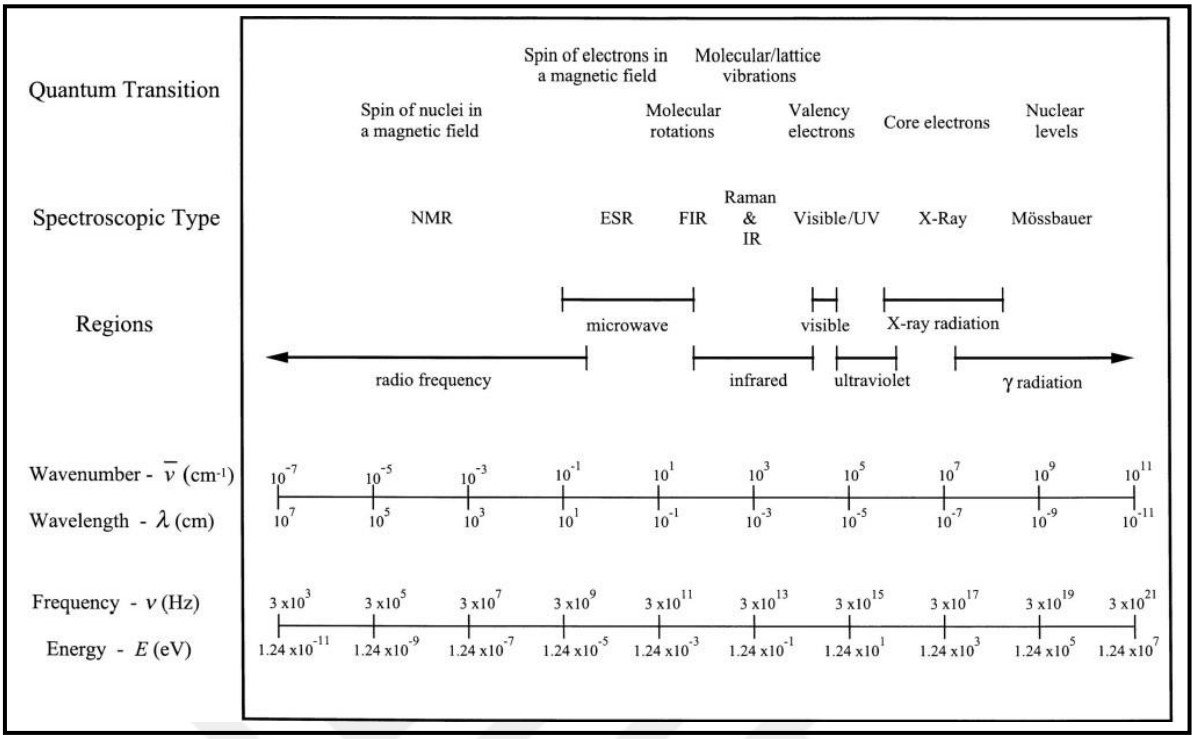

Figure 2.12: Spectrum Types, Wavenumbers, Wavelengths, Frequencies, and Energies in the Spectrum are Shown, Along with Different Regions of the Electromagnetic Spectrum and the Quantum Transitions Attributed to Each Region [Geiger, 2004: 8].

In vibration spectroscopy, the molecular vibration due to the absorption of light is measured (El-Azazy, 2018: 2).

Molecular vibration is divided into two main categories:

a. Stretching; Distance between two atoms. Stretching vibrations can be symmetrical or anti-symmetrical.
b. Bending vibrations; Slope among two bonds. Bending vibrations are of four categories; scissoring, rocking, wagging, and twisting (El-Azazy, 2018: 2). The schematic representation of molecular vibrations can be found in figure.

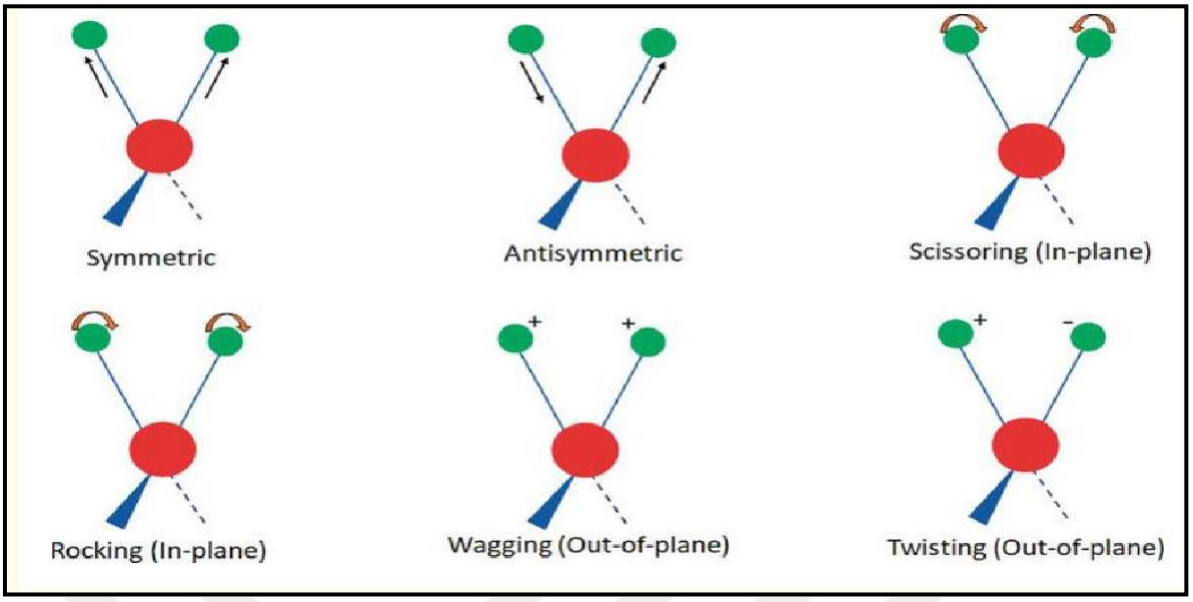

Figure 2.13: The Schematic Representation of Molecular Vibrations [El-Azazy, 2018: 3].

In biological systems, differences in the concentration, structure, and functions of biomolecules occur due to genetic modifications, and metabolic or environmental factors. To monitor these differences, vibrational spectroscopy detects differences in spectral bands by obtaining in quality and quantitative knowledge about the positions, width, and density of the spectral bands (Kucuk Baloglu & Severcan, 2018: 12).

2.3.3 Infrared Spectroscopy

Based on the vibrations of a molecule's atoms, infrared spectroscopy studies the transition between vibrational energy levels (Haris, & Severcan, 1999: 208). The electromagnetic spectrum range between 0.78-1000 μm is defined by the term infrared (Bozkurt, 2006: 19). In a molecule that absorbs infrared light, a vibrating electric dipole moment must shift (Kocak, 2007: 34). The Beer-Lambert law states that the band strengths of infrared spectroscopic analysis absorption spectra are straight commensurate to the concentrations of the relevant molecules' functional groups (Gurbanov, Bilgin, & Severcan, 2016: 849). Infrared spectroscopy, which is an important analytical technique, provides the opportunity to study many sample types such as films, liquids, solutions, fibres, pastes, surfaces, powders, and gases (Mollaoglu Dogan et al., 2018: 3; Stuart, 2004: 1). The molecular makeup of each sample is revealed by IR spectroscopy, which analyzes by absorbing infrared radiation by functional groups as N-H or C-H, and C=O or P=O (for example,

functional groups of tissue or biofluid components like nucleic acids, proteins, or carbohydrates in biological samples) (Dogan, Lasch, Neuschl, Millrose, Alberts, Schughart, Naumann, & Brockmann, 2013: 2; Severcan, Bozkurt, Gurbanov, & Gorgulu, 2010: 622). It can act a significant role in the structural characterization of molecules and is of great importance technique for comprehending the structure of biomolecules. The three primary sections of the infrared spectrum, far, middle, and near, are in the range of 400-4 cm^{-1}, 4000-400 cm^{-1}, and 14000-4000 cm^{-1}, respectively (Kucuk Baloglu & Severcan, 2018: 12; Bozkurt, 2006: 19).

In this thesis investigation, the mid-infrared wavelength section of 4000-650 cm^{-1} is used.

2.3.4 Fourier Transform Infrared (FTIR) Spectroscopy

The Michelson Interferometer principle serves as the foundation for Fourier Transform Infrared (FTIR) spectrometry (Stuart, 2006: 1). In Figure 2.3.7, the fundamental pieces of an FTIR spectrometer are schematically depicted. The progress of IR spectroscopy has been aided by the incorporation of the Fourier-transform method into spectrometers. As a result, the IR spectra are of higher quality and the data collection process is quicker (Mollaoglu Dogan et al., 2018: 3). An interferogram is a signal created as a result of the route length differences between two beams. In order to create an interferogram, FTIR spectroscopy relies on the concept of radiation interference between two beams (Stuart, 2006: 1). Infrared radiation exits the source and travels through an interferometer to the sample. An interferometer measures the wavelength of light using the radiation interference between two beams. A beam splitter also produces the interferogram. The interferogram is created by the interference recombination of two beams with differing travel lengths in the beam splitter. When IR radiation is supplied, some of it is absorbed while the remainder travels to the detector, where it is measured as the total interferogram from all IR wavelengths. The Fourier transform is a mathematical procedure that transforms the interferogram's intensity against time spectrum into the IR spectrum's intensity versus frequency spectrum (Kepenek, 2017: 13).

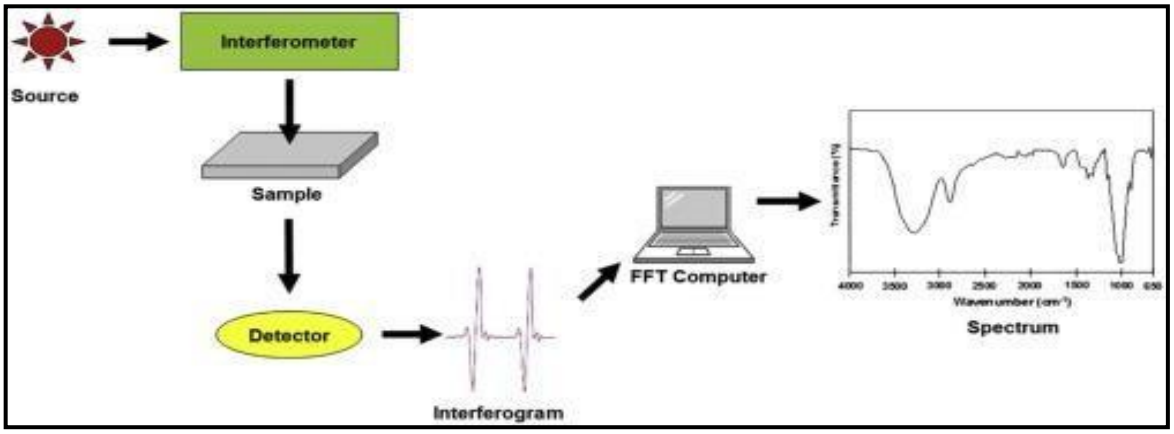

Figure 2.14: The Fundamental Components of an FTIR Spectrometer [Undavalli, Ling, & Khandelwal, 2021].

Qualitative and quantitative information about functional groups is obtained by using the FTIR technique in biological systems, and vibration energy levels of functional groups are taken as a basis for this technique. A system-specific spectrum is obtained in which the band of each functional group may be viewed at the same time (Sahin, Bilge, Kazancı, & Severcan, 2013: 9). The bands in the obtained spectrum; Field changes, changes in bandwidth, and shifts in peak positions provide functional and structural information about the studied sample (Simsek Ozek, Sara, Onur, &Severcan, 2010: 42; Cakmak, Togan, & Severcan, 2006: 55). In the 1980s, FTIR spectroscopy was widely used in biological systems thanks to the advent of sophisticated interferometry and multivariate statistical methods, and it is still used today all over the world (Kepenek, 2017: 8).

2.3.5 Attenuated Total Reflectance Fourier Transform Infrared (ATR-FTIR) Spectroscopy

Transflection, Transmission, and Attenuated Total Reflection (ATR) are the three primary sampling techniques used in FTIR spectroscopy. The Transflecion mode relies on the detection of IR radiation's absorption after it has passed through the sample, been reflected off the substrate, and been retransmitted from the matter. A drawback of this method is the thickness of the sample. Because of the sample and substrate (such as calcium fluoride) before radiation is detected, the transmission mode transmits IR radiation. In transmission mode, high-quality spectra can be acquired, however there is a sample preparation stage. This process takes time. Furthermore, pricey IR transparent substrates are employed. Total

internal reflection is phenomena that is used in ATR spectroscopy (De Bruyne, Speeckaert, & Delanghe, 2017: 3). The angle of incidence at the matter and crystal surfaces must be larger than the crucial angle when a radiation beam penetrates a crystal in order for the incident radiation to undergo total internal reflection (Mollaoglu Dogan et al., 2018: 5). Beyond the crystal and surrounding medium, internal reflection produces a standing wave that vanishes or is near-field in nature. The absorption qualities can be seen as the disappearing wave weakens when the samples are created directly in the ATR crystal. The disappearing wave loses energy at the same frequencies as the absorbance of the sample (Minnes, Nissinmann, Maizels, Gerlitz, Katzir, & Raichlin, 2017: 2). The penetration depth of radiation depends on some factors, these are; crystal material, angle of incidence, wavelength, refractive index of the sample. Only a slim matter layer close to the ATR crystal is shown by the ATR spectrum (Dogan et al., 2013: 2). ATR cells utilize crystals done materials like diamond, ZnSe, Ge, Si, and thallium/iodide. The low water solubility and high refractive index of these materials allow them to be used as ATR crystals. ATR mode allows the measurement of aqueous samples such as blood, serum, or solid samples such as fully hydrated tissue samples. Unlike the conduction and transflexion modes, ATR requires little preparation in some samples and none in some samples, and the thickness of the sample is negligible. Potential molecular interactions between the sample and the crystal surface could cause issues with the ATR technique (Mollaoglu Dogan et al., 2018: 5; Dogan et al., 2013: 2).

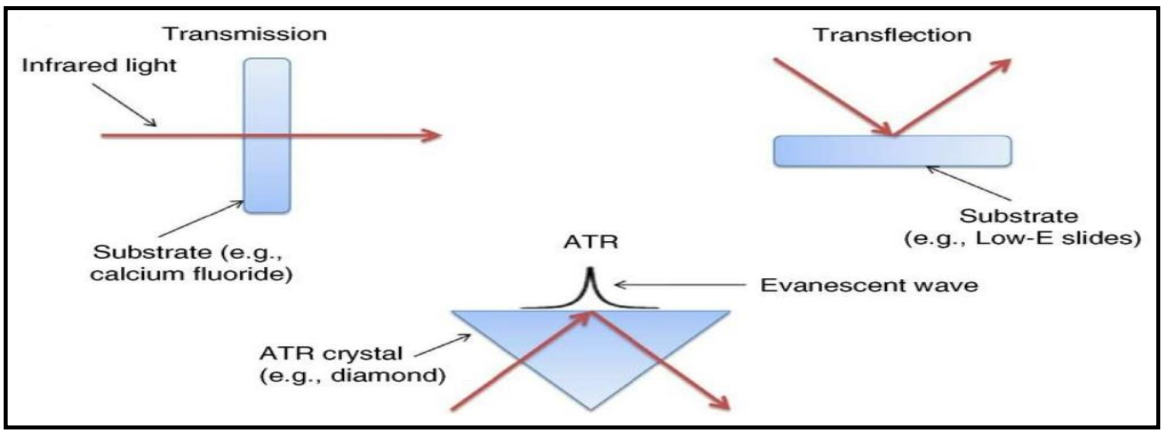

Figure 2.15: The Three Major Sampling Modes for FTIR Spectroscopy [Baker, Trevisan, Bassan, Bhargava, Butler, Dorling, Fielden, Fogarty, Fullwood, Heys, Hughes, Lasch, Martin-Hirsch, Obinaju, Sockalingum, Sulé-Suso, Strong, Walsh, Wood, Gardner, & Martin, 2014: 1772].

2.3.5.1 Advantages of FTIR and ATR-FTIR spectroscopy

a. One drop of serum, for example, can be used as a little quantity of sample for analysis using FTIR spectroscopy (Dogan et al., 2021: 557).
b. FTIR spectroscopy works with high sensitivity and detects differences without the use of external agents (Garip, Cetin Gözen, & Severcan, 2009: 1301; Severcan et al., 2010: 622).
c. The speed of the FTIR spectroscopy method is one of its most significant benefits. It is very useful because it does not require preliminary preparation for sample preparation and the time to learn about the spectral parameters is short (Gurbanov, & Tuncer, 2021: 24).
d. This tecnique is a practical, reproducible, easy-to-apply, operator-independent, and cost-effective technique (Gurbanov, & Tuncer, 2021: 24; Dogan et al., 2021: 550)
e. Considering all of the ESR, X-ray diffraction, NMR, and CD spectroscopy techniques, the FTIR technique is more cost-effective (Haris, & Severcan, 1999: 208).
f. From field values of bands, changes in peak position, and changes in bandwidth, we can learn important structural and functional information about biological materials (Simsek Ozek et al., 2010: 42).

Since IR spectroscopy has many advantages as listed above, it is used in the diagnosis of diabetes (Severcan et al., 2010), cancer (Abbas, Simsek Ozek, Emri, Koksal, Severcan, & Severcan, 2018), neurological (Yonar, Ocek, Tiftikcioglu, Zorlu, & Severcan, 2018), infectious diseases (Barauna, 2021), determination of the effects of drugs and vaccines (Dogan et al., 2021), membrane studies (Ezer, Sahin, Kazancı, 2017) protein structure characterization studies (Haris & Severcan, 1999), biomedical applications of body fluids (Lasch, Beekes, Schmitt, & Naumann, 2007), molecular characterization of bacteria (Kepenek, Gözen, & Severcan, 2018), comparison of bacteria or strains (Garip et al., 2009) and cell line classification and discrimination (Ozek, Tuna, Erson-Bensan, & Severcan, 2010).

Tissue sections, bacterial isolates, and biofluids such as saliva, urine, cerebrospinal fluid, serum, and plasma can be used in these studies (Bozkurt, Bilgin, Severcan, 2007; Garip et al., 2009; Barboza da Silva, Vincente de Carvalho, Schneider, & Corbellini, 2022; Gok et al., 2016; Yonar et al., 2018; Dogan et al., 2021; Elkadi, Hassan, Elanany, Byrne, &

Ramadan, 2021). In addition, the fact that these biosamples are easily available and informative, coupled with the fact that the IR technique requires a fast and small amount of samples, makes IR spectroscopy an ideal technology for the early detection of diseases.

In this thesis, the impact of pyridostigmine in myasthenia gravis disease was investigated via infrared spectroscopy in human blood serum samples.

The advantages of ATR-FTIR mode:

a. In addition to the small amount of sample sufficient, the sample is analyzed by placing it directly on the crystal.
b. Spectral data is obtained in a short time without noise (Garip Ustaoglu, Kaygusuz, Bilgin, & Severcan, 2021: 361).

2.3.5.2 Analysis of serum samples in infrared spectroscopy

Body fluids are highly informative due to their contents. For instance, urine, saliva, and serum. They are also easily obtainable. Thanks to these advantages, they can be used especially in the diagnosis of diseases and in determining their therapeutic effects such as drugs/vaccine (Dogan et al., 2021: 550). The levels of proteins in the serum vary when conditions such as illness occur and are directly related (De, Rana, Akpinar, Miranda, Arvizo, Bunz, & Rotello, 2009: 461). Thanks to the changes in the chemical composition of the serum in pathological conditions such as disease, it can be used as a clinical material in the diagnosis of disease (Psychogios, Hau, Peng, Guo, Mandal, Bouatra, Sinelnikov, Krishnamurthy, Eisner, Gautam, Young, Xi, Knox, Dong, Huang, Hollander, Pedersen, Smith, Bamforth, Greiner, McManus, Newman, Goodfriend, & Wishart, 2011: 2). Containing more than 300 types of protein, in addition, to amino acids, carbohydrates, and lipids, the serum also contains up to 114,000 metabolites in different concentrations (Byrne, Bonnier, Mclntyre, & Parachalil, 2020: 1). Using tissues and biological fluids, FTIR spectroscopy provides rapid, label-free diagnostic and therapeutic monitoring that requires small samples. Biofluids, especially serum, were analyzed with the FTIR technique, enabling the detection of many different diseases. Spectral biomarkers were determined by spectroscopic analysis and became the ideal diagnostic tool (Baker, Hussain, Lovergne, Untereiner, Hughes, Lukaszewski, Thiéfin, & Sockalingum, 2016: 1803). Malignant pleural mesothelioma is a disease associated with other advanced respiratory disorders. Limitations

in its differentiation from other diseases cause late diagnosis of the disease. By using serum samples, it was differentiated from lung cancer and benign exudative effusions with FTIR technique and presented as a new approach for diagnosis (Yonar, Severcan, Gurbanov, Sandal, Yilmaz, Emri, & Severcan, 2022). Atherosclerosis, which has a high mortality rate, is suitable for diagnosis by infrared spectroscopy from serum samples. It has been reported that fingerprints specific to atherosclerosis patients have been determined (Peters, Backhaus, Pfützner, Raster, Burgard, Demirel, Böckler, & Hakimi, 2017: 20). Glioma can only be detected at an advanced stage because it does not have specificity in clinical findings. Analysis of serum samples with infrared spectroscopy for early and rapid diagnosis has yielded an efficient result (Chen, Meng, Qu, Cheng, Chen, Yang, Gao, & Lv, 2021: 2). It is possible to detect breast cancer, which is especially widespread in women, from serum samples by infrared spectroscopy method (Backhaus, Mueller, Formanski, Szlama, Meerpohl, Eidt, & Bugert, 2010: 173). *Paracoccidioidomycosis* is an infection caused by a genus of fungi. Diagnostic methods such as microscopic examination are limited. In the diagnosis of paracoccidioidomycosis, the fingerprints specific to the disease detected in the infrared spectrum by analyzing the serum sample have proven that infrared spectroscopy can be used in the diagnosis of infectious with serum samples (Koehler, Scroferneker, Pereira, Preira de Souza, Cavalcante, Mendes, & Corbellini, 2022).

In addition, in this thesis study, the effect of pyridostigmine treatment in myasthenia gravis disease was investigated using the FTIR technique from serum samples. The FTIR technique has been shown to be an ideal method for the therapeutic monitoring of serum samples.

3. MATERIAL AND METHODS

3.1 PATIENTS AND SAMPLES COLLECTION

The experimental protocol of this study was approved by the ethics committee of Istanbul Bezmialem Vakıf University (Approval no: 15.10.2018-6032). Throughout the study, each participant's informed consent was obtained. Each patient had their fasting blood drawn into an EDTA-free blood collection tube (red-top tube), which was then transported in less than five minutes to the lab. The serum is separated from the cellular component by centrifugation at 3000 rpm for 15 minutes. Afterwards, serum samples were aliquoted as 0.5 ml and 200 µL into cryogenic tubes and stored at -85 °C until used in spectroscopy experiments (Gajjar, Trevisan, Owens, Keating, Wood, Stringfellow, Martin-Hirsch & Martin, 2013: 3920).

Control and patient blood samples were obtained in cooperation with Izmir Bakırcay University and Bezmialem Vakıf University laboratories.

Group 1: A control group of age- and sex-matched healthy individuals

Group 2: A Patient group not using pyridostigmine or any medication: MG

Group 3: A Patient group using pyridostigmine medication: MG+M

Table 3.1: Demographic Data of Healthy Individuals and Patients.

	Healthy Individuals (C)	**MG**	**MG+M**
n	42	24	15
Sex [n (%)]			
Male	15 (46.33)	9 (53.77)	9 (60.88)
Female	27 (39.88)	15 (44.80)	6 (52.16)
Age Average	42.19	48.16	57.40

Clinical information and blood test results of MG+M and MG are given in table 3.2 and table 3.3. According to the results of biochemistry, it is indicated by N if it is in the normal

Table 3.2: Clinical Information of MG Patients.

ID	Age	Sex	MG Type	Anti-AchR Ab	Anti-MuSK Ab	Iron	Ferritin	HDL	LDL	CRP
A.T	24	Female	Ocular	(-)	(-)	-	-	-	-	-
B.Y	47	Male	Ocular	(-)	(-)	N	N	H	H	-
E.T	46	Male	Ocular	(-)	(-)	N	N	N	H	-
H.G	59	Female	Ocular	(-)	(-)	-	-	-	-	-
K.C	25	Female	Ocular	(-)	(-)	L	N	N	H	N
N.S	64	Male	Ocular	(-)	(-)	N	N	L	H	-
S.A.S	39	Male	Ocular	(-)	(-)	-	-	-	-	-
V.A	56	Female	Ocular	(-)	(-)	N	N	N	N	N
F.B	18	Male	Generalized	(-)	(-)	N	N	N	N	N
F.E	58	Female	Generalized	(-)	(-)	N	N	N	H	-
H.S	67	Male	Generalized	(-)	(-)	N	N	L	H	-
M.S	73	Male	Generalized	(-)	(-)	N	N	N	N	-
S.T	49	Female	Generalized	(-)	(-)	N	N	N	H	-
Y.A	65	Male	Generalized	(-)	(-)	N	N	N	H	-
Y.B	21	Female	Generalized	(-)	(-)	N	N	N	N	-
F.E.L	58	Female	Ocular	(+)	(-)	-	-	-	-	-
C.K	73	Female	Generalized	(+)	(-)	L	N	N	N	N
E.G	28	Female	Generalized	(+)	(-)	L	N	N	N	-
F.O	44	Female	Generalized	(+)	(-)	N	N	N	N	-
H.A	59	Female	Generalized	(+)	(-)	N	N	N	H	-
H.Y	65	Male	Generalized	(+)	(-)	N	N	L	N	-
O.Y	37	Female	Generalized	(+)	(-)	N	L	H	H	-
Y.M	35	Female	Generalized	(+)	(-)	L	L	N	N	N
N.G	46	Female	Ocular	(+)	(+)	N	N	N	N	N

Table 3.3: Clinical Information of Patients Using Pyridostigmine (MG+M).

ID	Age	Sex	MG Type	Anti-AchR Ab	Anti-MuSK Ab	Iron	Ferritin	HDL	LDL	CRP
A.C	50	Male	Ocular	(-)	(-)	N	N	N	H	N
H.I.S	72	Male	Ocular	(-)	(-)	-	-	-	-	-
H.E	56	Female	Ocular	(-)	(-)	N	N	N	H	N
M.Z.K	59	Male	Ocular	(-)	(-)	N	N	L	H	N
O.K.A	59	Male	Ocular	(-)	(-)	N	N	N	N	N
V.A	56	Female	Ocular	(-)	(-)	N	N	N	H	N
E.A	41	Female	Generalized	(-)	(-)	N	N	N	H	N
M.B	58	Male	Generalized	(-)	(-)	N	N	L	N	-
S.S	81	Female	Ocular	(-)	(+)	L	L	N	H	N
F.F.T.T	19	Female	Ocular	(+)	(-)	L	N	N	N	N
G.A	60	Female	Generalized	(+)	(-)	N	N	N	H	-
I.Y	77	Male	Generalized	(+)	(-)	-	-	-	-	-
S.H	29	Male	Generalized	(+)	(-)	N	N	H	N	-
M.O	78	Male	Generalized	(+)	(+)	N	N	N	N	-
S.E	66	Male	Generalized	(+)	(+)	-	-	-	-	-

3.2 ATR-FTIR SPECTROSCOPY EXPERIMENT

3.2.1 Spectral Data Collection

Prior to spectroscopic analysis, frozen serum samples were thawed and mixed at room temperature.

The spectra were collected by Perkin Elmer-Frontier FTIR spectrometer and Miracle, PIKE Zn/Se crystalline ATR unit at Bilecik Şeyh Edebali University. 1 µL of serum sample was placed on the crystal plate and dried under very light nitrogen gas for 2 minutes to remove excess free water. Spectra were collected in the region of 4000-650 cm^{-1} at a resolution of 4 cm^{-1} and 32 scan. To avoid the influence of molecules in the air, before obtaining the sample spectra, the background spectrum of the air was first recorded under the same conditions as the samples and automatically subtracted from all spectra. Spectrum one and OPUS Spectrum software version 8.5.29 were used to record spectra.

3.2.2 Spectral Analysis

Three random aliquodes from each sample were scanned three and four times. Detailed spectral analyzes were applied to the average spectra of the replicates to detect macromolecular content and structural changes.

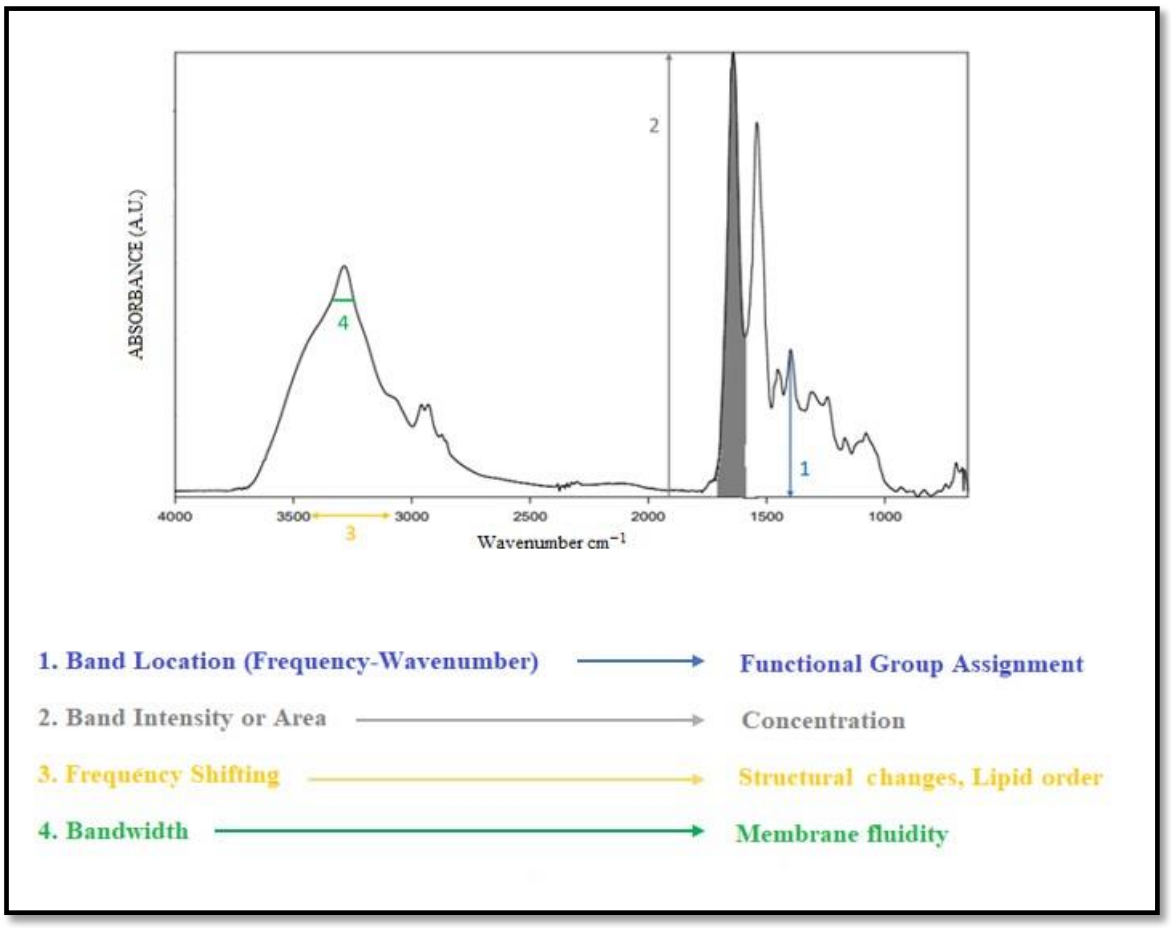

Figure 3.1: Spectral Parameters.

The above figure 3.1 shows the spectral parameters of an infrared spectrum. Functional groups can be appointed according to the position of the peaks. The shifts in band frequency values provide knowledge about the structural changes of the molecules involved, while the increase or decrease in the band areas/intensity provides concentration information. Additionally, data on the fluidity of the membrane can be gleaned by analyzing the bandwidth of the lipid bands. The spectra's various spectral parameters, including band area, bandwidth, and band frequency values, were measured, and thorough analyses were conducted. The average raw spectra underwent baseline correction as a preprocessing step.

Band areas were measured with method enforced as integration method B in the data acquisition software package OPUS from Bruker Optics. After calculating the band areas, the band area ratios were calculated and a detailed spectral analysis was performed. Possible experimental errors were avoided by calculating the band area ratios. Band positions were measured relative to the center of mass of the bandwidth, which corresponds to 75% of the band intensity. This width was also used as the bandwidth for the relative lipid dynamics measurements. Utilizing OPUS Spectrum software version 8.5.29, these changes were determination and their spectrum analyzed.

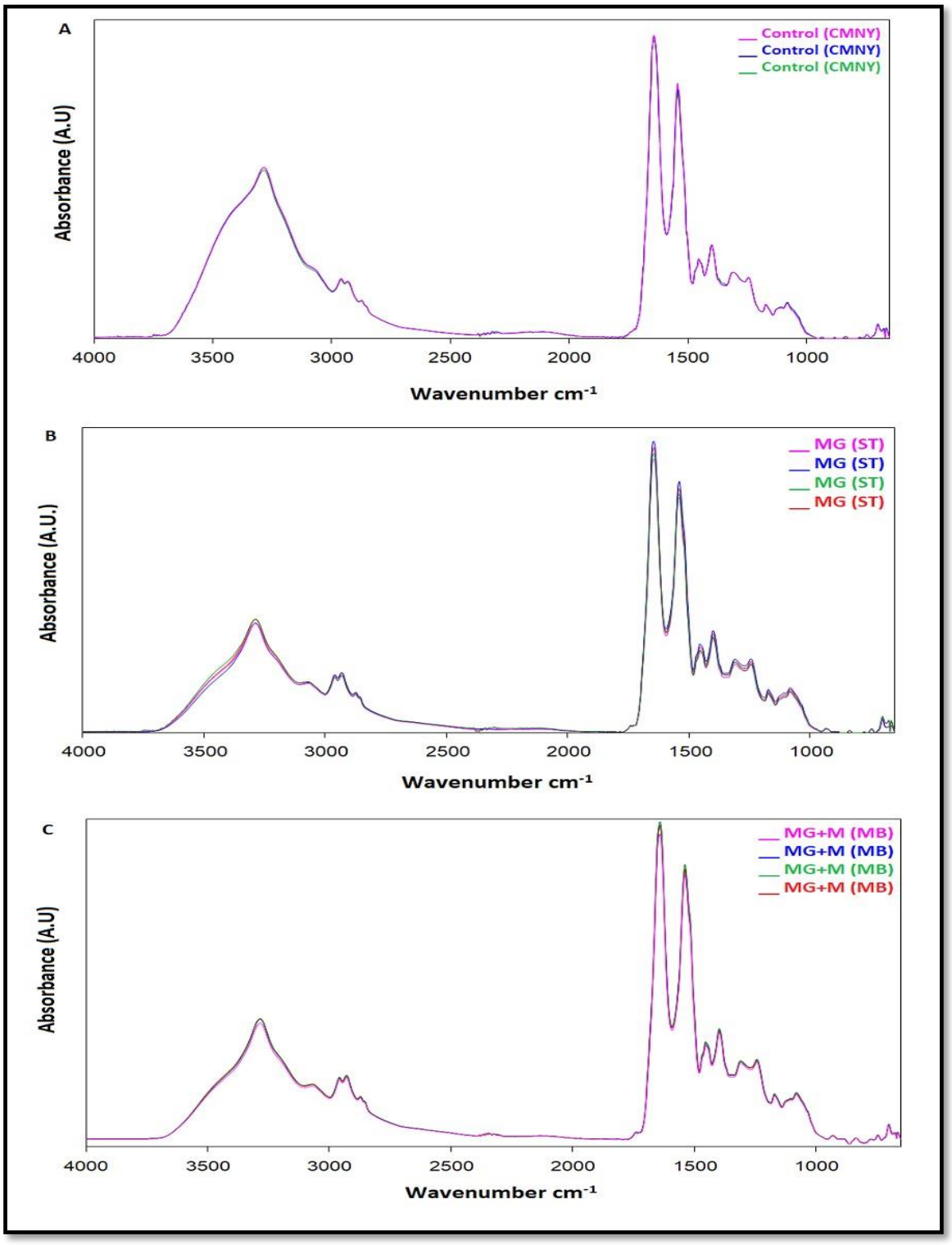

Figure 3.2: a) Whole Region View of 3 Spectra of a Control Sample. b) Whole Region View of 4 Spectra of a Myasthenia Gravis (MG) Patients Sample. c) Whole Region View of 4 Spectra of a Pyridostigmine-user Patients (MG+M).

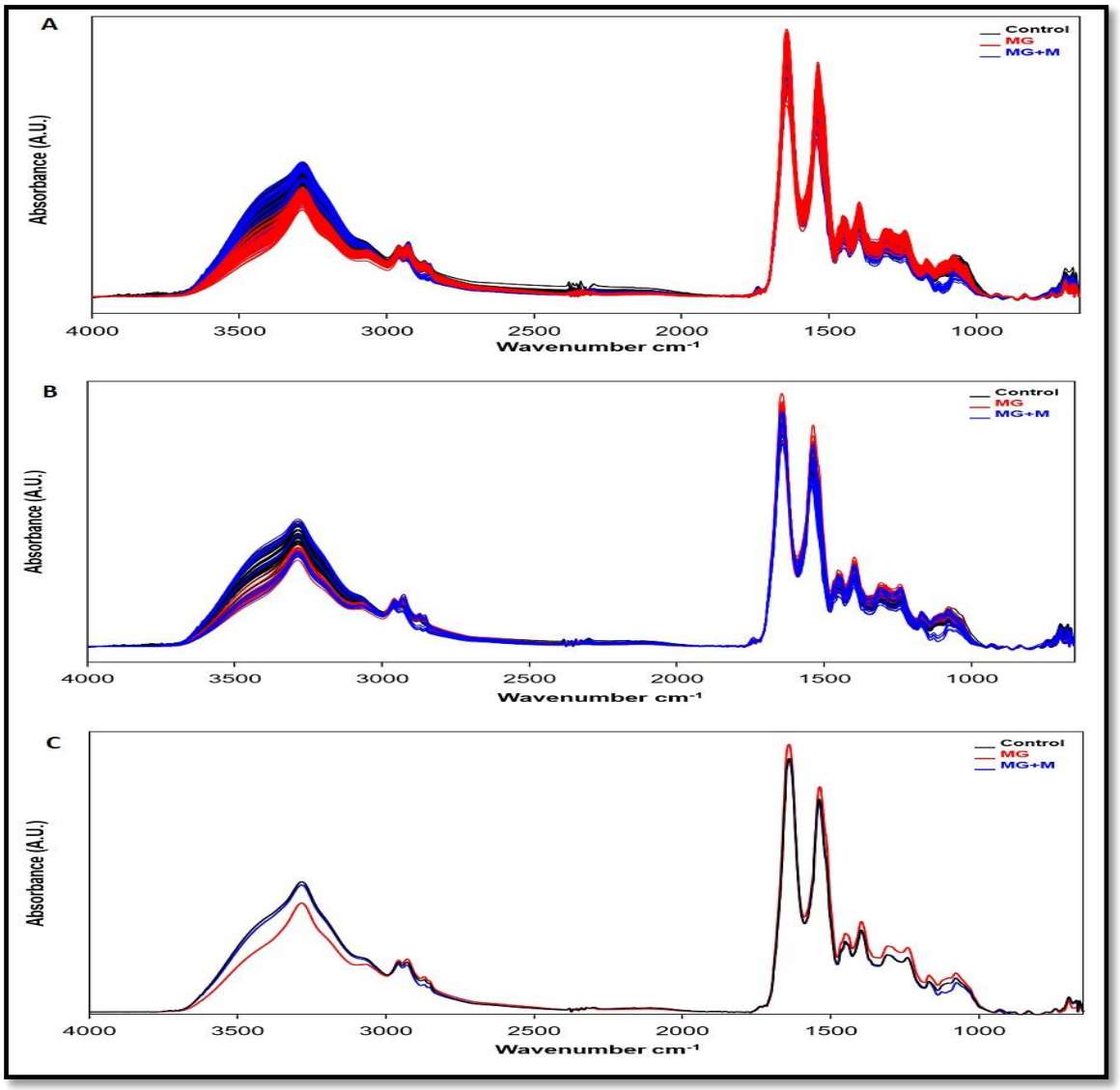

Figure 3.3: a) Whole Region View of 3 and 4-replicated Spectra of MG, MG+M and Control Group. b) Average Spectrum Whole Region View of 3 and 4 Replicate Spectra of MG, MG+M, and Control Group. c) Whole Region View of the Average Spectra of MG, MG+M, and the Control Group.

3.2.3 Statistical Data Analysis

To compare the spectral variations of the control, MG patient, and MG+M patient groups and to determine the significance level, statistical analysis was carried out. The statistical analysis program used was Graphpad Prism 8.0.2. (La Jolla, CA, ABD). The one-way ANOVA statistical test was used to examine group differences (Tamhane T2 post-hoc test with Brown-Forsythe and Welch ANOVA, Dunn post-hoc test with Kruskal Wallis). "Mean ± Standard Error of Mean (SEM)" was used to present the results. P values less than 0.05 were considered significant, and significance was expressed as follows:

*$p \leq 0.05$, **$p \leq 0.01$, ***$p \leq 0.001$, ****$p<0.0001$, ****$p<0.0001$.

+$p \leq 0.05$, ++$p \leq 0.01$, +++$p \leq 0.001$, ++++$p<0.0001$

4. RESULTS

In this thesis study, blood serum samples of 42 healthy controls, 24 Myasthenia gravis patients not using any medication, and 15 Pyridostigmine-user MG patients were compared by using infrared spectroscopy to determine the role of Pyridostigmine therapy in Myasthenia Gravis disorders.

4.1 SPECTRUM OF HUMAN SERUM SAMPLES AND BAND ASSIGNMENT

Figure 4.1 displays the average control spectra in the 4000-650 cm^{-1} range. The average spectra of all the groups were interactive baseline-corrected and normalized to the Amid A band for visual display that is focused at 3284 cm^{-1}. Minimum-maximum normalization was used.

The severe peaks were labelled in the figure whose assignments are given in table 4.1. Band 3, which is not clearly seen in the figure, is shown in the box as enlarged by taking its second derivative.

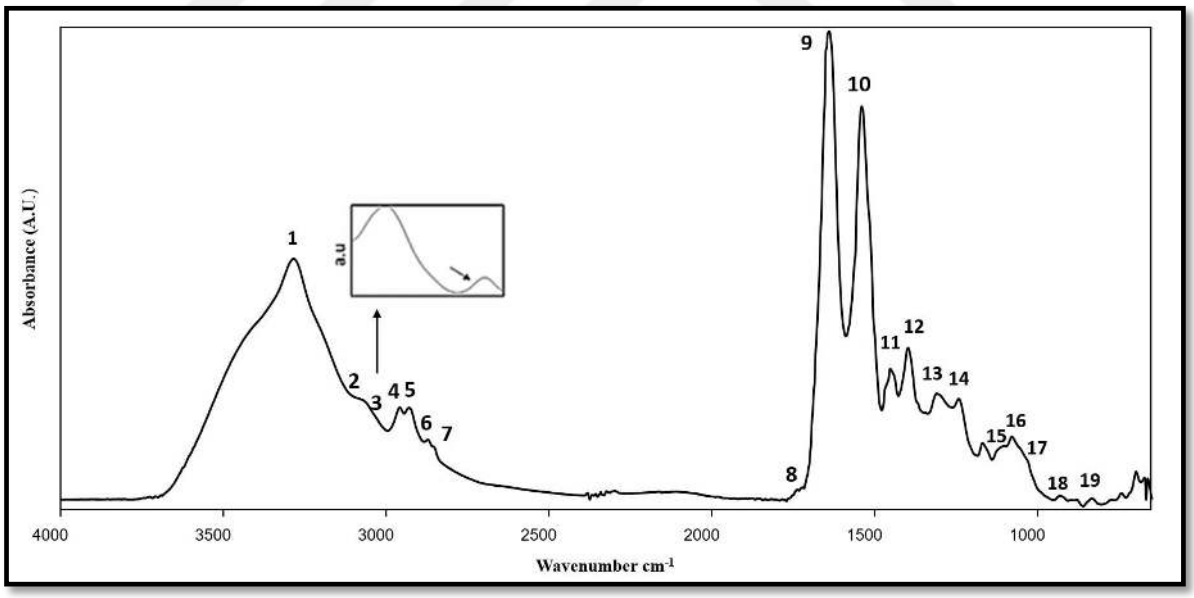

Figure 4.1: The Representative Average Spectrum of a Control Group in the 4000-650 cm^{-1} Region.

Table 4.1: An FTIR Spectrum Band Assignment For a Serum Sample [Dogan et al., 2021: 552; Elibol, Severcan, Jakubowska-Dogru, Dursun, Severcan, 2022; Wood, B. R. 2016].

Band No	Wavenumber (cm^{-1})	Band Assignments
1	**3284**	Amide A (mainly N–H stretching of hydrogen-bonded amide groups of proteins with some contribution from the O–H stretching of polysaccharides and intermolecular hydrogen bonding of proteins and glycogen)
2	**3062**	Amide B band: overtone of Amide I: protein
3	**3008**	Olefinic H–C=C–H stretching vibration: unsaturated lipids
4	**2958**	CH_3 antisymmetric stretching: mainly lipids and proteins with minor contribution from carbohydrates and nucleic acids
5	**2929**	CH_2 antisymmetric stretching: mainly lipids with minor contribution from proteins, carbohydrates, nucleic acids
6	**2872**	CH_3 symmetric stretching: mainly protein, with minor contribution from lipids, carbohydrates, nucleic acids
7	**2854**	CH_2 symmetric stretching: mainly lipids with minor contribution from proteins, carbohydrates, nucleic acids
8	**1738**	Ester C=O stretching: trygliceride, cholesterol esters
9	**1642**	Amide I (proteins, C=O stretching [80%])
10	**1541**	Amide II (proteins, N-H bending [60%] and the C-N stretching [40%])
11	**1454**	CH_2 asymmetric bending: mainly lipids, minor contribution from protein
12	**1398**	COO- symmetric stretching: fatty acids and aminoacids
13	**1310**	Amide III: C–N stretching and N–H bending
14	**1243**	PO_2– asymmetric stretching: mainly nucleic acid with minor contribution of phospholipids
15	**1127**	RNA, υ(C=O) ribose
16	**1080**	PO_2– symmetric stretching: nucleic acids and phospholipids
17	**1030**	C—O stretching: carbohydrates (glycogen, glucose)
18	**932**	Z-form DNA
19	**835**	A-form and B-form helix conformation of DNA

4.2 GENERAL COMPARISON OF THE SPECTRA OF CONTROL, PATIENT, AND MG+M PATIENT GROUPS

The analyses were performed in three distinct regions: the amide A (3600–3100 cm^{-1}), the C–H stretching (3000–2800 cm^{-1}), and the fingerprint (1800–800 cm^{-1}) ranges.

Protein from N-H and O-H stretching, as well as a small amount of polysaccharides, carbohydrates, and bound water, make up the majority of the amide A band. The protein from the N-H vibration makes up the amide B band.

When we compare the patient (MG), pyridostigmine user-patient (MG+M), and control spectra in the 3600-3100 cm^{-1} region, there is little difference between the control and MG+M spectra. The MG+M patient spectrum resembles the control spectrum when compared according to the patient group.

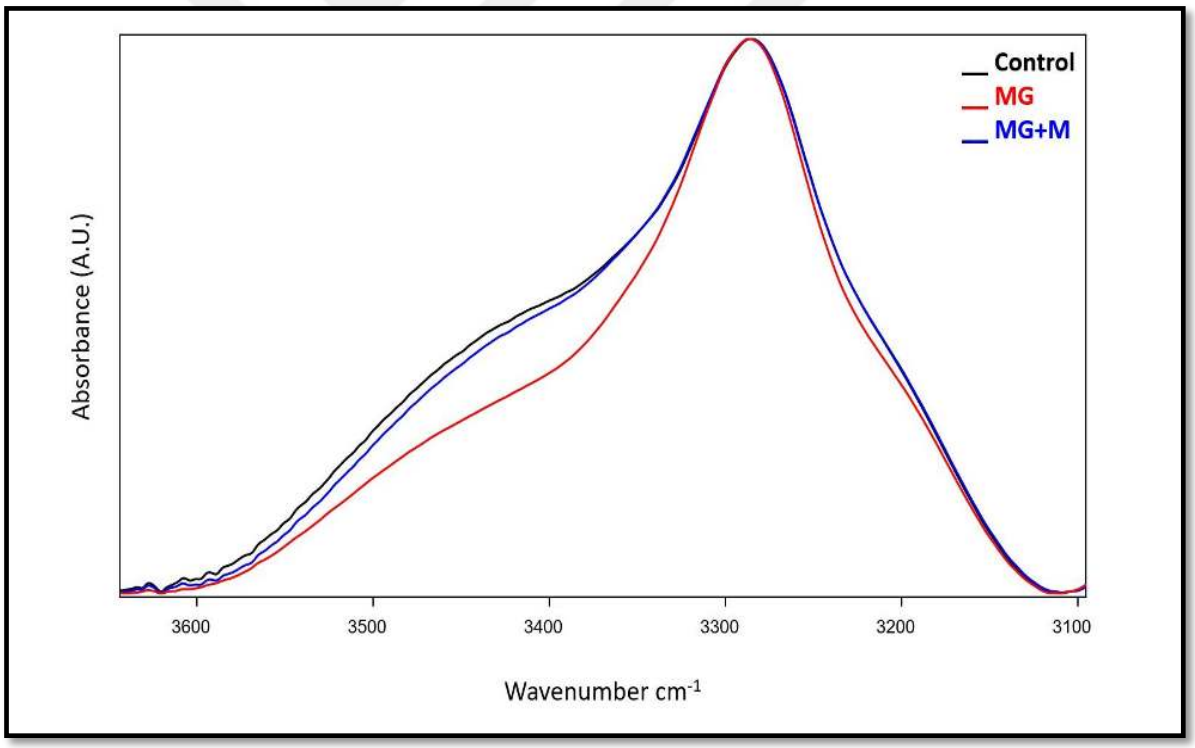

Figure 4.2: The Average Infrared Spectra of the Control, Patient (MG), and Pyridostigmine user-patient (MG+M) in the 3600-3100 cm^{-1}.

The C-H vibration region is shown in Figure 4.3. The C-H vibration region contains; a CH_3 antisymmetric band located at 2958 cm^{-1}, a CH_2 antisymmetric band located at 2929 cm^{-1}, a CH_3 symmetric band located at 2872 cm^{-1}, and CH_2 symmetric band located at 2854 cm^{-1}. In this region, lipid acyl chains give rise to CH_2 symmetric and antisymmetric stretch bands, which monitor saturated lipids in the C-H stretching region. Proteins are responsible for the weak CH_3 symmetric stretch band, while lipids and proteins both contribute equally to the CH_3 antisymmetric band (Dogan et al., 2021: 551). The visual comparison reveals that the 2958 CH_3 and 2929 CH_2 antisymmetric bands in the patient's spectra are more intense or wider than those of the control. Additionally, an increase in the area or intensity of the 2854 CH_2 symmetric and 2872 CH_3 symmetric bands is seen. The MG+M patient spectra resemble the control spectra when compared to the patient group in the 3000–2800 C–H vibration region.

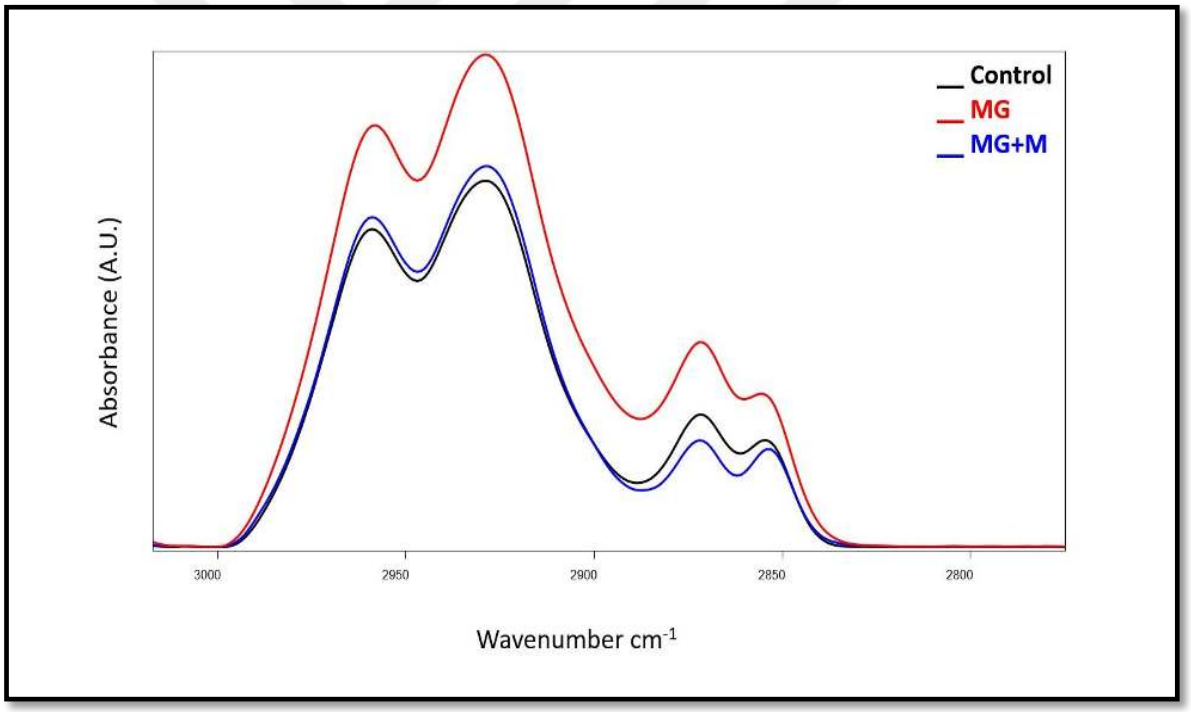

Figure 4.3: Representation of the C-H Vibration Region of the Control, Patient (MG), and Pyridostigmine user-patient Spectra (MG+M).

In figure 4.3, the control spectrum is shown in black, the patient spectrum is in red, and the Pyridostigmine user-patient (MG+M) spectrum is shown in blue. The spectra are shown in the 3000-2800 cm^{-1} frequency range and normalized according to the Amide A band located at 3284 cm^{-1} after baseline correction for a visual demonstration.

There are a number of bands originated from lipids, proteins, carbohydrates, and nucleic acids in the fingerprint region which is located in between 1800 and 800 cm^{-1}. In the current study, the fingerprint region was splited into two sections. Figure 4.4 illustrates the initial section which covers the spectral range of 1800-1500 cm^{-1}. This region contains well known protein bands namely the amide I band, located at 1642 cm^{-1}, and the amide II band, located at 1541 cm^{-1}. Furthermore, the triglyceride/ cholesterol ester band is also located around 1738 cm^{-1} in this region. The C=O stretching vibration of the amide groups is the primary cause of the amide I band. Amid II band originates from the vibrations of Proteins' C-N stretching and N-H is originated (Dogan et al., 2021: 552).

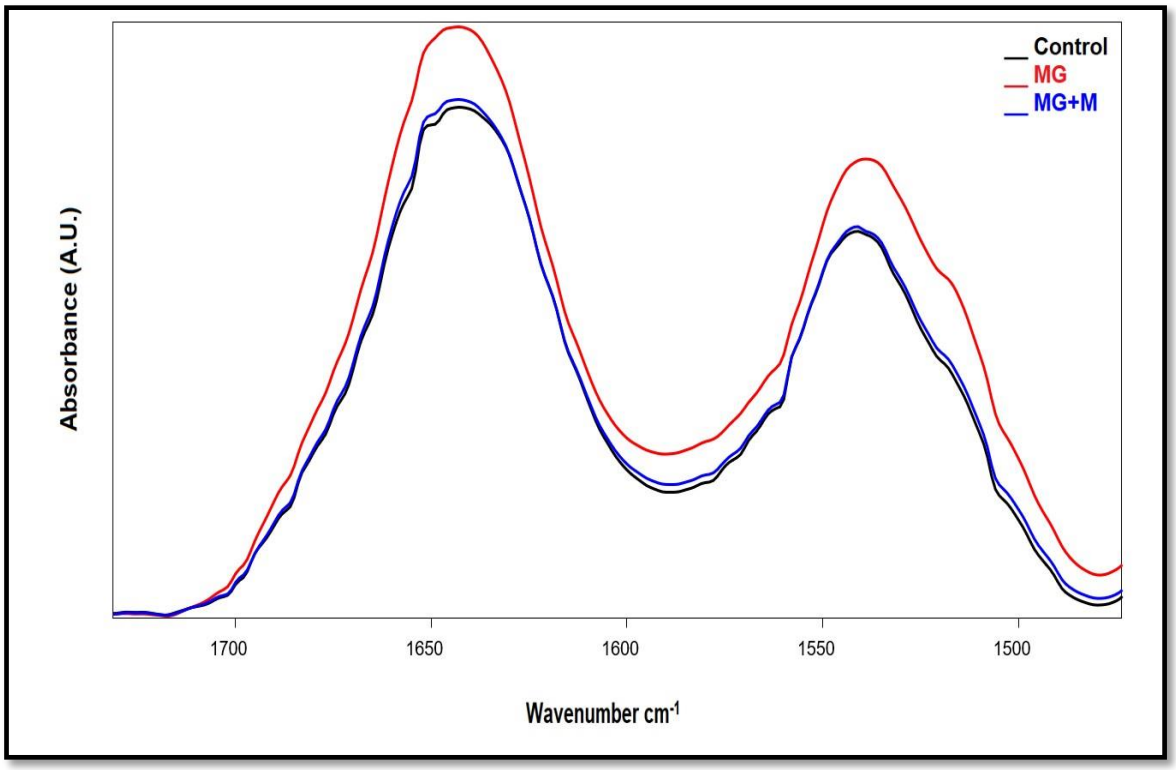

Figure 4.4: Representative Spectra of Amide I and Amide II Bands of the Control, Patient (MG), and Pyridostigmine user-patient MG+M) Spectra.

In figure 4.4, the control spectrum is shown in black, the patient spectrum is red, and the Pyridostigmine user-patient (MG+M) spectrum is blue. The spectra are shown in the 1800-1500 cm^{-1} frequency range and normalized according to the Amide A band located at 3284 cm^{-1} after baseline correction for a visual demonstration.

The other important part of the fingerprint region is the 1500-800 cm^{-1} region which contains functional groups belong to all biomolecules in the system of interest. Figure 4.5 displays this region. The CH_2 bending band at 1454 cm^{-1}, which is primarily originated from lipids, provides details on the composition and structure of lipids. It contains a small amount of protein additive (Simsek Ozek et al., 2010: 44). The band located at 1398 cm^{-1} is caused by COO- symmetric stretching vibrations in the side chains of amino acids and fatty acids (Dogan et al., 2021: 552). The N-H bending and C-N stretching of proteins are the cause of the amide III bands to be appeared at 1310 cm^{-1} (Dogan et al., 2021: 551). Information about Nucleic acids and phospholipids in sera is obtained from PO_2 antisymmetric stretch band at 1243 cm^{-1} (Dogan et al., 2021: 554). Nucleic acids are typically identified by the band PO_2 symmetric stretch band at 1080 cm^{-1} (Gok et al., 2016: 6). The polysaccharide's C-O stretching is the cause of the band at 1030 cm^{-1} (Kepenek et al., 2018: 11). There is a specific DNA band at 933 cm^{-1} caused by the vibrations of the deoxyribose ring (Garip, Bayari, Severcan, Abbas, Lednev, & Severcan, 2016: 025008-8). DNA's A and B form helix conformation is revealed by the band at 835 cm^{-1} (Dogan et al., 2021:552).

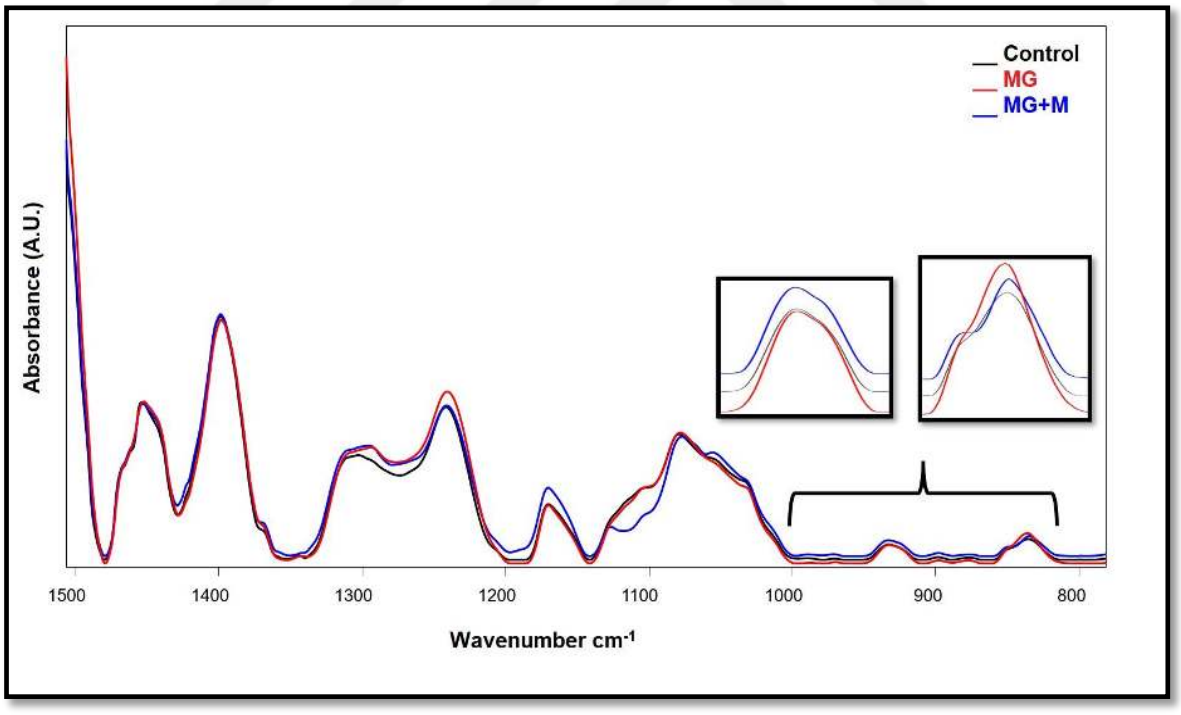

Figure 4.5: Representation of Fingerprint Region of the Control, Patient (MG), and Pyridostigmine user-patient (MG+M) Spectra.

In figure 4.5, The control spectrum is shown in black, the patient spectrum is in red, and the Pyridostigmine user-patient (MG+M) spectrum is shown in blue. After baseline correction, the spectra are displayed in the 1500–800 cm^{-1} frequency range and normalized using the Amide I band, which is present in the 1642 cm^{-1} region.

In the 1500-800 cm^{-1} range, dramatic differences between the control and MG patient and Pyridostigmine user groups are seen. Figure 4.5 illustrates it in detail. Although the use of Pyridostigmine has the same effect as MG, the use of Pyridostigmine has brought the DNA band closer to control.

4.3 COMPARISON OF BAND AREA RATIOS IN PATIENTS, CONTROL AND MG+M PATIENTS SPECTRA

According to Beer's Lambart law, the intensity and/or area of the infrared absorption bands rising from a particular functional group of the molecule of interest is straight proportional to the concentration of that molecule (Dogan et al., 2021: 551). Therefore, we used the areas under the bands for concentration knowledge about biomolecules. The areas used to evaluate the spectroscopic data and the ratios of these areas are shown in Table 4.2.

Table 4.2: The Implications of Band Area Ratios [Dogan et al., 2021: 553; Teker, Ceylani, Keskin, Samgane, Mansuroglu, Baba, Allahverdi, Acıkgoz, Gurbanov, 2023].

Band Area Ratios	Implications
$A_{3286}/A_{1639+1538}$	Amide A Content
$A_{2929}/A_{2929+2854}$	Saturated Lipid Concentration
$A_{1639}/A_{1642+1541}$	Protein Concentration
$A_{1241+1080}/A_{1642+1541}$	Nucleic acid/Protein ratio
A_{1241}/A_{2958}	Protein Phosphorylation
$A_{835}/A_{1241+1080}$	DNA Concentration
A_{1642}/A_{1541}	Protein Structural Changes
A_{1741}/A_{1538}	Protein Carbonylation

Table 4.2: The implications of band area ratios [Dogan et al., 2021: 553; Teker, Ceylani, Keskin, Samgane, Mansuroglu, Baba, Allahverdi, Acıkgoz, Gurbanov, 2023] ‘‘Table Continued’’.

Band Area Ratios	**Implications**
$A_{1741}/A_{2929+2854}$	Triglyceride Concentration
$A_{1030}/A_{1639+1538}$	Glucose/Protein ratio
A_{2929}/A_{2958}	Aliphatic Chain Length
A_{930}/A_{1080}	Z Form DNA Concentration
A_{1127}/A_{835}	RNA/DNA ratio

Table 4. 3: Numerical Comparison of Area Ratios of Patient Serum Biomolecules with the Control Group and Patient Serum Biomolecules with the MG+M Patient Group.

Area Ratios	**Implications**	**Control**	**MG**	**MG+M**
A_{2929} / $A_{2929+2854}$	Saturated Lipid Concentration	0,923±0,001	0,931±0,002↑**	0,921±0,001↓+++
A_{1639} /$A_{1639+1538}$	Protein Concentration	0,536±0,001	0,549±0,002↑****	0,546±0,002↑**
$A_{1241+1080}$ /$A_{1639+1538}$	Nucleic acid/Protein ratio	0,0315±0,0005	0,0337±0,0004↑**	0,034±0,001↑**
A_{1241} /A_{2958}	Protein Phosphorylation	2,746±0,025	2,879±0,019↑***	2,700±0,073
A_{835} /$A_{1241+1080}$	DNA Concentration	0,163±0,003	0,190±0,004↑****	0,145±0,012 ↓++
A_{1639} /A_{1538}	Protein Structural Changes	1,154±0,004	1,218±0,009↑****	1,206±0,012↑**
$A_{3286}/A_{1639+1538}$	Amide A Content	1,876±0,03481	1,303±0,02048↓****	1,706±0,1344↓+
A_{1741}/A_{1538}	Protein Carbonylation	0,002588± 0,0001867	0,003229± 0,0002865	0,003620± 0,0003915
$A_{1741}/A_{2929+2854}$	Triglyceride Concentration	0,09429± 0,004160	0,1093± 0,007862	0,1131± 0,007630
$A_{1030}/A_{1639+1538}$	Glucose/Protein ratio	0,00110±0,00004	0,00105±0,00003	0,00095±0,00005
A_{2929}/A_{2958}	Aliphatic Chain Length	1,503±0,046	1,569±0,049	1,700±0,090
A_{930}/A_{1080}	Z Form DNA Concentration	0,2803± 0,006887	0,3022± 0,007560	0,2475± 0,01709 ↓+
A_{1127}/A_{835}	RNA/DNA ratio	0,2537± 0,01079	0,1898± 0,007665 ↓****	0,4117± 0,07843 ↑+

A more detailed numerical representation of band ratios is given in Table 4.3. The units of measurement are "mean ± Standard Error of Mean (SEM)". A graphical representation of it is presented in Figure 4.6 for better comprehension. Although changes were observed in the parameters of protein carbonylation, triglyceride concentration, glucose/protein ratio, and aliphatic chain length, they were not included in the bar graphs because no statistically significant changes were recorded.

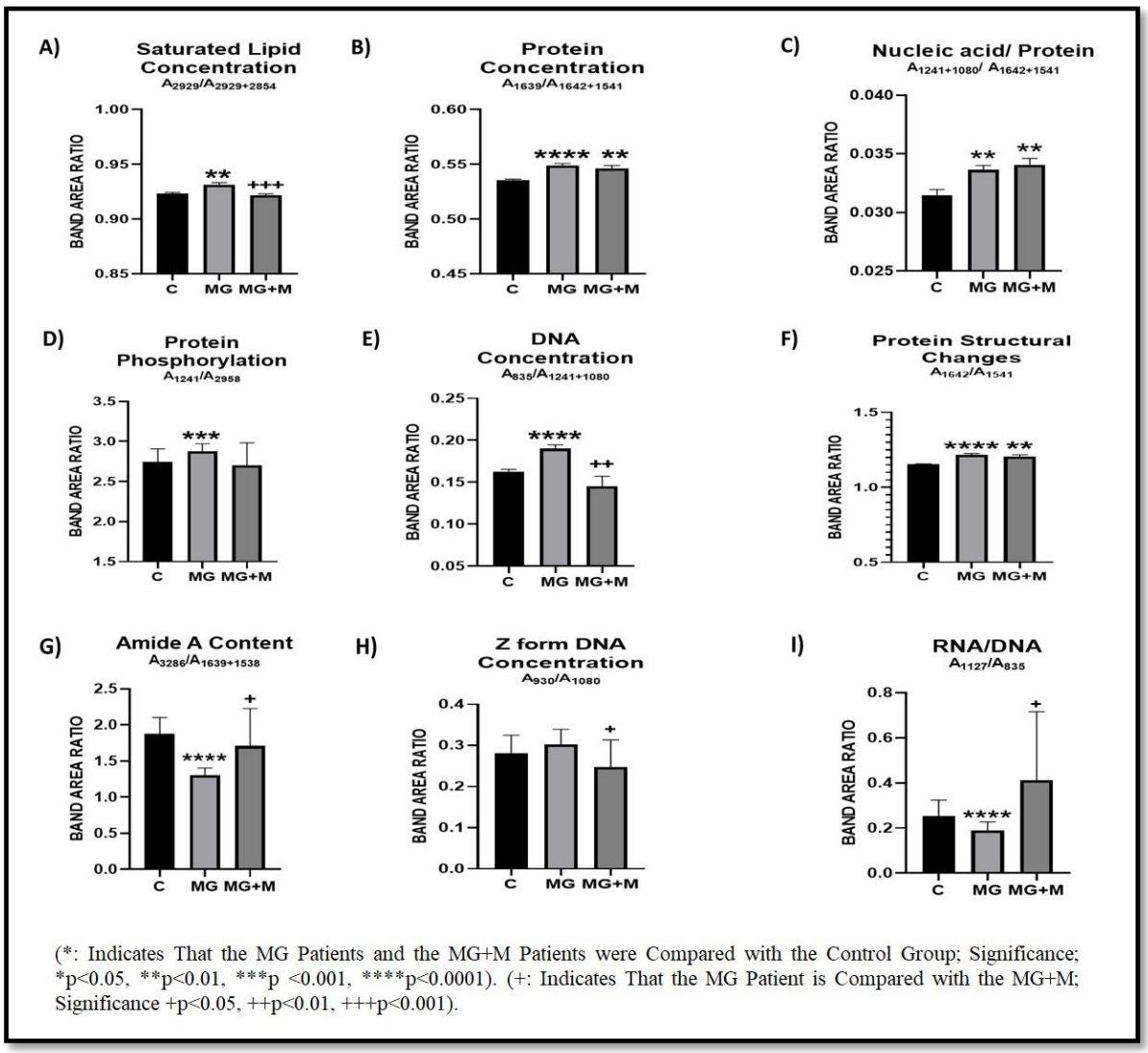

Figure 4.6: Comparison of Area Ratios of Serum Biomolecules of Control, MG and MG+M groups.

Calculating the area ratios connected to biomolecules in our sera samples revealed significant alterations, as shown in Table 4.3 and Figure 4.6. According to the findings, the use of pyridostigmine reduced the high effect of MG on saturated lipid, DNA concentration, and protein phosphorylation and approaches the control values. However, it has been observed that Pyridostigmine does not change the effect of MG on protein concentration, protein structural change, and Nucleic acid/Protein ratio parameters.

4.4 EFFECTS OF PYRIDOSTIGMINE ON LIPID ORDER AND DYNAMICS

Shifts in the position of the CH_2 antisymmetric stretching band, which is a lipid band, give information about the lipid order, that is, the flexibility of the lipid acyl chain. If this value shifts to low wavenumbers, lipid ordering increases, and the shift to high wavenumbers shows increased lipid disordering (Severcan, Sahin, Kazancı, 2005a: 220). This is a structural parameter. Changes in the bandwidth of the CH_2 antisymmetric stretching band give knowledge about lipid dynamics, a functional parameter. An increase in bandwidth indicates an increase in lipid dynamics, and a decrease in bandwidth indicates a decrease in lipid dynamics (Severcan et al., 2005a: 220). It has been observed that MG disease has no effect on the order of the lipid chain, but significantly reduces the lipid dynamics. It has been observed that lipid order is decreased in patients using Pyridostigmine, and lipid dynamics is increased more than in control. These changes are seen in Figure 4.7. The numerical representation is given in Table 4.4. The units of measurement are "mean ± Standard Error of Mean (SEM)".

Table 4.4: Numerical Comparison of Lipid Bandwidth and Band Position in MG, MG+M and Control Spectra (*: Indicates That the MG and the MG+M were Compared with the Control Group. Significance; *p<0.05, **p<0.01, ***p <0.001, ****p<0.0001). (+: Indicates That the MG is Compared with the MG+M ; Significance +p<0.05, ++p<0.01, +++p<0.001).

Information	C	MG	MG+M
CH_2 antisymmetric stretching bandwidth	7.692±0.06848	7.206±0.07506↓****	8.515±0.1238↑**** ↑++++
CH_2 antisymmetric stretching band position (wavenumber cm^{-1})	2929± 0.1655	2929±0.1707	2926±0.1200↓**** ↓++++

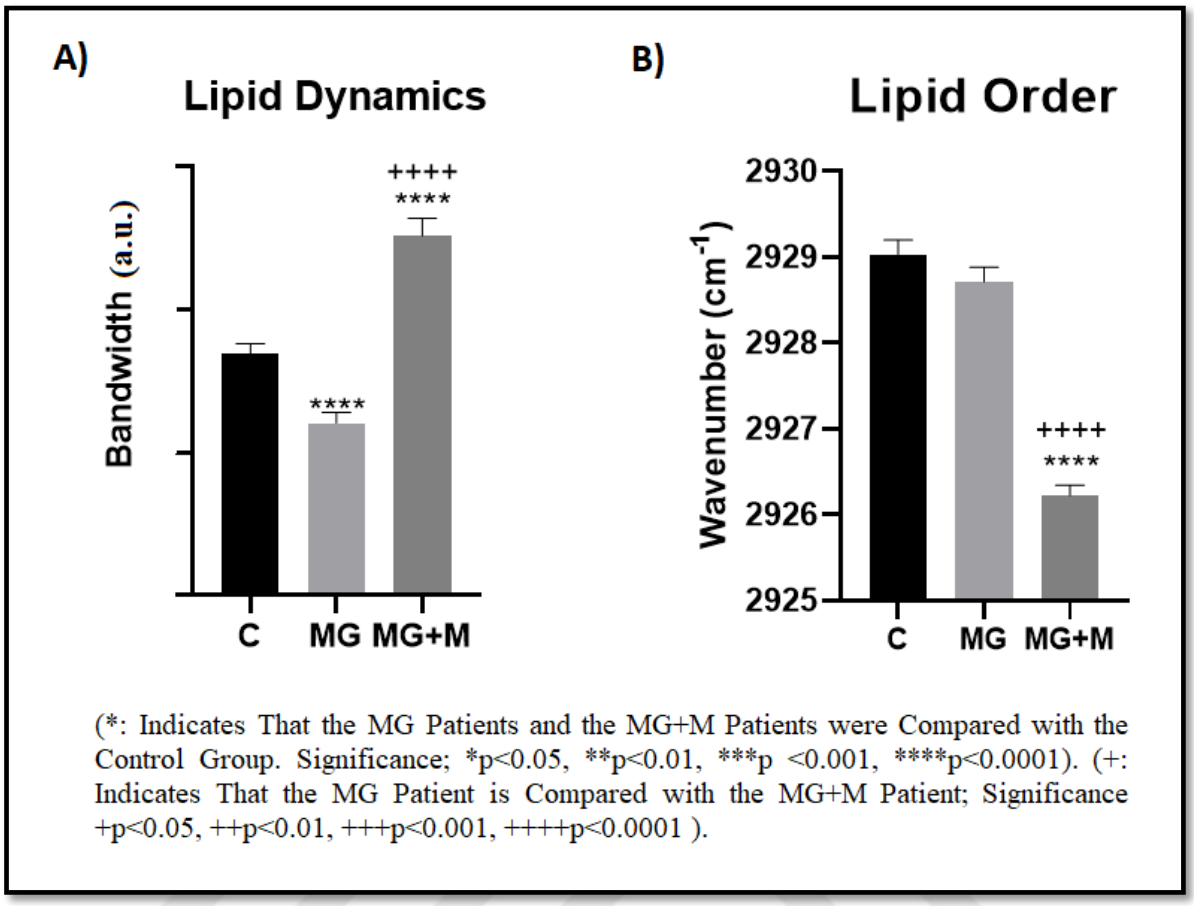

(*: Indicates That the MG Patients and the MG+M Patients were Compared with the Control Group. Significance; *p<0.05, **p<0.01, ***p <0.001, ****p<0.0001). (+: Indicates That the MG Patient is Compared with the MG+M Patient; Significance +p<0.05, ++p<0.01, +++p<0.001, ++++p<0.0001).

Figure 4.7: Comparison of Lipid Bandwidth and Band Position in MG, MG+M and Control Spectra.

4.5 LIPID PEROXIDATION RESULTS RELATED TO THE USE OF PYRIDOSTIGMINE

The olefinic band, which is a weak band located at a wavelength of 3008 cm^{-1}, represents unsaturated lipids. This band gives information about lipid peroxidation. The decrease in the area of the band corresponds to an increase in lipid peroxidation (Sills, Moore & Mendelsohn, 1994: 118). The area of the olefinic band was calculated from the baseline corrected and vector-normalized spectra. Changes in lipid peroxidation levels between groups are shown in Figure 4.8. The olefinic band area is used as the lipid peroxidation index (Severcan, Gorgulu, Turker Gorgulu & Guray, 2005b: 38). The unsaturated/saturated lipid ratio refers to the unsaturation index. It was calculated by taking the area ratio of the olefinic band (unsaturated lipid) to the CH_2 antisymmetric (saturated lipid) band (Garip Ustaoglu et

al., 2021:3). It is shown in Figure 4.8. The numerical representation is given in Tables 4.5 and 4.6. The units of measurement are "mean ± Standard Error of Mean (SEM)".

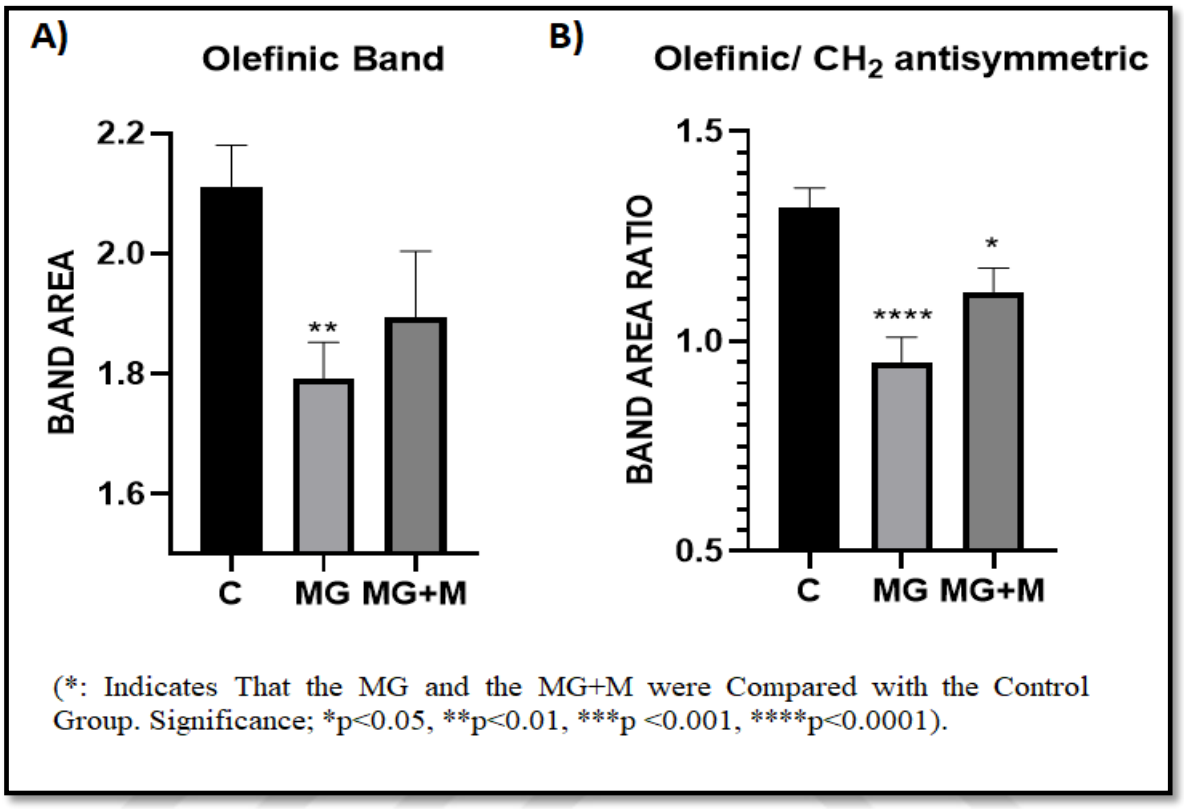

Figure 4.8: Comparison of Olefinic Band Area and Olefinic/CH_2 Antisymmetric Band Area Ratio in MG, MG+M, and Control Spectra. (*: Indicates That the MG and the MG+M were Compared with the Control Group. Significance; *p<0.05, **p<0.01, ***p <0.001, ****p<0.0001).

Table 4.5: Numerical Comparison of Olefinic Band Area and Olefinic/CH_2 Antisymmetric Band Area Ratio in MG, MG+M , and Control Spectra (*: Indicates That the MG and the MG+M were Compared with the Control Group. Significance; *p<0.05, **p<0.01, ***p <0.001, ****p<0.0001).

Information	C	MG	MG+M
Olefinic Band Area	2.112±0.06823	1.792±0.05994↓**	1.894±0.1092
Olefinic band/ CH_2 antisymmetric stretching band Area Ratio	1.317± 0.04802	0.9494±0.06025↓****	1.118±0.05688↓*

5. DISCUSSION AND CONCLUSION

This molecular-level study was conducted to determine the role of Pyridostigmine treatment in MG pathogenesis via infrared spectroscopy by comparing the serum of Pyridostigmine users and non-user patients and control group.

Autoantibodies attach to AChRs on the muscle membrane at the neuromuscular junction in the rare autoimmune condition known as myasthenia gravis. The most typical symptom of this condition, which weakens muscles, is a droopy eyelid (Gilhus, 2016: 2570). In the treatment of the disease, symptomatic treatment is applied at the first stage. The widespread use of acetylcholinesterase inhibitor in symptomatic therapy is pyridostigmine. Immunotherapies based on steroids and other immunosuppressants are applied to patients for whom acetylcholinesterase inhibitor therapy is not sufficient. Aside from patients with Anti-MuSK antibodies, other subgroups of Myasthenia Gravis patients also benefit from acetylcholinesterase inhibition. In the sera of 80% of MG ill, there are AChR antibodies (Yavuz, 2019: 23). Considering how Anti-AChR antibodies contribute to the development of Myasthenia Gravis: intracellular breakdown of surface AChRs; binding of AChR autoantibodies to AChR ligand binding sites thereby inhibiting acetylcholine binding and thereby channel opening; production of membrane attack complexes (MACs) in the sarcolemma and the breakdown of sarcolemma folds by triggering complement activation in neuromuscular connections; The disease is brought on by anti(MuSK and LRP4) antibodies, which disrupt the normal organization and operation of normal mechanisms in neuromuscular connections and interfere with the interactions of MuSK and LRP4 proteins (Guidon, 2019: 218). The enzyme acetylcholinesterase has an important function in the hydrolysis of acetylcholine. Pyridostigmine acts a key role in inhibiting this enzyme, thereby increasing the quantity of ACh at the neuromuscular junction. Consequently, neuromuscular transmission occurs (Farrugia & Goodfellow, 2020:2).

Muscle weakening that just affects the eye muscles in 20% of MG patients causes ptosis or diplopia (Hehir & Silvestri, 2018: 255). These patients with the ocular form of MG are likely to progress to generalized myasthenia gravis after 2 years. However, ocular MG patients can only be treated using acetylcholinesterase inhibitors (Hehir & Silvestri, 2018: 255). This shows the importance and widespread use of the drug pyridostigmine.

Pyridostigmine drug is used as a symptomatic therapy in MG disease. It is used as a long-term therapy in ills with mild disorder and as adjunctive trestment in ills with violent disorder taken immunotherapy (Maggi & Mantegazza, 2011: 691). Given all of these factors, the key purpose of this thesis is to evaluate the effectiveness of pyridostigmine treatment in people with Myasthenia Gravis. For this aim, in this study, 24 human sera samples from the patient group diagnosed with Myasthenia Gravis and not started any therapy, 15 from the patient group receiving only pyridostigmine therapy, and 42 from the healthy control group were examined. Body fluids like saliva, serum, plasma, and urine can be used for the early diagnosis of many disorders and the assessment of drug/vaccine effects because they are very informative and accessible (Dogan et al., 2021: 550). Containing more than 300 types of protein, as well as amino acids, carbohydrates, and lipids, the serum also contains up to 114,000 metabolites in different concentrations (Byrne, 2020:1). In cases such as disease, the protein levels in the serum change. This change is directly related to the disease (De, 2009: 461). Among the vibration spectroscopic techniques consisting of Raman, infrared, and Terahertz spectroscopy, infrared spectroscopy is widely used in medicine. The molecular makeup, concentration, structure, and function of biomolecules can be changed by pathological circumstances, environmental variables, or genetic changes. FTIR is a very effective approach for identifying chemical changes brought on by these factors, especially when used in combination with multivariate analysis techniques and ATR-FTIR spectroscopy (Dogan et al., 2021: 549). Articles on FTIR studies using serum samples have been published previously. In a study, it has been shown that the FTIR spectroscopy technique was used by using serum samples in the diagnosis of COVID-19, which causes the corona epidemic that we are still under its influence (Zhang, Xiao, Wang, Peng, Chen, Zhang, Zhang, Guo, Wang, Luo, Zhou, Xu, 2021: 2191). Another corona study using FTIR spectroscopy to investigate the possibility that the CoronaVac vaccination alters the biological properties of human serum biomolecules (Dogan et al., 2021). Moreover, it has been shown that FTIR spectroscopy in human pleural fluid, when used together with chemometric analysis, successfully distinguishes mesothelioma cancer, which is rare cancer, and other chest disorder (Abbas et al., 2018: 105003-1; Yonar, Sandal, Emri & Severcan, 2015:626a). By using serum samples, it was also differentiated from lung cancer and benign exudative effusions with FTIR technique coupled with chemometrics and presented as a new approach for diagnosis (Yonar et al., 2022). In this thesis study, the impact of pyridostigmine

treatment in Myasthenia Gravis disease was investigated using the FTIR technique from serum samples. With a minimal amount of material and no need of external agents, FTIR is a useful technique that allows accurate and synchronous monitoring of macromolecular functional groups in biological systems. Infrared spectroscopic analysis for concentration determination is governed by Beer-Lambert's equation, which states that the intensity of the bands in the absorption spectra or the integrated band area is straight proportional to the concentration of the relevant functional group (Gurbanov et al., 2016: 849). In order to determine the relative concentration of the biomolecules, the areas under the bands were computed.

Concentration changes of biomolecules were accurately determined using band area ratios. Also, changes due to any experimental artifacts are avoided by using band area ratios. Band area ratios provide information on the content, concentration, structural changes, and lipid asymmetry of biological molecules.

As it is known, disease states cause metabolic changes and increase in proteins, increase in reactive oxygen species, and as a result, oxidative stress and lipid peroxidation occur as a result. Lipid peroxidation is a process in which oxidants, like free radicals, attack lipids, particularly unsaturated fatty acids, which are generally characterized by shortening of the acyl chain length and contain carbon-carbon double bonds. In this case, the long acyl chains are broken down into shorter acyl chains. The carbon-carbon double bonds are attacked and thus saturated lipids are formed (Ayala, Muñoz & Argüelles, 2014:1; Olusi, 2002: 1163). Since the unsaturated bonds become saturated, it is thought to contribute to the significant increase in the number of saturated lipids in the patient group (Garip Ustaoglu, Ali, Rakib, Blezer, Heijningen, Dijkhuizen &Severcan: 2021:8). Saturated lipid concentration increased in MG. With the use of pyridostigmine the MG-induced increased in saturated lipid concentration decrease band approached to the control value indicating the recovery effect of pyridostigmine. In addition, the decrease in the olefinic band area corresponds to the increase in lipid peroxidation. As seen in Figure 4.8, lipid peroxidation increases dramatically in MG patients. It was observed that the increase in lipid peroxidation level in MG compared to the control decreased with the use of pyridostigmine. Similarly, when the olefinic/CH_2 antisymmetric band area ratio was examined, it was observed that lipid

peroxidation increased in MG patients. A decrease in lipid peroxidation is observed in patients using pyridostigmine.

Amide A band located at 3284 mostly contains protein as well as polysaccharide, glycogen, and bound water. As seen in Figure 4.2, the spectrum of Control and MG+M patients is very similar, with little difference. However, the spectrum of MG patients is different compared to the control. It differs compared to the control and MG+M spectrum. When the amide A content was calculated, a decrease was observed in MG patients compared to the control. An increase was observed in MG+M patients compared to MG patients and approached the control values.

For the purpose of determining protein concentration, the ratios of the Amide I/(Amid I + Amide II) band area were examined. Protein levels were significantly higher in MG patients than in the control group (Fig. 4.6b). The increase in protein levels may be owing to an increase in muscle or glycolytic enzymes in general, transport proteins, or other proteins like creatine kinase. It has been noted in earlier studies that protein levels rise in diseases of the muscles (Alagaratnam, 2008:1553; Ralbovsky, Dey, Galfano, Dey & Lednev, 2020: 7). The using of pyridostigmine did not change the effect of MG on the protein concentration parameter. Pyridostigmine prevents the destruction of acetylcholine by cholinesterase, allowing nerve impulses to be transmitted more freely across the neuromuscular junction. Thus, muscle-nerve transmission is ensured. It is known that anti-MuSK MG antibodies replay less favorably to acetylcholinesterase inhibitors than other MG subgroups. For this reason, the use of pyridostigmine may not have affected the protein concentration of the patients, since muscle-nerve conduction cannot be adequately achieved in every patient.

As seen in Figure 4.6c, nucleic acid/protein ratio increased significantly in the patient group. The ratio of nucleic acid to protein amount decreases since protein amount rises. However, the dramatic increase in nucleic acid/protein ratio indicates an increase in nucleic acid concentration. This increase is due to an increase in the amount of nucleic acids. Indeed, as seen in the DNA concentration band in Figure 4.6e, the amount of DNA increases dramatically in the MG. The increase in DNA concentration can result from injured and dying cells. Damage-associated molecular patterns that can also stimulate interferon type 1 production can release endogenous molecules. It may be endogenous DNA or RNA, or nuclear components such as cytosolic proteins. It is called sterile inflammation for it is not

caused by a pathogenic infection (Payet, You, Fayet, Dragin, Berrih-Aknin, Le Panse, 2022a: 4). Another supporting finding is that the elimination of apoptotic thymocytes, which supports the release of endogenous nucleic acids from necrotic thymocytes, is impaired due to the decrease of macrophages in the thymus in AChR-MG (Payet, Hemery, Truffault, Bondet, Duffy, Michel, Fadel, Guihaire, Demeret, Berrih-Aknin, Le Panse, 2022b: 7). When other studies in the literature are taken into consideration, it has been reported that myasthenia gravis disease differs in the expression of miRNAs and increases the transcription of genes related to blood cell traffic and apoptosis (Sabre, Punga & Punga, 2020:1; Park, Jung, Lee & Hong, 2016: 41). This information supports the increase in DNA concentration and nucleic acid/protein ratio in MG. The significant reduction in DNA concentrations of patients using pyridostigmine may be due to cell damage and decreased transcript profiles of genes involved in apoptosis. The using of pyridostigmine reduced the enhancing effect of MG on DNA concentration and brought the changes closer to control. However, it did not change the effect of MG in the Nucleic acid/Protein ratio. When looking at the RNA/DNA ratio, which provides information about the ratio of nucleic acids, there is a decrease in the proportion of MG ills compared to the healty indivuduals. This rate increased in MG+M patients compared to MG patients. The increase observed in patients taking pyridostigmine is also higher compared to the control group. The increase here may be due to a decrease in DNA concentration. For RNA concentration, only the area of the RNA band was calculated. This parameter was changes observed but statistically significant change was no. The band area of the RNA band located at 1127 was measured. This band area is increased in the RNA concentration of patients using pyridostigmine. This increase supports the increase in RNA/DNA concentration and the increase in RNA concentration band area ratio.

The Z-form DNA is a left-handed release and contains deoxycytidine in anti-conformation and deoxyguanosine in synform. When the Z-form DNA concentration was examined, there was no statistically significant change, although an increase in the bar graph was observed in MG ills compared to the control. However, compared to MG patients, Z-form DNA concentration was decreased in MG+M patients (Figure 4.6h). It is known in the literature that Z-DNA functions functionally in transcription. However, some works have shown that the effect of this function is related to the particular gene under investigation (Gurbanov, Tunçer, Mingu, Severcan & Gozen, 2019: 5).

A significant increase in protein phosphorylation was observed in MG (Seen in Figure 4.6d). This is an important parameter in the arrangement of many physiological processes like transcription, survival, and regulation of cell death, including signal transduction (Nemes, Gellert, Almási, Vági, Sáray, Kádár, Salánki, 2017:1). The use of pyridostigmine reduced the enhancing effect of MG in protein phosphorylation and brought it closer to control. This can tell that inactivated proteins are activated or vice versa.

The difference in the amide I/amide II area ratio reveals a change in protein structure because the amide I band is produced by 80% C=O stretching while the amide II band is produced by 60% N-H bending and 40% C-N stretching (Garip Ustaoglu et al., 2021: 362). In MG patients, the rate of protein structural alterations (seen in Figure 4.6f) is increased. This scenario is supported by increases in DNA and nucleic acid concentrations, which will also impact protein production. It has been shown in the literature that beta plaques of toxic proteins (amyloid beta and alpha-synuclein) formed in neurological disturbances like neurodegenerative disorders have an antiparallel structure (Cerf, Sarroukh, Tamamizu-Kato, Breydo, Derclaye, Dufrêne, Narayanaswami, Goormaghtigh, Ruysschaert, Raussens, 2009: 415; Rodriguez, Ivanova, Sawaya, Cascio, Reyes, Shi, Sangwan, Guenther, Johnson, ZhangJiang, Arbing, Nannenga, Hattne, Whitelegge, Brewster, Messerschmidt, Boutet, Sauter, Gonen, Eisenberg, 2015: 1). In addition, the increase in aggregate beta structures with the disease supports the denaturation of the protein structure in neurological diseases (Lam, Graber, Gentry, Bieschke, 2016: 2). The function of proteins is closely related to their structure. Therefore, changes in the structure affect the normal functions of proteins. Pyridostigmine did not change the effect of MG on the protein structural change parameter. The use of pyridostigmine does not alter the pathophysiological process that causes and maintains MG but acts as an important player in nerve conduction by inhibiting AChE.

The vibrations of the corresponding functional group in the lipid molecules give the CH_2 antisymmetric stretch band (Gurbanov et al., 2016: 849). Shifts in the position of the CH_2 antisymmetric stretching band, which is a lipid band, give information about the lipid order, that is, the flexibility of the lipid acyl chain. If this value shifts to low wavenumbers, lipid ordering increases, and high wavenumbers show increased lipid disordering if shifts to wavenumbers. This is a structural parameter (Severcan, 2005: 220). It has been observed

that MG disease has no effect on the flexibility of the lipid chain. When the impact of pyridostigmine on lipid order was examined, it was observed that it increased lipid order.

Changes in the bandwidth of the CH_2 antisymmetric stretching band give knowledge about lipid dynamics, which is a functional parameter. An increase in bandwidth indicates an increase in lipid dynamics, and a decrease in bandwidth indicates a decrease in lipid dynamics (Severcan et al., 2005: 220). It was observed that lipid dynamics, namely lipid diffusion, decreased significantly in MG disease. Pyridostigmine, on the other hand, increases lipid dynamics in the opposite direction more than control. This should be considered as a negative side effect.

Changes to lipids and proteins, such as saturation level, packaging, and composition, can also affect the interaction of lipids and proteins and may affect lateral distribution. All these are parameters associated with the arrangement of the membrane. The shift of the CH_2 band to low-frequency values in the use of pyridostigmine indicates that acyl chain flexibility decreases e.g. lipid order increases. This may indirectly indicate that as the lipid order increases, the membrane thickness increases accordingly. The variation in membrane thickness will disturb the conformation of the proteins in the membrane. These changes in membrane fluidity and thickness can result in disturbances in cell function.

The investigation of structural and functional alterations in the biomolecules of biological systems induced by environmental or disease circumstances, the early detection of pathological conditions and diseases, and therapeutic monitoring are done using the special spectroscopy method known as FTIR. The ATR-FTIR approach, in particular, provides a fantastic chance to identify molecular alterations that result in changes in vibrational energy levels that can be observed by applying a tiny quantity of sample to the crystal without the requirement for preparatory preparation (Dogan et al., 2021:550).

There are different spectroscopy studies on Myasthenia gravis in the literature. In MG patients, it is aimed to remove the thymus to prevent the production of abnormal antibodies that cause the disease by performing thymectomy and to improve the symptoms. In a study, MG patients underwent phosphorus 31 (31P) magnetic resonance (MR) spectroscopy to assess muscle metabolism both before and after thymectomy (Ko, Huang, Hsieh, Ng, Lee, Lee, Lin, Chen, & Lee, 2008: 162). In a separate MR research, patients with myasthenia

gravis and various autoantibodies had their intrinsic tongue muscles' muscle lipid content examined using proton magnetic resonance spectroscopy. It has been shown that oxidative metabolism is impaired in individuals with AChR MG and MuSK MG due to the decline in creatine phosphocreatine in the muscles of the tongue (Lavrnic, Dakovic, Peric, Rakocevic-Stojanovic, Basta, Marjanovic, Stosic-Opincal, & Lavrnic, 2011: 25).

A structural investigation of immunotherapeutic peptides for autoimmune Myasthenia Gravis was carried out by Jung et al., showing that cyclic extended peptides can be used as useful tools for optimizing the affinity of peptide antigens derived from the phage library. In this study, the NMR spectroscopy technique was used (Jung, Yi, Lee, Lee, Jung, Yang, Eu, Im, & Kim, 2007: 14987). In another study, a comparison of Laser Correlation Spectroscopy and Radioimmunoassay in Myasthenia Gravis was done, and its educational value was provided (Alcinova, Arkhipova, Sidnev, Sanadze, Dedaev, Karganov, 2014:1).

In this thesis study, the serum of patients using and not using pyridostigmine and the control group were compared in order to examine the molecular effect of pyridostigmine medication in the etiology of MG. According to the findings, the use of pyridostigmine reduced the elevated effect of MG on saturated lipid, DNA concentration, and protein phosphorylation and approaches to the control values.

In conclusion, these findings unequivocally demonstrate the recovery impact of pyridostigmine against MG-induced changes in serum biomolecules. Furthermore, the FTIR technique can be used as a useful technique in therapeutic monitoring. Protein functions like receptor binding, and signal transduction will be regulated and affected by the drug. In the future, it will be possible to design drugs with fewer side effects (Sanganahalli, Joshi & Joshi, 2000: 89).

REFERENCES

Abbas, S., Simsek Ozek, N., Emri, S., Koksal, D., Severcan, M. & Severcan, F. (2018). Diagnosis of malignant pleural mesothelioma from pleural fluid by Fourier transform-infrared spectroscopy coupled with chemometrics. J. Biomed. Opt., 23(10), 105003-1- 14.

Alagaratnam, S. (2008). Serum protein profiling in mice: identification of Factor XIIIa as a potential biomarker for muscular dystrophy. Proteomics, 8, 1552–1563.

Alcinova, I., Arkhipova, E., Sidnev, D., Sanadze, A., Dedaev, S. & Karganov, M. (2014). ISRN Immunology, 2014, 1-6.

Al-Zwaini, I. J. & Al-Mayahi, A. (2019). Introductory Chapter: Myasthenia Gravis - An Overview. IJ. Al-Zwaini, & A. Al-Mayahi (Ed.), Selected Topics in Myasthenia Gravis (1-10). IntechOpen: DOI: 10.5772/intechopen.85761

Andrews, D. L. (2017). Electromagnetic Radiation. Lindon, JC. (Ed.), Encyclopedia of Spectroscopy and Spectrometry (Third Edition) (427-431). Oxford: Academic Press. https://doi.org/10.1016/B978-0-12-409547-2.11153-9

Ayala, A., Muñoz, M. & Argüelles, S. (2014). Lipid Peroxidation: Production, Metabolism, and Signaling Mechanisms of Malondialdehyde and 4-Hydroxy-2-Nonenal. Oxidative Medicine and Cellular Longevity, 1-31.

Aydogan, O. (2019). PDTP-DFBT ve PC71BM Organik güneş hücresi malzemelerinin moleküllerinin titreşimsel spektroskopik özelliklerinin incelenmesi (Master Thesis). Retrived from Ulusal Tez Merkezi– Türkiye & Eskisehir (560624).

Backhaus, J., Mueller, R., Formanski, N., Szlama, N., Meerpohl, H-G., Eidt, M. & Bugert, P. (2010). Diagnosis of breast cancer with infrared spectroscopy from serum samples. Vibrational Spectroscopy, 52(2), 173-177.

Baker, M. J. Hussain, S. R., Lovergne, L., Untereiner, V., Hughes, C., Lukaszewski, R. A., Thiéfin, G. & Sockalingum, G. D. (2016). Developing and understanding biofluid vibrational spectroscopy: a critical review. Chemical Society Reviews, 45, 1803-1818.

Baker, M. J., Trevisan, J., Bassan, P., Bhargava, R., Butler, H. J., Dorling, K. M., Fielden, P. R., Fogarty, S. W., Fullwood, N. J., Heys, K. A., Hughes, C., Lasch, P., Martin-Hirsch, P. L., Obinaju, B., Sockalingum, G. D., Sulé-Suso, J., Strong, R. J., Walsh, M. J., Wood, B. R., Gardner, P. & Martin, F. L. (2014). Using Fourier transform IR spectroscopy to analyze biological materials. Nature Protocols, 9, 1771-1791.

Barauna, V. G., Singh, M. N., Barbosa, L. L., Marcarini, W. D., Vassallo, P. F., Mill, J. G., Ribeiro-Rodrigues, R., Campos, L. C. G., Warnke, P. H. & Martin, F. L. (2021). Ultrarapid on-site detection of sars-cov-2 infection using simple atr-ftir spectroscopy and an analysis algorithm: high sensitivity and specificity. Analytical Chemistry, 93, 2950-2958.

Barboza da Silva, J., Vincente de Carvalho, A. E., Schneider, C. & Corbellini, V. A. (2022). Saliva may predict quality of life in psoriasis as measured by Fourier transform infrared spectroscopy (FTIR) and chemometrics. Photodiagnosis and Photodynamic Therapy, 39, 103017.

Becker, W. M., Reece, J. B. & Poenie, M. F. (1995). The World of the Cell (3rd). The Benjamin/Cummings.

Beloor Suresh, A. & Asuncion, R, M. D. Myasthenia Gravis, StatPearls [Internet], 2021, Available from: https://www.ncbi.nlm.nih.gov/books/NBK559331/?report=classichttps://www.ncbi.nlm.nih.gov/books/NBK559331/

Berrih-Aknin, S., Frenkian-Cuvelier, M., & Eymard, B. (2014). Diagnostic and clinical classification of autoimmune myasthenia gravis. Journal of Autoimmunity, 48-49, 143-148.

Bozkurt, O. (2006). The Effect of Diabetes on Rat Skeletal Muscle Tissues at Molecular Level (Master Thesis). Retrived from Ulusal Tez Merkezi– Türkiye & Ankara (181163).

Bozkurt, O., Bilgin, M. D. & Severcan, F. (2007). The effect of diabetes mellitus on rat skeletal Extensor digitorum longus muscle tissue An FTIR study. Spectroscopy-An International Journal, 21(3), 151- 160.

Braz, L. P., Shiau Ng, Y., Gorman, G. S., Schaefer, A. M., McFarland, R., Taylor, R. W., Turnbull, D. M., & Whittaker, R. G. (2021). Neuromuscular junction abnormalities in mitochondrial disease. Neurology: Clinical Practice, 11(2), 97-104.

Byrne, H. J., Bonnier, F., Mclntyre, J. & Parachalil, D. R. (2020). Quantitative analysis of human blood serum using vibrational spectroscopy. Clinical spectroscopy, 2, 1-15.

Cakmak, G., Togan, I. & Severcan, F. (2006). 17_-Estradiol induced compositional, structural and functional changes in rainbow trout liver, revealed by FT-IR spectroscopy: A comparative study with nonylphenol. Aquatic Toxicology, 77, 53–63.

Campbell, I. D. & Dwek, R. A. (1984). Biological spectroscopy. USA: Benjamin/Cummings Publishing Company.

Cerf, E., Sarroukh, R., Tamamizu-Kato, S., Breydo, L., Derclaye, S., Dufrêne, Y. F., Narayanaswami, V. Goormaghtigh, E., Ruysschaert, J. M. & Raussens, V. (2009). Antiparallel beta-sheet: a signature structure of the oligomeric amyloid beta-peptide, Biochemical Journal, 421(3), 415-23.

Chen, F., Meng, C., Qu, H., Cheng, C., Chen, C., Yang, B., Gao, R. & Lv, X. (2021). Human serum mid-infrared spectroscopy combined with machine learning algorithms for rapid detection of gliomas. Photodiagnosis and Photodynamic Therapy, 1-17.

Conti-Fine, B. M., Milani, M., & Kaminski, H. J. (2006). Myasthenia gravis: past, present, and future, The Journal of Clinical Investigation. 116(11), 2843- 2854.

Conti-Fine, B. M., Milani, M. & Wang, W. (2008). CD4+ T Cells and Cytokines in the Pathogenesis of Acquired Myasthenia Gravis. Ann. N.Y. Acad. Sci., 1132, 193–209.

Dalakas, M. C. (2015). Future perspectives in target-specific immunotherapies of myasthenia gravis. Ther Adv Neurol Disord, 8(6), 316–327.

Dalakas, M. C. (2018). Immunotherapy in myasthenia gravis in the era of biologics. Nature Reviews Neurology, 15, 113-124.

De Bruyne, S., Speeckaert, M. M. & Delanghe, J. R. (2017). Applications of mid-infrared spectroscopy in the clinical laboratory setting. Critical Reviews in Clinical Laboratory Sciences, 1- 20.

De, M., Rana, S., Akpinar, H., Miranda, O. R.,Arvizo, R. R., Bunz, U. H. F. & Rotello, V. M. (2009). Sensing of proteins in human serum using conjugates of nanoparticles and green fluorescent protein. Nature chemistry, 1(6), 461-465.

Dogan, A., Gurbanov, R., Severcan, M. & Severcan, F. (2021). CoronaVac (Sinovac) COVID-19 vaccine-induced molecular changes in healthy human serum by infrared spectroscopy coupled with chemometrics. Turkish Journal of Biology, 45, 549- 558.

Dogan, A., Lasch, P., Neuschl, C., Millrose, M. K., Alberts, R., Schughart, K., Naumann, D. & Brockmann, G. A. (2013). ATR-FTIR Spectroscopy Reveals Genomic Loci Regulating the Tissue Response in High Fat Diet Fed BXD Recombinant Inbred Mouse Strains. BMC genomics, 14 (386), 1-17.

Du, F. H., Mills, E. A., & Mao-Draayer, Y. (2017). Next-generation anti-CD20 monoclonal antibodies in autoimmune disease treatment. Autoimmunity Highlights, 8(12), 1-12.

El-Azazy, M. (2018). Infrared Spectroscopy - A Synopsis of the Fundamentals and Applications. El-Azazy, M. (Ed.), Infrared Spectroscopy- Principles, Advances, and Applications (1-22). IntechOpen. DOI: 10.5772/intechopen.82210

Elibol, B., Severcan, M., Jakubowska-Dogru, E., Dursun, I. & Severcan, F. (2022). The structural effects of Vitamin A deficiency on biological macromolecules due to ethanol consumption and withdrawal: An FTIR study with chemometrics. Journal of Biophotonics.

Elkadi, O. A., Hassan, R., Elanany, M., Byrne, H. J. & Ramadan, M. A. (2021). Identification of Aspergillus species in human blood plasma by infrared spectroscopy and machine learning. Spectrochimica Acta Part A: Molecular and Biomolecular Spectroscopy, 248, 1- 13.

Emery, W., & Camps, A. (2017). Basic Electromagnetic Concepts and Applications to Optical Sensors. Introduction to Satellite Remote Sensing Atmosphere, Ocean, Cryosphere and Land Applications (43-83). Elsevier. https://doi.org/10.1016/B978-0-12-809254-5.00002-6

Ezer, N., Sahin, I. & Kazancı, N. (2017). Alliin interacts with DMPC model membranes to modify the membrane dynamics: FTIR and DSC Studies, Vibrational Spectroscopy, 89, 1- 8.

Farrugia, M. E. & Goodfellow, J. A. (2020). A Practical Approach to Managing Patients with Myasthenia Gravis—Opinions and a Review of the Literature. Frontiers in Neurology, 604.

Freifelder, D., (1982). Physical Chemistry. Applications to biochemistry and molecular biology, Freeman, W. H. (Ed), New York.

Gajjar, K., Trevisan, J., Owens, G., Keating, P. J., Wood, N. J., Stringfellow, H. F., Martin-Hirsch, P.L. & Martin, F. L. (2013). Fourier-transform infrared spectroscopy coupled with a classification machine for the analysis of blood plasma or serum: a novel diagnostic approach for ovarian cancer, Analyst. 138(14), 3917-26.

Garip Ustaoglu, S., Ali, M. H. M., Rakib, F., Van Heijningen, F. C. L., Dijkhuizen, R. M. & Severcan F. (2021). Biomolecular changes and subsequent time-dependent recovery in hippocampal tissue after experimental mild traumatic brain injury, Scientific Reports, 11, 12468.

Garip Ustaoglu, S., Kaygusuz, H., Bılgın, M. D. & Severcan, F. (2021). Novel approaches for COVID-19 diagnosis and treatment: a nonsystematic review. Turkish Journal of Biology, 45, 358-371.

Garip, S. (2012). Investigation of drug-related changes on bone tissues of rat animal models in healthy and disease states (Master Thesis). Retrived from Ulusal Tez Merkezi– Türkiye & Ankara (293097).

Garip, S., Bayari, S. H., Severcan, M., Abbas, S., Lednev, I. K. & Severcan, F. (2016). Structural effects of simvastatin on liver rat [corrected] tissue: Fourier transform infrared and Raman microspectroscopic studies. J. Biomed. Opt. 21(2), 25008 (Erratum in: J Biomed Opt, 21(4),49801).

Garip, S., Cetin Gözen, A. & Severcan, F. (2009). Use of Fourier transforms infrared spectroscopy for rapid comparative analysis of Bacillus and Micrococcus isolates. Food Chemistry, 113, 1301– 1307.

Geiger, C. A. (2004). An Introduction to Spectroscopic Methods in the Mineral Sciences and Geochemistry. A. Beran & E. Libowitzky (Ed.), Spectroscopic Methods in Mineralogy (1-42). Eötvös University Press.

Gervasoni, J., Primiano, A., Marini, F., Sabino, A., Biancolilo, A., Calvani, R., Picca, A., Marzetti, E., Persichilli, S., Urbani, A., Servidei, S., & Primiano, G. (2020). Fourier-Transform Infrared Spectroscopy of Skeletal Muscle Tissue: Expanding Biomarkers in Primary Mitochondrial Myopathies. Genes, 11, 1522, 1-8.

Gilhus, N. E. (2016). Myasthenia Gravis. The new england journal o f medicine, 375(26), 2570-2581.

Gilhus, N. E., & Verschuuren, J. J. (2015). Myasthenia gravis: subgroup classification and therapeutic strategies. Lancet Neurol, 14, 1023-1036.

Gilhus, N. E., Tzartos, S., Evoli, A., Palace, J., Burns, T. M. & Verschuuren, J. J. (2019). Myasthenia gravis. Nature Reviews disease primers, 5(30), 1-19.

Gilhus, N. E., Skeie, G. O., Romi, F., Lazaridis, K., Zisimopoulou, P. & Tzartos, S. (2016). Myasthenia gravis-autoantibody characteristics and their implications for therapy. Nature reviews neurology, 12, 259-268.

Gok, S., Aydin, O. Z., Sural, Y. S., Zorlu, F., Bayol, U. & Severcan, F. (2016). Bladder cancer diagnosis from bladder wash by Fourier transform infrared spectroscopy as a novel test for tumor recurrence, J. Biophotonics, 1–9.

Guidon, A. C. (2019). Neuromuscular Junction Disorders. In: Cho, T., Bhattacharyya, S., Helfgott, S. (Ed.), Neurorheumatology (217-224), Springer, Cham. https://doi.org/10.1007/978-3-030-16928-2_23

Gurbanov, R. (2010). The effects of selenium on stz-induced diabetic rat kidney plasma membrane (Master Thesis). Retrived from Ulusal Tez Merkezi– Türkiye & Ankara (255463).

Gurbanov, R., & Tuncer, S. (2021). The Use of Fourier-Transform Infrared Spectroscopy to Determine Potential Starch-based Prebiotics. KSU J. Agric Nat, 24 (1), 22-30.

Gurbanov, R., Bilgin, M. & Severcan, F. (2016). Restoring Effect of Selenium on the Molecular Content, Structure and Fluidity of Diabetic Rat Kidney Brush Border Cell Membrane. Biochimica et Biophysica Acta, 1858, 845–854.

Gurbanov, R., Tunçer, S., Mingu, S., Severcan, F. & Gozen, A. G. (2019). Methylation, sugar puckering and Z-form status of DNA from a heavy metal-acclimated freshwater Gordonia sp. Journal of Photochemistry & Photobiology, B: Biology, 111580, 1- 11.

Ha, J. C., & Richman, D. P. (2015). Myasthenia gravis and related disorders: Pathology and molecular pathogenesis. Biochimica et Biophysica Acta (BBA) - Molecular Basis of Disease, 1852(4), 651-657.

Haris, P. I. & Severcan, F. (1999). FTIR spectroscopic characterization of protein structure in aqueous and non-aqueous media. Journal of Molecular Catalysis B: Enzymatic, 7, 207–221.

Hashimoto, K., Badarla, V. R., Kawai, A. & Ideguchi. T. (2019). Complementary vibrational spectroscopy. Nature communications, 10: 4411.

Hehir M. K., & Silvestri, N. J. (2018). Generalized Myasthenia Gravis Classification, Clinical Presentation, Natural History, and Epidemiology. Neurol Clin, 36, 253–260.

Hill, M. (2003). The Neuromuscular Junctıon Disorders. J Neurol Neurosurg Psychiatry, 74, ii32- ii37.

Hübscher, S. G. (2003). Iron overload, inflammation, and fibrosis in genetic haemochromatosis. J Hepatol, 38(4), 521-5.

Hughes, B. W., Kusner, L. L., & Kaminski, H. J. (2006). Molecular architecture of the neuromuscular junction. Muscle & Nerve, 33, 445-461.

Juel, V. C., & Massey, J. M. (2007). Myasthenia gravis. Orphanet Journal of Rare Diseases, 2 (44), 1-13.

Jung, H. H., Yi, H. J., Lee, S. K., Lee, J. Y., Jung, H. J., Yang, S. T., Eu, Y. J., Im, S. H., & Kim, J. I. (2007). Biochemistry, 46, 14987-14995.

Kaminski, H. J. (2018). Treatment of Myasthenia Gravis. H. J. Kaminski, L. L. Kusner (Ed.), Myasthenia Gravis and Related Disorders, Springer Nature, 169- 187.

Kepenek, E. S. (2017). Molecular adaptations in cadmium and lead resistant environmental species (Doctoral Thesis). Retrieved from Ulusal Tez Merkezi– Türkiye & Ankara (489518).

Kepenek, E. S., Gözen, A. G. & Severcan, F. (2018). Molecular characterization of acutely and gradually heavy metal acclimated aquatic bacteria by FTIR spectroscopy. Journal of Biophotonics, 1- 20.

Kinik, S. T., Tuncer, A. M. & Altay, C. (1999). Transferrin receptor on peripheral blood lymphocytes in iron deficiency anemia. Br J Haematol, 104(3), 494-8.

Ko, S. F., Huang, C. C., Hsieh, M. J., Ng, S. H., Lee, C. C., Lee, C. C., Lin, T. K., Chen, M. C. & Lee, L. (2008). 31P MR Spectroscopic Assessment of Muscle in Patients with Myasthenia Gravis before and after Thymect. Radiology, 247, 162- 169.

Kocak, M. (2007). Interactions of Cholesterol Reducing Agent Simvastatin with Phospholipid Model Membranes (Master Thesis). Retrived from Ulusal Tez Merkezi– Türkiye & Ankara (199298).

Koehler, A., Scroferneker, M. L., Pereira, B. A.S., Preira de Souza, N. M., Cavalcante, R., Mendes, R. P. & Corbellini, V. A. (2022). Using infrared spectroscopy of serum and chemometrics for diagnosis of paracoccidioidomycosis. Journal of Pharmaceutical and Biomedical Analysis, 221.

Kucuk Baloglu, F., & Severcan, F. (2018). Characterization and Differentiation of Adipose Tissue by Spectroscopic and Spectral Imaging Techniques. L. Szablewski (Ed.), Adipose Tissue (11- 27). IntechOpen. DOI: 10.5772/intechopen.75156

Lam, H. T., Graber, M. C., Gentry, K. A. & Bieschke, J. (2016). Stabilization of α-Synuclein Fibril Clusters Prevents Fragmentation and Reduces Seeding Activity and Toxicity, Biochemistry, 55(4), 675-685.

Lasch, P., Beekes, M., Schmitt, J. & Naumann, D. (2007). Detection of preclinical scrapie from serum by infrared spectroscopy and chemometrics. Anal Bioanal Chem, 387(5), 1791–1800.

Lavrnic, D., Dakovic, M., Peric, S., Rakocevic-Stojanovic, V., Basta, I., Marjanovic, I., Stosic-Opincal, T. & Lavrnic, S. (2011). Journal of the Neurological Sciences, 302, 25–28.

Maggi, L. & Mantegazza, R., (2011). Treatment of myasthenia gravis: focus on pyridostigmine. Clinical Drug Investigation, 31(10), 691- 701.

Mamrut, S., Avidan, N., Truffault, F., Staun-Ram, E., Sharshar, T., Eymard, B., Frenkian, M., Pitha, J., de Baets, M., Servais, L., Berrih-Aknin S. & Miller, A. (2017). Methylome and transcriptome profiling in Myasthenia Gravis monozygotic twins. Journal of Autoimmunity, 82, 62- 73.

McBride, J. A., & Striker, R. (2017). Imbalance in the game of T cells: What can the CD4/CD8 T-cell ratio tell us about HIV and health. PLoS Pathog., 13(11), e1006624.

MCGrogan, A., Sneddon, S., & de Vries, C. S. (2010). The Incidence of Myasthenia Gravis: A Systematic Literature Review. Neuroepidemiology, 34, 171-183.

Menon, D., Barnett, C., & Bril, V. (2020). Novel Treatments in Myasthenia Gravis. Front. Neurol., 11,8538). 1-12.

Minnes, R., Nissinmann, M., Maizels, Y., Gerlitz, G., Katzir, A. & Raichlin, Y. (2017). Using Attenuated Total Reflection– Fourier Transform Infra-Red (ATR-FTIR) spectroscopy to distinguish between melanoma cells with a different metastatic potential. Nature, Scientific Reports, 7: 4381, 1- 7.

Mollaoglu Dogan, A. Ozyurt, I. & Severcan, F. (2018). Applications of Infrared Spectroscopy and Microscopy in Diagnosis of Obesity. El-Azazy, M. (Ed.), Infrared Spectroscopy- Principles, Advances, and Applications (1-22). IntechOpen. DOI: 10.5772/intechopen.81216

Montano, V., Gruosso, F., Carelli, V., Comi, GP., Filosto, M., Lamperti, C., Mongini, T., Musumeci, O., Servidei, S., Tonin, P., Toscano, A., Modenese, A., Primiano, G., Valentino, ML., Bortolani, S., Marchet, S., Meneri, M., Tavilla, G., Siciliano, G., & Mancuso, M. (2020). Primary mitochondrial myopathy. Neurology: Genetics, 6(6), 1-11.

Mousa Abbas, S. A. (2016). Biophysical characterization of proteins in solution and human fluids for cancer diagnosis applications using Fourier transform infrared spectroscopy (Doctoral Thesis). Retrived from Ulusal Tez Merkezi– Türkiye & Ankara (442185).

Nalbantoglu, M. & Uzun Adatepe, N. (2015). Miyastenia Gravis ve Diğer Nöromusküler İleti Bozukluğu Hastalıkları, Akın Eraslan Balcı (Ed). Mediyasten Hastalıkları ve Cerrahisi (229- 246).

Nemes, K., Gellert, A., Almási, A., Vági, P., Sáray, R., Kádár, K. & Salánki, K. (2017). Phosphorylation regulates the subcellular localization of Cucumber Mosaic Virus 2b protein, Scientific Reports, 7, 13444.

Oger, J. & Frykman, H. (2015). An update on laboratory diagnosis in myasthenia gravis. Clinica Chimica Acta, 444, 126-131.

Olusi, S. (2002). Obesity is an independent risk factor for plasma lipid peroxidation and depletion of erythrocyte cytoprotectic enzymes in humans. Int J Obes, 26, 1159–1164.

Omar, A., Marwaha, K., & Bollu, P. C. Physiology, Neuromuscular Junction, StatPearls [Internet], 2022, Available from: https://pubmed.ncbi.nlm.nih.gov/29261907/

Owe J. F, Daltveit A. K. & Gilhus N. E. (2006). Does myasthenia gravis provide protection against cancer. Acta Neurol Scand, 113(183), 33–36.

Ozdemir, Z., & Alagöz, M. A. (2018). Anticholinesterases, I. J. Al-Zawaini, A. Al-Mayahi (Ed.), Selected Topics in Myasthenia Gravis, Intecopen, 1-13. DOI: 10.5772/intechopen.81994.

Ozek, N. S., Tuna, S., Erson-Bensan, A. E. & Severcan, F. (2010). Characterization of microRNA-125b expression in MCF7 breast cancer cells by ATR-FTIR spectroscopy. Analyst, 135(12), 3094–3102.

Park, K. H., Jung, J., Lee J. H., & Hong, Y. H. (2016). Blood Transcriptome Profiling in Myasthenia Gravis Patients to Assess Disease Activity: A Pilot RNA-seq Study. Exp Neurobiol, 25(1), 40-7.

Pasnoor, M., Dimachkie, M. M., Farmakidis, C., & Barohn, R. J. (2018). Diagnosis of Myasthenia Gravis. Neurol Clin, 36, 261–274.

Payet, C. A., You, A., Fayet, O. M., Dragin, N., Berrih-Aknin, S. & Le Panse, R. (2022a). Myasthenia Gravis: An Acquired Interferonopathy?, Cells, 11(7), 1218.

Payet, O. M., Hemery, E., Truffault, F., Bondet, V., Duffy, D., Michel, F., Fadel, E., Guihaire, J., Demeret, S., Berrih-Aknin, S. & Le Panse, R. (2022b). Central Role of Macrophages and Nucleic Acid Release in Myasthenia Gravis Thymus, Annals of Neurology, Epub ahead of print, PMID: 36571580.

Peters, A. S., Backhaus, J., Pfützner, A., Raster, M., Burgard, G., Demirel, S., Böckler, D. & Hakimi, M. (2017). Serum-infrared spectroscopy is suitable for diagnosis of atherosclerosis and its clinical manifestations. Vibrational Spectroscopy, 92, 20-26.

Psychogios, N., Hau, D.D., Peng, J., Guo, A. C., Mandal, R., Bouatra, S., Sinelnikov, I., Krishnamurthy, R., Eisner, R., Gautam, B., Young, N., Xia, J., Knox, C., Dong, E., Huang, P., Hollander, Z., Pedersen, T. L., Smith, S. R., Bamforth, F., Greiner, R., McManus, B., Newman, J. W., Goodfriend, T. & Wishart, D. S. (2011). The Human Serum Metabolome. Plus one, 6(2), e16957, 1-23.

Punga, A. R., Maddison, P., Heckmann, J. M., Guptill, J. T. & Evoli, A. E. (2022). Epidemiology, diagnostics, and biomarkers of autoimmune neuromuscular junction disorders. The Lancet Neurology, 21(2), 176-188.

Querol, L. & Illa I. (2013). Myasthenia gravis and the neuromuscular junction. Curr Opin Neurol, 26(5), 459- 465.

Ragheb, S., Bealmear, B. & Lisak, R. (1999). Cell-surface expression of lymphocyte activation markers in myasthenia gravis. Autoimmunity, 31(1), 55-66.

Ralbovsky, N. M., Dey, P., Galfano, A., Dey, B.K. & Lednev, I. K. (2020). Diagnosis of a model of Duchenne muscular dystrophy in blood serum of mdx mice using Raman hyperspectroscopy. Scientific Reports, 10:11734,

Rodriguez, J. A., Ivanova, M. I., Sawaya, M. R., Cascio, D., Reyes, F. E., Shi, D., Sangwan, S., Guenther, E. L., Johnson, L. M., Zhang, M., Jiang, L., Arbing, M. A., Nannenga, B. L., Hattne, J., Whitelegge, J., Brewster, A. S., Messerschmidt, M., Boutet, S., Sauter, N. K., Gonen, T. & Eisenberg, D. S. (2015). Structure of the toxic core of α-synuclein from invisible crystals, Nature, 525, 486-490.

Romi, F., Hong Y. & Gilhus, N. E. (2017). Pathophysiology and immunological profile of myasthenia gravis and its subgroups. Current Opinion in Immunology, 49, 9– 13.

Sabre, L., Punga, T., & Punga, A. R. (2020). Circulating miRNAs as Potential Biomarkers in Myasthenia Gravis: Tools for Personalized Medicine. Frontiers in immunology, 11, 213.

Sahin, I., Bilge, D., Kazancı, N. & Severcan, F. (2013). Concentration-dependent effect of melatonin on DSPC membrane. Journal of Molecular Structure, 1-23.

Sanganahalli, B. G., Joshi, P. G. & Joshi, N. B. (2000). Differential effects of tricyclic antidepressant drugs on membrane dynamics—a fluorescence spectroscopic study. Life Sciences, 68(1), 81-90.

Sathasivam, S. (2014). Diagnosis and management of myasthenia gravis. Progress in Neurology and Psychiatry, 18(1), 6-14.

Sen, I., Bozkurt, O., Aras, E., Heise, S., Brockmann, G. A., & Severcan, F. (2015). Lipid Profiles of Adipose and Muscle Tissues in Mouse Models of Juvenile Onset of Obesity Without High Fat Diet Induction: A Fourier Transform Infrared (FT-IR) Spectroscopic Study, Appl. Spectrosc., 69, 679-688.

Severcan, F., Bozkurt, O., Gurbanov, R. & Gorgulu, G. (2010). FT-IR spectroscopy in the diagnosis of diabetes in rat animal model. Journal of Biophotonics, 3(8- 9), 621- 631.

Severcan, F., Gorgulu, G., Gorgulu, T. S., Guray, T. (2005b). Rapid monitoring of Diabetes-Induced Lipid peroxidation by Fourier Transform Infrared Spectroscopy, Analytical Biochemistry, 339, 36-40.

Severcan, F., Sahin, I. & Kazancı. N. (2005a). Melatonin strongly interacts with zwitterionic model membranes-evidence from Fourier transform infrared spectroscopy and differential scanning calorimetry, Biochimica et Biophysica Acta (BBA) - Biomembranes, 1668(2), 215-222.

Sieb, J. P. (2014). Myasthenia gravis: an update for the clinician. Clinical and experimental immunology, 175(3), 408- 418.

Sills, R. H., Moore, D. J. & Mendelsohn, R. (1994). Erythrocyte peroxidation: Quantitation by Fourier transform infrared spectroscopy, Analytical Biochemistry, 218, 118-123.

Simsek Ozek, N., Sara, Y., Onur, R. & Severcan, F. (2010). Low-dose simvastatin induces compositional, structural, and dynamic changes in rat skeletal extensor digitorum longus muscle tissue. Bioscience reports, 30, 41- 50.

Singh, B. R., Wasacz, F. M., Strand, S., Jakobsen, R. J., & DasGupta, B. R. (1990). Structural Analysis of Botulinum Neurotoxin Types A and in Aqueous and Nonpolar Solvents by Fourier Transform Infrared, Second Derivative UV Absorption, and Circular Dichroic Spectroscopies. Journal of Protein Chemistry, 9 (6), 705- 713.

Sirin-Inan, N. G. (2018). Myasthenia gravis hastalarında nöromüsküler kavşak işlevlerinin elektrofizyolojik değerlendirilmesi (Master Thesis). Retrieved from: Ulusal Tez Merkezi – Türkiye & Istanbul (552885).

Spahıu, E. (2015). ATR-FTIR Evaluation of structural and functional changes on murine macrophage cells upon activation and suppression by immunotherapeutic oligodeoxynucleotides (Master Thesis). Retrived from Ulusal Tez Merkezi– Türkiye & Ankara (416391).

Stief, T. (2014). Edıtorial: Hemostasis activation in inflammation: Kallıkrein, thrombin, 1 ΔO2. Hemostasis Laboratory, 7(3-4), 323-329.

Stuart, B. H. (2004). Infrared Spectroscopy, Fundamentals, and Applications. England: John Wiley & Sons, Ltd.

Stuart, B. H. (2006). Infrared Spectroscopy of Biological Applications. Encyclopedia of Analytical Chemistry, 1-31.

Teker, H. T., Ceylani, T., Keskin, S., Samgane, G., Mansuroglu, S., Baba, B., Allahverdi, H., Acıkgoz, E & Gurbanov, R. (2023). Age-related diferences in response to plasma exchange in male rat liver tissues: insights from histopathological and machine-learning assisted spectrochemical analyses. Biogerontology.

Trakas, N., & Tzartos, S. J. (2018). Immunostick ELISA for rapid and easy diagnosis of Myasthenia Gravis. Journal of immunological methods, 460, 107-112.

Trouth, Dabi, Solieman, Kurukumbi, & Kalyanam (2012). Myasthenia Gravis: A Review. Autoimmune Diseases, 2012, 1-11.

Turner, C. (2007). A review of myasthenia gravis and its management. Current Anaesthesia & Critical Care, 18, 15-23.

Undavalli, V. K., Ling, C., & Khandelwal, B. (2021). Impact of alternative fuels and properties on elastomer compatibility. Aviation Fuels, 113- 132.

Van Beekvelt, M. C., van Engelen, B. G., Wevers, R. A., & Colier, W. N. (1999). Quantitative Near-Infrared Spectroscopy Discriminates between Mitochondrial Myopathies and Normal Muscle. Ann Neurol, 46, 667-670.

Vincent, A. (2002). Unraveling the pathogenesis of myasthenia gravis. Nature reviews immunology, 2, 797-804.

Vincent, A., Palace, J., & Hilton-Jones, D. (2001). Myasthenia gravis, The Lancet, 357, 2122–2128.

Wang, Z. & Yan, Y. (2017). Immunopathogenesis in Myasthenia Gravis and Neuromyelitis Optica. Frontiers in Immunology, 8:1785, 1- 14.

Watanabe, O. (2013). Isaacs's syndrome and associated diseases. Rinsho Shinkeigaku, 53(11), 1067- 1070.

Wood, B. R. (2016). The importance of hydration and DNA conformation in interpreting infrared spectra of cells and tissues. Chemical Society Reviews, 7, 45. 1980- 1998.

Yangın, M. N., Zorlu, Y., & Severcan, F. (2022). Diagnosis and Treatment Methods of Autoimmüne Myasthenia Gravis: A Systematic Review. Journal of Health Sciences, 4(2), 104-116.

Yavuz, Z. (2019). Myasthenia Gravis Klinik ve Demografik Özellikleri (Dissertation for specialty in medicine). Retrived from Ulusal Tez Merkezi – Türkiye & Ankara. (602539).

Yonar, D., Ocek, L., Tiftikcioglu, BI., Zorlu, Y. & Severcan, F. (2018). Relapsing-Remitting Multiple Sclerosis diagnosis from cerebrospinal fuids via Fourier transform infrared spectroscopy coupled with multivariate analysis. Nature-Scientific reports, 8(1025), 1- 13.

Yonar, D., Sandal, A., Emri, S. & Severcan, F. (2015). A Novel Method for Early Diagnosis of Malignant Pleural Mesothelioma from Human Serum Samples: ATR-FTIR Spectroscopy. Biophysical Journal, 108(2), Supplement 1, p626a.

Yonar, D., Severcan, M., Gurbanov, R., Sandal, A., Yilmaz, U., Emri, S. & Severcan, F. (2022). Rapid diagnosis of malignant pleural mesothelioma and its discrimination from lung cancer and benign exudative effusions using blood serum. Biochimica et Biophysica Acta (BBA) - Molecular Basis of Disease, 1868.

Zhang, B., Shen, C., Bealmear, B., Ragheb, S., Xiong, W., Lewis, R. A., Lisak, R. P., & Mei, L. (2014). Autoantibodies to Agrin in Myasthenia Gravis Patients. Plos one, 9(3), 1- 6.

Zhang, L., Xiao, M., Wang, Y., Peng, S., Chen, Y., Zhang, D., Zhang, D., Guo, Y., Wang, X., Luo, H., Zhou, Q. & Xu, Y. (2021). Fast Screening and Primary Diagnosis of COVID-19 by ATR-FT-IR. Anal. Chem., 93(4), 2191- 2199.